Electronic Structure and Phase Equilibria in Ternary Substitutional Alloys: A Tight-Binding Approach

by

Ariel Javier Sebastián Traiber

Lic. en Ciencias Físicas, University of Buenos Aires, 1989
S.M., Materials Science, MIT, 1991

Submitted to the Department of Materials Science and Engineering
in partial fulfillment of the requirements for the degree of

Doctor of Philosophy in Materials Science

at the

MASSACHUSETTS INSTITUTE OF TECHNOLOGY

June 1995

Author .....
Department of Materials Science and Engineering
May 5, 1995

Certified by .....
Samuel M. Allen
Professor of Physical Metallurgy
Thesis Supervisor

Accepted by .....
Carl V. Thompson II
Professor of Electronic Materials
Chair, Departmental Committee on Graduate Students

Electronic Structure and Phase Equilibria in Ternary Substitutional Alloys: A Tight-Binding Approach

by

Ariel Javier Sebastián Traiber

Submitted to the Department of Materials Science and Engineering
on May 5, 1995, in partial fulfillment of the
requirements for the degree of
Doctor of Philosophy in Materials Science

Abstract

The goal of this thesis is to develop and apply alloy theory methods to transition metals and alloys (particularly ternary systems) based on the tight-binding (TB) model of atomic cohesion in studies of stability and phase equilibria. At least two factors make this kind of formalism desirable: it can bring a clear understanding of the underlying physical mechanisms that many times get obscured in first-principles calculations, and it is easily adapted to complex problems and multicomponent solutions, at low computational cost.

The original physical insight given by the TB method is demonstrated by the study of the relation between the atomic local environment and the relative stability of simple phases, through the calculation of the moments of the electronic density of states. We show that the relative stability of phases related to the Bain transformation is mainly controlled by the moment of order five, and we have identified the main contributions to this moment.

We present a model for cohesive energy based on the assumption that it can be written as the sum of a band-structure contribution and a repulsive short-range contribution. We have calculated the band contribution using a TB Hamiltonian with d states and applied the linearized Green's function method based on the recursion technique. For the repulsive part of the energy we employ a Born-Mayer potential. The model was used to study total energies for Mo. We show that a six-moment approximation to the band energy is sufficient to reproduce more accurate results, using the standard recursion method, for the energetics of this transition metal.

We describe a reliable and consistent scheme to study phase equilibria in ternary substitutional alloys based on the TB approximation. The TB electronic parameters are obtained from linear muffin-tin orbital calculations. The transfer integrals are scaled in distance with an orbital-dependent exponential decay parametrization, while the on-site energies are scaled via a polynomial parametrization. The computed density of states and band structures compare very well with those obtained in more

accurate *ab initio* calculations.

This study includes disordered, partially ordered and ordered alloys. Disordered alloys are studied within the tight-binding coherent-potential approximation formalism extended to multicomponent alloys. The energies of ordered systems are obtained through effective pair interactions computed with the general perturbation method, and compared with those obtained from a recursion technique. Partially ordered alloys are studied with a novel simplification of the molecular coherent-potential approximation combined with the general perturbation method. The TB scheme proved to be a consistent and reliable way to treat the electronic structure of alloys, and it has the capability of assisting in the design of materials with specific electronic properties.

The formalism is applied to study bcc-based ternary Zr-Ru-Pd alloys. These alloys show promising applications as medical implant devices because of their potentially good biocompatibility, corrosion and wear resistance, and toughness. Using the energetic parameters obtained with the aforementioned TB scheme, we apply the cluster-variation method to study phase equilibria for these alloys. The results are consistent with the experimental evidence. We also show how it is possible to explain within this formalism the observed behavior of the electronic specific heat coefficient, γ, for the $Zr_{0.5}$(Ru,Pd) system.

Thesis Supervisor: Samuel M. Allen
Title: Professor of Physical Metallurgy

Acknowledgments

I would like to thank my advisor, Prof. Sam Allen, for his constant interest in the developing of my research, and my life as a graduate student. It has been a pleasure working with him all these years.

Most of my doctoral work was done under the direction of Dr. Patrice Turchi at the Theory and Modeling Group of the Chemistry and Materials Science Department, Lawrence Livermore National Laboratory, in California. I will be always indebted to Dr. Turchi for giving me the unique opportunity, as a graduate student, to work at Lawrence Livermore. I thank him for his constant availability and support, his wiliness to sharing his extensive knowledge at any time, and for his contagious enthusiasm for science, and encouragement to go on, even at times of uncertainty or frustration.

Thanks are due to Professors Gerd Ceder and Sidney Yip for their advice and service on my thesis committee.

Many thanks to Dr. Tony Gonis for the enlightening discussions, and to Dr. Phillip Sterne for sharing his superb computer knowledge that made my life so much easier at Lawrence Livermore. Thanks also to past and present post-docs of the Theory Group: Marcel Sluiter, Prabhakar Singh, Leszek Reinhard and Jan van Ek, for sharing their knowledge and expertise; to Rose Coleman and Margie Altenbach for helping in dealing with the bureaucratic ways of a National Lab, and to Maria Jose Caturla for being such an easy-going office-mate, and for sharing innumerable lunches at the Central Cafeteria.

To all my friends in Cambridge/Boston, Northern California, Argentina, and other faraway places: thank you for your love, support, and best wishes. Special thanks to Sue and Kathy for their wonderful friendship.

Finally, I want to say a big 'Thank you' to my parents for their love and support, and to Doug, for being there. Things got harder when he was not around but, even from afar, he was a constant source of encouragement.

This thesis is dedicated to the memory of

Peter Grasty (1956-1995).

Peter and I started graduate school at the same time,

and we both received our Master's degrees

in Materials Science in 1991.

He was an unpretentious, kind, and caring human being.

His memory will always live within all of us,

who have enjoyed his wonderful friendship.

Contents

List of Figures

List of Tables

Chapter 1

Introduction

Myriad experimental data have been collected over several decades about metals and alloys; e.g., heats of formation, phase equilibria, melting points, composition and structure of compounds, and interactions between alloying elements. Yet, only in the last twenty years have fundamental theories evolved to the point of being able to make quantitative predictions related to this wealth of information. The breakthrough came in the sixties when Hohenberg, Kohn, and Sham [1, 2] showed that it was possible to transform the complicated many-electron problem into an effective one-electron problem which could, in principle, be solved using the so-called local density approximation (LDA). Their theory, known as density functional theory (DFT), offered the possibility of obtaining a reliable prediction of cohesive and structural properties of simple metals, transition metals (TM), and intermetallics, from first principles. With the advent of fast computers and improved computational codes, one can now compute the ground-state properties of complex solids with tens of atoms in a periodically repeated unit cell. And with the addition of some statistical mechanics, calculations from first-principles are also beginning to shed light on the origins of phase transitions and the structure of phase diagrams for alloys.

At the same time that these *ab initio* (or first-principles) methods were evolving, two simpler models were also being (re)developed: the Nearly Free Electron (NFE) model and the Tight-Binding (TB) model. These models offer, at least, two important advantages. First, they provide direct physical and chemical insight into

the origin of bonding and structure at the atomic level. Second, since they are not first-principles approaches, they provide a way to study finite-temperature properties and disordered materials that does not require extreme computational efforts. These two models have different underlying assumptions and hence applicability. The NFE approximation regards the valence electrons as a gas of free electrons that is only weakly perturbed by the underlying ionic lattice, while the TB approximation considers that the valence states are formed by the weak overlap of atomic orbitals. While the NFE approximation is a valid description of the *sp*-bonded simple metals, the TB approximation is a reasonable description of the *d*-bonded transition metals and most intermetallics. (Transition elements appear with the filling of the $3d$, $4d$, and $5d$ shells.) It is now established that the *d* electrons, although fairly localized in the atoms, do occupy band states responsible for many typical, particularly cohesive, properties of these elements [3].

Trends in cohesive and structural properties of transition metals and alloys have been well characterized by simple TB models. For instance, in the case of cohesive properties, the approximately parabolic variation of the cohesive energy, the bulk modulus, and the equilibrium atomic volume, across the TM series has been remarkably well reproduced with Friedel's rectangular band model [4]. The predicted cohesive energies are about 2 eV/atom too small, primarily because the model ignores the *sp* band, and the hybridization between the *sp* band and the *d* band can increase the cohesive energy. This model is also known as the "second-moment approximation" because the band energy is characterized solely by the second moment of the electronic density of states. In contrast, the prediction of structural stability requires a much more accurate evaluation of the actual shape of the TB density of states. The rectangular band, with its uniform density of states, is unable to discriminate between the energies of different crystal structures and one must go beyond the second moment to get sufficiently accurate results.

In principle and increasingly in practice, it is possible to solve fully dynamic calculations for the equations of motion of the ions. Such a simulation is called *molecular dynamics* (MD), and provides a picture of the processes occurring at high tempera-

ture. The implementation of MD simulations within a first-principles approach [5] is now well known and the ground-state energy and equilibrium atomic configuration of crystalline defects, interfaces, glasses and liquids may be predicted with some success, albeit with extreme computational effort. This still restricts the MD simulations to a small number of atoms and quite short simulation times. For studies of mechanical and deformation properties, simulation cells containing at least several hundred atoms are required and one cannot use the *ab initio* approach. To perform such simulations, we have to resort to some approximations. For instance, tight-binding molecular-dynamics methods have been used to study semiconductors and covalent systems such as Si, C and Si-C (see for example [6, 7]) as a compromise between the computational effort demanded by *ab initio* approaches, and the limitations imposed for the more widely used empirical potential methods which present problems of transferability and are not able to account for electronic structure effects of the lattice.

Chapter 3 addresses the issues raised in the previous two paragraphs. We start by examining the elements of the TB approximation and describing the TB Hamiltonian. Next, we present a novel analysis of the moments of the electronic density of states using a TB model, with so-called canonical parameters, as it relates to the relative stability of simple phases. The model concentrates particularly on the tetragonal or Bain transformation that takes an fcc into a bcc cell, as commonly found in relation to martensitic transformations. Finally, we describe a new TB total energy model with potential application in molecular-dynamics studies.

Solid solutions with ordered phases ("intermetallic compounds") that exhibit desirable mechanical properties such as ductility and high strength are promising candidates for special applications. Possible uses range from the high-temperature alloys for gas turbines to bearing surfaces and mechanical joints. Because materials designed for optimum performance rarely consist of binary systems, the ability to model higher-order systems is especially needed. In order to develop these materials, the fundamental physical issues must be understood. Theories capable of predicting the type of ordering, the existence of structural transformations, and the phase equilibria

are fundamental tools in this endeavor. In the last decade, there has been considerable improvement in the calculation of both energies of formation of disordered and ordered alloys, and multisite effective interactions based on band structure calculations. Such energetic quantities can be used to obtain fairly accurate predictions of phase stability at $T = 0$ K (ground-states). The effective interactions may then be used in combination with statistical models for phase diagram determination.

We present in Chapter 4 a reliable and consistent formalism, based on a TB approximation, to study the electronic structure and phase stability of multicomponent transition-metal alloys. We show how this simple scheme can be used to assist in the design of materials with specific electronic properties. First, we characterize the TB parameters computed with the linear muffin-tin orbital method, with direct application to the Zr-Ru-Pd alloy. The coherent-potential approximation to study disordered alloys is then presented, followed by an account of the generalized perturbation method. We then describe an approximation to study partially ordered systems. Results for the ternary Zr-Ru-Pd and its binary subsystems illustrate the methodology.

Two ways of determining the equilibria at finite temperatures have proven to be most useful: the cluster-variation method (CVM) introduced by Kikuchi [8, 9] and the Monte Carlo simulation technique (MC) [10]. These methods are based on an Ising-model-type description of the lattice and need energy parameters as input. The CVM is based on an analytical calculation of the configurational entropy S. The equilibrium states are obtained by a minimization of the appropriate free energy (F or Ω). The MC method is a method of computer simulation of a system with many degrees of freedom. Briefly, it is used to simulate any averaging with a probability distribution, and it is usually performed in the grand canonical scheme. At a given temperature and fixed chemical potentials, atoms are exchanged with a reservoir of atoms with a probability which is defined in such a way that the equilibrium state is reached after a sufficient number of atomic replacements. This method yields the equilibrium configuration but not the thermodynamic functions.

In Chapter 5, the energetic parameters obtained with the methodology described

in Chapter 4 will be used in combination with the CVM to study phase equilibria in binary and pseudo-binary alloys. The formalism will be illustrated with the ternary Zr-Ru-Pd alloy. From these results, we propose an explanation for the observed behavior of the electronic specific heat coefficient for the $Zr_{0.5}$(Ru,Pd) pseudo-binary alloy.

Chapter 2 presents background information which will be useful in subsequent chapters. It includes a section on notation and units, definitions for electronic density of states and band energies, a compilation of experimental facts regarding the Zr-Ru-Pd system, and a description of the bcc-based lattice structures. Chapter 6 presents a summary and the conclusions of this work. Finally, suggestions for future research are given in Chapter 7.

Chapter 2

Background

2.1 Units and Notation

Atomic units will be used throughout this thesis. The unit of energy is the Rydberg (Ry) which corresponds to the ionisation potential of the hydrogen atom: 1 Ry = 2.18 10^{-18} J = 13.5 eV. The unit of length is the atomic unit (au) which is the first Bohr radius: 1 au = 5.29 10^{-11} m = 0.529 Å. In atomic units, the following relationships hold: $\hbar/2m = 1$ and $e^2/4\pi\epsilon_o = 2$, where $\hbar$ is the Planck's constant divided by 2π, m is the electron mass, e is the magnitude of the electronic charge, and ϵ_o is the permitivity of free space. Energies of bulk materials and effective pair interactions will be usually given in Ry/atom. Conversion to other units may be achieved by using 1 mRy/atom = 1.32 kJ mol^{-1} = 0.314 kcal mol^{-1}. Electronic density of states will be given in States/Ry-atom.

Dirac's *bra* and *ket* notation will be use to express most of the mathematics of quantum mechanics formulations. The *ket* represents a wave function, $\psi \equiv |\psi\rangle$, while a *bra* is its hermitian conjugate, $\psi^* \equiv \langle\psi|$. We often use atomic orbitals, which we could note $|n, \lambda\rangle$, where n specifies a particular lattice site, and λ is a particular orbital.

Dirac's notation is based on the understanding that

$$\langle \phi | \psi \rangle = \int_{all\ space} \phi^* \, \psi \, \mathrm{d}\mathbf{r}. \tag{2.1}$$

The average or expectation value of a physical quantity represented by an operator H for a system characterized by the state ψ is given by

$$\langle \psi | H | \psi \rangle = \int \psi^* \, H \, \psi \, \mathrm{d}\mathbf{r}, \tag{2.2}$$

while the matrix element between states ϕ and ψ is given by

$$\langle \phi | H | \psi \rangle = \int \phi^* \, H \, \psi \, \mathrm{d}\mathbf{r}. \tag{2.3}$$

If $\{\psi_i\}$ is a basis set, the *trace* of the operator H is given by

$$\mathrm{Tr}H = \sum_i \langle \, \psi_i \, | \, H \, | \, \psi_i \, \rangle. \tag{2.4}$$

Finally the operator identity is written as

$$I = \sum_i | \, \psi_i \, \rangle \langle \, \psi_i \, |. \tag{2.5}$$

2.2 Density of States and Band Energies

Given a Hamiltonian H for a particular system, we could attempt to solve the (one-electron) Schrödinger equation

$$H|\psi_n\rangle = E_n|\psi_n\rangle, \tag{2.6}$$

and obtain the eigenfunctions $|\psi_n\rangle$ and eigenvalues E_n. On the other hand, most of the information we need is contained in the (total) density of states (DOS) given by

$$n(E) = \frac{1}{N} \sum_n \delta(E - E_n), \tag{2.7}$$

where $\delta(x)$ is the Dirac function and N is the number of lattice sites. If we define the operator $\delta(E-H)$ according to $\delta(E-H)|\psi_n\rangle = \delta(E-E_n)|\psi_n\rangle$, then the DOS can be rewritten as the trace over this operator:

$$n(E) = \frac{1}{N} \operatorname{Tr} \delta(E-H). \tag{2.8}$$

It is often useful to express the eigenfunctions $|\psi_n\rangle$ as a linear combination of atomic orbitals (LCAO) $|\phi_{i\alpha}\rangle$:

$$|\psi_n\rangle = \sum_{i\alpha} \mathrm{a}_{n,i\alpha} |\phi_{i\alpha}\rangle, \tag{2.9}$$

where i is a site index for the atomic site and α denotes the type of orbital, e.g., $3s, 3p_x, 3p_y$, etc.

It is possible then to define a partial density of states when the physical situation requires the knowledge of separate contributions to the total DOS. For instance, the local DOS for an orbital λ located on site i is given by

$$n_{i\lambda}(E) = \langle\, \phi_{i\lambda} \mid E - H \mid \phi_{i\lambda} \,\rangle = \delta(E - \epsilon_i^{\lambda}), \tag{2.10}$$

where ϵ_i^{λ} is the corresponding eigenvalue. If there are q orbitals in each site, then

$$n_i(E) = \sum_{\lambda=1}^{q} n_{i\lambda}(E) \tag{2.11}$$

is the DOS for site i, and the total DOS is given by

$$n(E) = \frac{1}{N} \sum_{i,\lambda} n_{i\lambda}(E). \tag{2.12}$$

Notice in this expression that the total DOS is normalized to the (total) number of states per site:

$$q = \int_{-\infty}^{\infty} n(E)\, \mathrm{d}E. \tag{2.13}$$

To avoid working with delta functions, we introduce the resolvent operator (or one-electron Green's function) $G(z) = (z-H)^{-1}$, defined for any complex number z.

Using the following identity,

$$\delta(x) = \lim_{\epsilon \to 0^+} -\frac{1}{\pi} \operatorname{Im} \left(\frac{1}{x + i\epsilon}\right), \tag{2.14}$$

we can then write

$$\delta(E - H) = -\frac{1}{\pi} \operatorname{Im} G(E^+), \tag{2.15}$$

where E^+ means we take the limit $z = E + i\epsilon, \epsilon \to 0^+$.

Finally, the density of states is expressed as

$$n(E) = -\frac{1}{\pi N} \operatorname{Im} \operatorname{Tr} G(E^+), \tag{2.16}$$

while the partial density of states on site i with orbital λ is given by

$$n_{i\lambda} = -\frac{1}{\pi} \operatorname{Im} \langle i\lambda | G(E^+) | i\lambda \rangle. \tag{2.17}$$

If E_{F} is the Fermi energy, the number of electrons per atom is given by

$$N_e = \int_{-\infty}^{E_{\mathrm{F}}} \mathrm{d}E \, n(E). \tag{2.18}$$

It is also interesting to define the integrated DOS $N(E)$:

$$N(E) = \int_{-\infty}^{E} \mathrm{d}E' \, E' \, n(E') = \frac{1}{\pi} \operatorname{Im} \operatorname{Tr} \ln G(E'^+). \tag{2.19}$$

Then, at zero temperature, $N_e = N(E_{\mathrm{F}})$. Finally, the band energy is defined as the sum of one-electron energies

$$E_b = \int_{-\infty}^{E_{\mathrm{F}}} \mathrm{d}E \, E \, n(E), \tag{2.20}$$

and the corresponding grand-potential $\Omega_b = E_b - N_e E_{\mathrm{F}}$ is given by

$$\Omega_b = -\int_{-\infty}^{E_{\mathrm{F}}} \mathrm{d}E \, N(E). \tag{2.21}$$

2.3 The Zr-Ru-Pd system

We will illustrate the formalism developed in Chapters 4 and 5 with the ternary Zr-Ru-Pd alloy. This system is one of a family of alloys under study with possible applications in medical implant devices. For example there are already surgical implants which are made in part of Co-Cr-Mo alloys. Zirconium-ruthenium-palladium alloys have attracted interest because of potentially good biocompatibility. In addition, preliminary experimental work has shown that $Zr_{0.5}$(Ru,Pd) alloys are extremely tough and wear resistant, properties which are desirable in implant device materials [11]. Intermediate compositions in the the Zr-Pd binary system crystallize with a β-brass (or $B2$-type) structure but undergo a martensitic transformation at 620°C; these binary alloys lack ductility at room temperature. The addition of Ru seems to stabilize the high-temperature $B2$ phase at room temperature and significant ductility has been recently reported in these ternary alloys. Equiatomic Ru-Zr alloys also form a $B2$-type structure which is stable up to its melting point. Ruthenium seems likely to substitute for palladium atoms in the ternary $B2$ alloy.

Figure 2-1 from Ref. [11] shows the variation of hardness and martensite transformation temperatures in the ternary alloy at $c_{\mathrm{Zr}} = 0.5$. The structure of the martensite was found to be of B_f or $B33$-type and experimental observations suggest a structural relationship between matrix and martensite which involves two kinds of shuffle-type displacive operations that take the $B2$ structure into $B19$ and finally into $B33$ [12].

2.4 Bcc-based lattice structures

The formalism that we are going to present in this thesis is not limited to any particular type of lattice structure. For sake of simplicity, and unless so noted, we will limit the application of the theory to the study of bcc-based systems. Structurbericht notation will be used throughout this work to designate the different structures which are derivatives of the bcc lattice (see Fig. 2-2). $A2$ designates the disordered bcc lattice. $B2$ is the β-brass structure which can be thought of as two interpenetrating

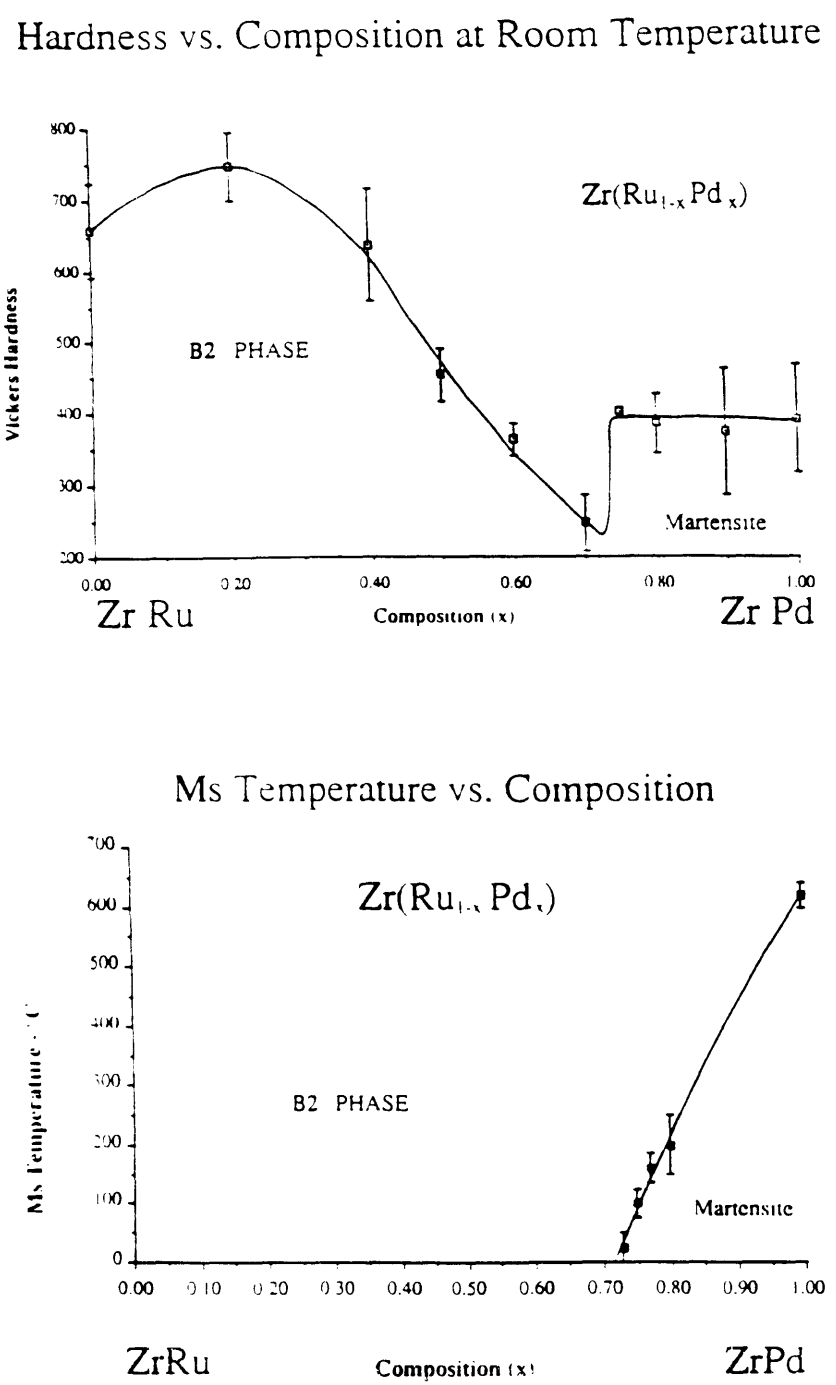

Figure 2-1: (a) Variation of hardness with composition at room temperature of the pseudo-binary system $Zr_{0.5}(Pd_cRu_{1-c})_{0.5}$. (b) Martensite transformation temperature on cooling versus composition for the same system. (Both from Ref. [11]).

primitive cubic lattices with different compositions. The $D0_3$ structure is a further NaCl-type ordering of one of the sublattices in the $B2$ structure. If the composition of this sublattice differs from that of the disordered one, the Heusler or $L2_1$ structure results. The $B32$ structure can be thought as two interpenetrating cubic lattices with NaCl-type ordering. Finally the structure with $F\bar{4}3m$ symmetry is formed by four interpenetrating cubic lattices of different compositions (there is no Structurbericht symbol for this structure).

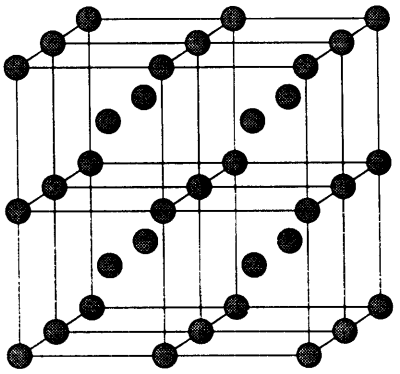

$A2$

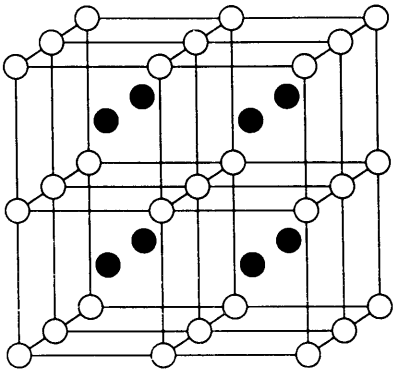

$B2$

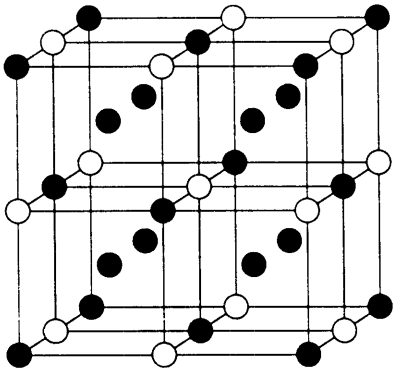

$D0_3$

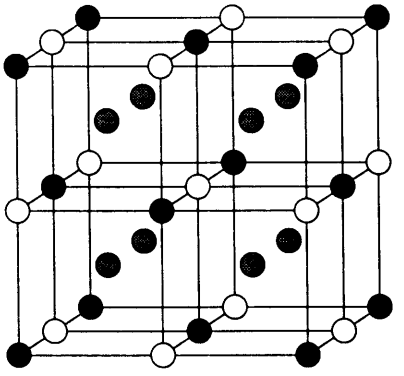

$L2_1$

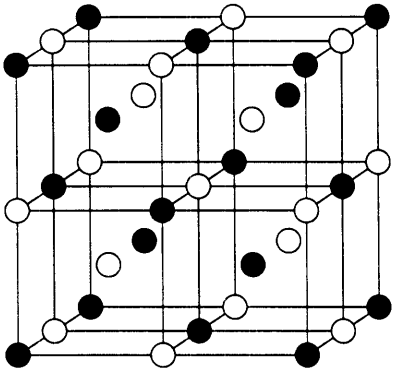

$B32$

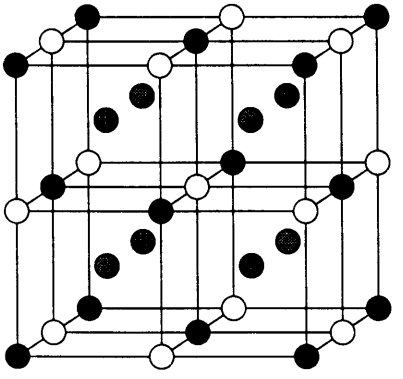

$F\bar{4}3m$

Figure 2-2: Bcc-based lattice structures

Chapter 3

General Description and Applications of the Tight-Binding Approximation

3.1 Introduction

It was well understood, since the early days of quantum mechanics, that the ground state of a piece of matter with 10^{22} atoms is described in principle by a wave function, obtained by solving the Scrödinger equation, which is function of the coordinates of all the electrons and nuclei. The exact wave function could never be calculated, but we will take for granted that it exists. *Ab initio* methods solve the Scrödinger equation by making significant approximations, but without resorting to experimental data. Semiempirical methods, which are able to incorporate most of the electronic effects, such as the TB method, inherit those same approximations. Two of those approximations will be readily accepted: The first one is the Born-Oppenheimer or adiabatic approximation: because of the large difference in mass between ions and electrons, the electrons can be considered as following instantaneously the motion of the ions. The electronic degrees of freedom are then removed and every ionic configuration possesses a well-defined electronic energy. Similarly, we are going to

neglect relativistic effects that are only important when dealing with heavy elements (e.g. $5d$ transition elements). Other approximations related specifically to the TB model will be discussed later.

The following section introduces the tight-binding Hamiltonian. Next, we present and discuss an analysis of the moments of the density of states for a particular structural transformation. Finally, an example of total-energy calculation within the TB approximation is described.

3.2 The Tight-Binding Hamiltonian

The tight-binding (TB) method is probably the simplest approach conceptually for describing energy bands. The basic approximation is to assume that all electronic wave functions of the metal system can be described by a basis of atomic-like orbitals. By knowing the wave functions and energies for the electron states in the free atom, we form the solid by bringing these atoms together and seek an expansion of the wave function of interest, $|\psi\rangle$, of the form

$$|\psi\rangle = \sum_{n,\lambda} a_n^\lambda |n,\lambda\rangle, \tag{3.1}$$

where $|n,\lambda\rangle$ is a wave function corresponding to an orbital of type λ on site n. Notice that for periodic systems, the resulting expansion coefficients a_n^λ are proportional to $e^{i\mathbf{K}.\mathbf{R}_n}$ for a state transforming according to wavenumber $\mathbf{K}$, and where $\mathbf{R}_n$ is a lattice site.

To simplify the computations, it is often assumed that the basis provided by the atomic wave-functions is not only complete but orthonormal as well, that is,

$$\langle n,\lambda|m,\mu\rangle = \delta_{n,m}\delta_{\lambda,\mu}. \tag{3.2}$$

This means that we are neglecting the overlap integrals between wave-functions on different sites, which is justified for transition metals since the d-electrons are fairly localized [3].

The lattice potential V^{lat} is assumed to be the sum of atomic potentials V^{at} centered on various lattice sites p,

$$V^{lat} = \sum_p V_p^{at}, \tag{3.3}$$

where $V_p^{at}|\mathbf{r}\rangle = V^{at}(r - \mathbf{R}_p)|\mathbf{r}\rangle$.

The one-electron Hamiltonian is then written as

$$H = T + \sum_p V_p^{at}, \tag{3.4}$$

where T is the kinetic-energy operator.

It is clear that $|\lambda, n\rangle$ is an eigenstate of the Hamiltonian corresponding to a free atom located on a site n, i.e., $H^{at} = T + V_p^{at}$. Then, we have

$$(T + V_p^{at})|n, \lambda\rangle = \epsilon_n^{\lambda}|n, \lambda\rangle, \tag{3.5}$$

where ϵ_n^{λ} is the atomic energy for the orbital λ.

Now, we are ready to compute the TB Hamiltonian matrix elements in the atomic orbital basis:

$$\langle n, \lambda|H|m, \mu\rangle = \langle n, \lambda| T + \sum_p V_p^{at} |m, \mu\rangle \tag{3.6}$$

$$= \epsilon_n^{\mu} \langle n, \lambda|m, \mu\rangle + \langle n, \lambda| \sum_{p \neq m} V_p^{at}|m, \mu\rangle. \tag{3.7}$$

Let us consider the second term of the right hand side of Eq. 3.7. For $n = m$, we define $\alpha_m^{\lambda,\mu}$, the crystal-field integral, as

$$\alpha_m^{\lambda,\mu} = \langle m, \lambda| \sum_{p \neq m} V_p^{at}|m, \mu\rangle. \tag{3.8}$$

The atomic potentials V^{at} are attractive, so $\alpha_m^{\lambda,\mu}$ are all negative and their effect is to shift the atomic levels ϵ_n^{λ}. In the case of crystalline systems with equivalent sites, these crystal fields are independent of the site m, and frequently diagonal, i.e.,

$\alpha_m^{\lambda,\mu} = \alpha^\lambda \delta_{\lambda,\mu}$ [15].

For $n \neq m$, we define the hopping or transfer integrals β as

$$\beta_{nm}^{\lambda\mu} = \langle n, \lambda | H | m, \mu \rangle \tag{3.9}$$

$$= \langle n, \lambda | \sum_{p \neq m} V_p^{at} | m, \mu \rangle. \tag{3.10}$$

These parameters are responsible for the mixing of atomic levels into molecular states which extend over the whole solid.

We notice that the $\beta_{nm}^{\lambda\mu}$ are the sum of two-center ($n = p \neq m$) and three-center ($n \neq p \neq m$) integrals. Usually we retain only the two-center integrals, which are much larger in magnitude than the three-center ones. These integrals are short-ranged (which is particularly true for transition metals, covalent elements, and their alloys) so it is usually sufficient to include only a small number (one or two) of neighboring shells.

Finally, using all the above definitions we can express the TB Hamiltonian as

$$H = \sum_{n,\lambda} |n, \lambda\rangle \tilde{\epsilon}_n^\lambda \langle n, \lambda| + \sum_{\substack{m,n \\ \mu,\lambda}} |n, \lambda\rangle \, \beta_{nm}^{\lambda\mu} \, \langle m, \mu| \,, \tag{3.11}$$

where $\tilde{\epsilon}_n^\lambda = \epsilon_o^\lambda + \alpha_n^\lambda$. Unless noted, we will drop the *tilde* on ϵ in the remainder of this thesis.

At this point it is convenient to introduce a sub-block matricial notation that we will need in the following section. Matrix operators will be shown in boldface. We first define the normalized atomic orbital vector $|\mathbf{n}_q\rangle$ as

$$|\mathbf{n}_q\rangle = \frac{1}{\sqrt{q}} \begin{pmatrix} |n, \lambda_1\rangle \\ \vdots \\ |n, \lambda_q\rangle \end{pmatrix}, \tag{3.12}$$

where q denotes the range of the atomic orbital space ($q = 9$ for full s-p-d bands).

Next, we define the following $q \times q$ matrices

$$[\boldsymbol{\beta}(\mathbf{R}_{n,m})]_{ij} = \beta_{nm}^{\lambda_i \lambda_j} \tag{3.13}$$

$$[\boldsymbol{\epsilon}(\mathbf{R}_n)]_{ij} = \epsilon_n^{\lambda_i}\ \delta_{\lambda_i,\lambda_j} \tag{3.14}$$

with $\mathbf{R}_{n,m} = \mathbf{R}_n - \mathbf{R}_m$. Finally, we can express the Hamiltonian operator as

$$\mathbf{H} = \left(\begin{array}{c|c|c} \mathbf{H}(\mathbf{R}_{1,1}) & \mathbf{H}(\mathbf{R}_{1,2}) & \cdots \\ \hline \mathbf{H}(\mathbf{R}_{2,1}) & \mathbf{H}(\mathbf{R}_{2,2}) & \cdots \\ \hline \vdots & \vdots & \ddots \end{array}\right), \tag{3.15}$$

where the $q \times q$ matrix sub-blocks $\mathbf{H}(\mathbf{R}_{n,m})$ are defined as

$$\mathbf{H}(\mathbf{R}_{n,m}) = \boldsymbol{\epsilon}(\mathbf{R}_n)\ \delta_{n,m}\ +\ \boldsymbol{\beta}(\mathbf{R}_{n,m}). \tag{3.16}$$

Transition metals (TM), metals with partially filled d and f shells, comprise most of the elements in the periodic table. Here, we are mainly concerned with $3d$ or $4d$ TM elements. They present fairly localized d states and also wider sp states. It will be necessary then to consider all possible types of bonding between orbitals with symmetry s, p and d. We recall that there are one s, three p, and five d-type orbitals. For instance, if we consider two neighboring atoms and the five d-states, we will find that there are just three types of bonds that may be formed which preserve the angular momentum along the bond axis. These are the fundamental integrals $dd\sigma(m = 0)$, $dd\pi(m = 1)$ and $dd\delta(m = 2)$. Likewise, we can study the possible integrals involving s and p orbitals. Figure 3-1 shows the results. In the crystal, we have to consider the angular variation of the hopping integrals between all combinations of s, p and d orbitals. The β's will result in linear combinations of the fundamental integrals for a fixed orientation of the crystal. These fundamental integrals are known as Slater-Koster (SK) parameters. The linear combinations, which are basically angular dependencies, were tabulated by Slater and Koster as a function of a set of direction cosines (l, m, n) [16].

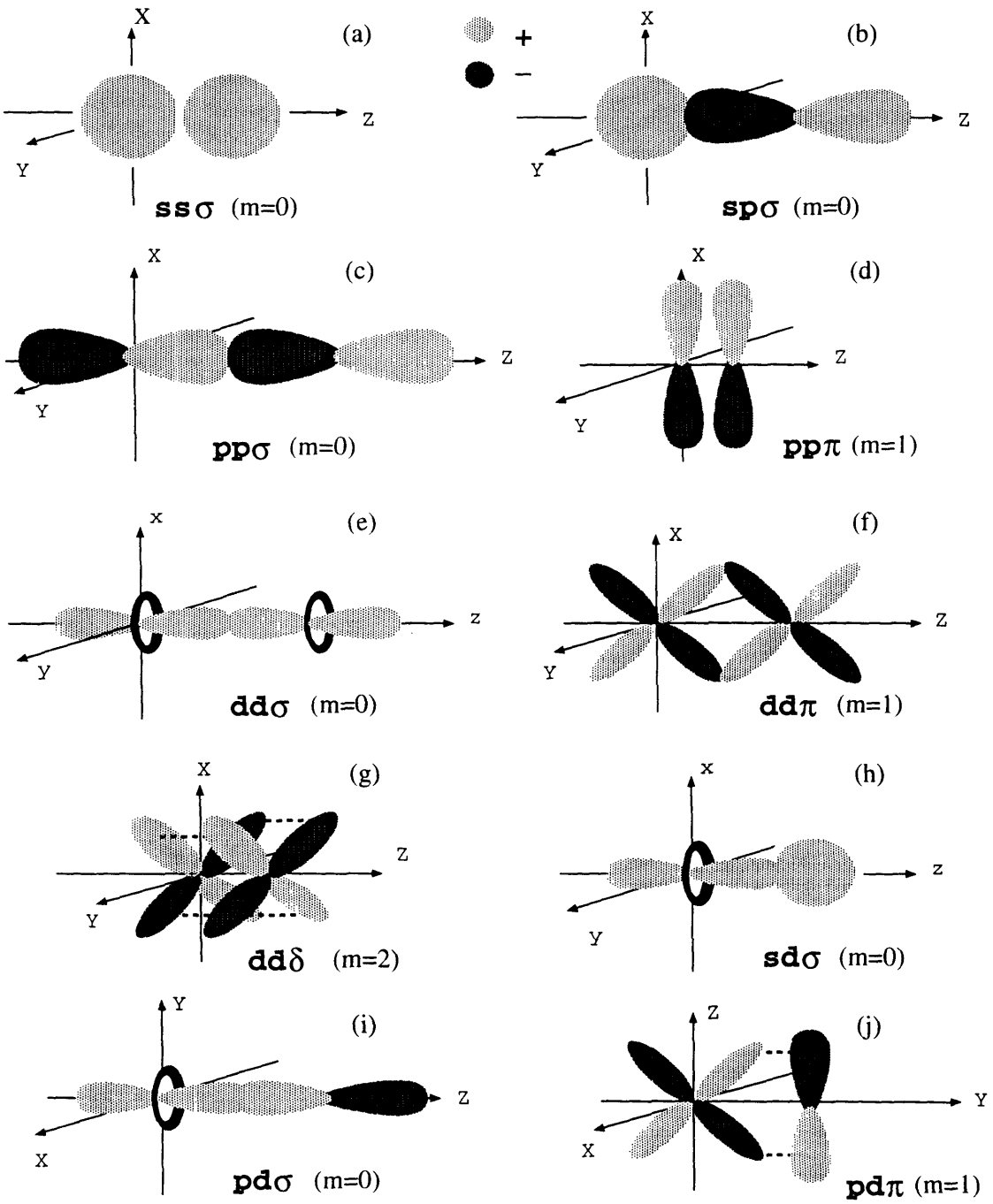

Figure 3-1: Schematic representation of the fundamental transfer integrals or Slater-Koster parameters. These integrals are formed between two atomic states with the same angular momentum component along the bond axis ($\hat{z}$ in this case).

Before continuing with the applications, we shall state the main approximations of the TB model:

- the effects of exchange and correlation between the electrons are neglected (these are fully incorporated in the *ab initio* methods);
- we assume that the basis of atomic wave functions is complete and orthogonal;
- we neglect the three-center integral contributions to the hopping integrals;
- the model ignores the spin-orbit coupling, which would require an additional term in the Hamiltonian proportional to $\tilde{L}\cdot\tilde{S}$, where $\tilde{L}$ and $\tilde{S}$ are the orbital and spin momentum operators, respectively. It can be shown that only intra-atomic spin-orbit couplings are important and that only the *width* of the (d) band is affected, not the energy levels. Even then, the effect is very small [3].

The validity or reasonableness of these assumptions may be justified with the analysis of the results.

The success of the TB approximation depends on the judicious choice or computation of Hamiltonian matrix elements (or parameters). Different approaches for determining these elements can be found in the literature. For a qualitative study of cohesive or structural trends in TM and alloys, "canonical" parameters give very reasonable results, and they will be used in the next section when the first TB application is discussed. On the other hand, the most common approach for quantitative studies is to assume that these matrix elements extend only to first or second neighbors, and treat them as disposable parameters by fitting them to more accurate band-structure calculations, such as the linearized augmented-plane-wave (LAPW) method [13]. Finally, in the scheme we will describe in the next chapter for the study of multi-component alloys, TB parameters are obtained from the linear muffin-tin orbital (LMTO) tight-binding method of Anderson [14]. This scheme has no adjustable parameters or functions to be fitted to experiments. Because of this, we may consider our results to be "first-principles."

3.3 Moment Analysis

3.3.1 Background

An important theorem derived by Cyrot-Lackmann [17] relates the moments of the local density of states to the topology of the local atomic environment. We define the pth moment of the local DOS as (we will consider systems with all sites being equivalent for simplicity)

$$\mu_p = \int_{-\infty}^{\infty} \mathrm{d}E\,(E - \bar{E})^p\, n(E), \tag{3.17}$$

with $\bar{E} = \int_{-\infty}^{\infty} \mathrm{d}E\, E\, n(E)$. The physical meaning of the first moments is straightforward. The moment of order zero gives the total number of states,

$$\mu_0 = \int \mathrm{d}E\, n(E) = q, \tag{3.18}$$

while the first moment is the center of gravity of the band. For a non-degenerate band this is equal to zero:

$$\begin{aligned} \mu_1 &= \int \mathrm{d}E\,(E - \epsilon_\lambda)\, n_\lambda(E) \\ &= \int \mathrm{d}E\,(E - \epsilon_\lambda)\, \delta(E - \epsilon_\lambda) \\ &= 0. \end{aligned} \tag{3.19}$$

The second moment, μ_2, is the moment of inertia of the DOS relative to the center of gravity. The square root of μ_2 is a measure of the width of the local DOS. The third moment, μ_3, measures the skewness or asymmetry of the DOS. A large negative value of μ_3 corresponds to a long tail in the DOS below, and a more compressed peak above, the center of gravity. The fourth moment, μ_4, measures the tendency for gap formation in the middle of the band. A precise criterion for discriminating between

unimodal or bimodal tendencies is given by the dimensionless parameter s [18]:

$$s = \frac{\mu_4 \mu_2 - (\mu_2)^3 - (\mu_3)^2}{(\mu_2)^3}. \tag{3.20}$$

If $s < 1$ the DOS tends to show bimodal behavior, otherwise it will tend to be unimodal.

Using Eq. 2.8 in Eq. 3.17 we obtain

$$\mu_p = \int \mathrm{d}E\,(E - \bar{E})^p \,\mathrm{Tr}\,\delta(E - H) = \mathrm{Tr}\,\mathbf{H}^p. \tag{3.21}$$

Applying the matrix operators, we can express the moment in the basis of atomic orbitals vectors. using the fact that $\sum_n |\mathbf{n}\rangle\langle\mathbf{n}| = \mathbf{I}$, where $\mathbf{I}$ is the $(q \times q)$ identity matrix (where we have dropped the q subscript in Eq. 3.12):

$$\begin{aligned}
\mathrm{Tr}\,\mathbf{H}^p &= \sum_n \mathrm{Tr}\,\langle\mathbf{n}|\,\mathbf{H}^p\,|\mathbf{n}\rangle & (3.22)\\
&= \sum_{n,m_1,\ldots,m_{p-1}} \mathrm{Tr}\,\langle\mathbf{n}|\,\mathbf{H}\,|\mathbf{m}_1\rangle\langle\mathbf{m}_1|\,\mathbf{H}\,|\mathbf{m}_2\rangle\cdots\langle\mathbf{m}_{p-1}|\,\mathbf{H}\,|\mathbf{n}\rangle & (3.23)\\
&= \sum_{n,m_1,\ldots,m_{p-1}} \mathrm{Tr}\,\underbrace{\mathbf{H}(\mathbf{R}_{n,m_1})\,\mathbf{H}(\mathbf{R}_{m_1,m_2})\cdots\mathbf{H}(\mathbf{R}_{m_{p-1},n})}_{p\ factors}. & (3.24)
\end{aligned}$$

For non-degenerate bands the expression above reduces to a product of transfer integrals $\langle n,\lambda|H|m,\gamma\rangle$ that can be seen to represent the hopping of electrons from an orbital λ centered on site n to an orbital γ centered on site m. Depending on whether the matrix element is site-diagonal or off-diagonal, these correspond to on-site and near-neighbor jumps. Figure 3-2 shows an example of four-hop circuits in an square lattice with first-nearest neighbor hopping integrals only. If we assume that the atomic energy levels are zero and neglect the crystal-field integrals (i.e. $\epsilon_n^\lambda = 0$) then

$$\mu_p = \sum \beta_{nm}^{\lambda\beta}\beta_{ml}^{\beta\gamma}\cdots. \tag{3.25}$$

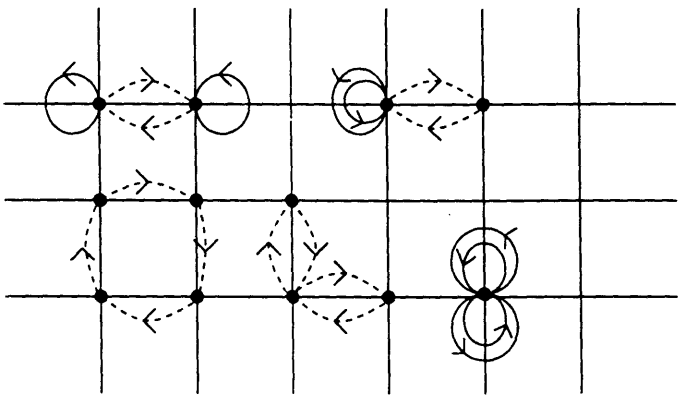

Figure 3-2: Example of four-jump paths in an square lattice with first nearest neighbor only. Solid lines refer to paths associated with on-site jumps, whereas paths associated with broken lines correspond to self-avoiding paths.

And in the case of the second moment

$$\mu_2 = \sum_{n,m} \sum_{\lambda,\mu} \beta_{nm}^{\lambda\mu} \beta_{mn}^{\mu\lambda}. \tag{3.26}$$

Each term in the previous equation represents an electron starting at site n, hopping on a neighboring site m and hopping back to n. Then the second moment is the sum of all such paths of two hops. This is easily generalized to higher-order moments.

Finally, we can state the moments theorem: the n'th moment of the local density of states is the sum over all paths of n hops that start and end at a particular lattice site. This is an important result because it tells us that by studying the local environment surrounding an atom we can make qualitative comments about the density of states, even if we do not know its precise form, through the calculations of its first few moments. For degenerate bands, we associate a matrix with each jump and then evaluate the trace of the product associated with each circuit (see Eq. 3.24). The contribution of a circuit is independent of the direction in which the path is described, of the position of the origin in the circuit, and of its orientation in the lattice since the trace of $\mathbf{H}^p$ is rotationally invariant and basis independent.

We will now show how the knowledge of the local environment through the moment analysis can help us understand the stability properties of some simple crystal

structures. To this end we used a canonical model that has been successfully applied to study the qualitative trends along the d-transition metals series [19]. In this model, only the (five) d-atomic orbitals are included in the orbital basis and crystalline-field integrals are neglected. The hopping integrals are then a linear combination of the fundamental SK parameters: $dd\sigma$, $dd\pi$, and $dd\delta$. Taking into account the symmetry of the d-orbitals, we can orient the $\hat{z}$ axis along the vector connecting sites i and j, $\mathbf{R}_{ij} = \mathbf{R}_i$-$\mathbf{R}_j$. In this case the matrix $\boldsymbol{\beta}$ (Eq. 3.13) is diagonal and given by:

$$\boldsymbol{\beta} = \begin{pmatrix} \mathrm{dd}\delta & & & & \\ & \mathrm{dd}\pi & & 0 & \\ & & \mathrm{dd}\pi & & \\ & 0 & & \mathrm{dd}\delta & \\ & & & & \mathrm{dd}\sigma \end{pmatrix} \tag{3.27}$$

for a given distance $|\mathbf{R}_{ij}|$. The order of atomic orbitals in the basis is $\{xy, yz, xz, x^2 - y^2, 3z^2 - r^2\}$. The moments μ_p can then be computed as

$$\mu_p = \sum_{n,m_1,\ldots,m_{p-1}} \mathrm{Tr}\, \boldsymbol{\beta}(\mathbf{R}_{n,m_1})\boldsymbol{\beta}(\mathbf{R}_{m_1,m_2}) \cdots \boldsymbol{\beta}(\mathbf{R}_{m_{p-1},n}). \tag{3.28}$$

Unfortunately, in a given structure, only one matrix $\boldsymbol{\beta}(\mathbf{R})$ will be diagonal along a particular vector $\mathbf{R}$. Using a rotation matrix, we can express the hopping integral matrix for any other step as [19]

$$\boldsymbol{\beta}(\mathbf{R}) = \mathbf{U}_\theta \, \boldsymbol{\beta}(\mathbf{R}_{i,j}) \, \mathbf{U}_\theta^{-1}, \tag{3.29}$$

where $\mathbf{U}_\theta$ is the (unitary) rotation matrix that corresponds to the real-space rotation of $\mathbf{R}_{i,j}$ onto $\mathbf{R}$.

The last point to consider is the explicit dependence of the transfer integrals on distance. Exponential and power laws have been considered in the literature. We are

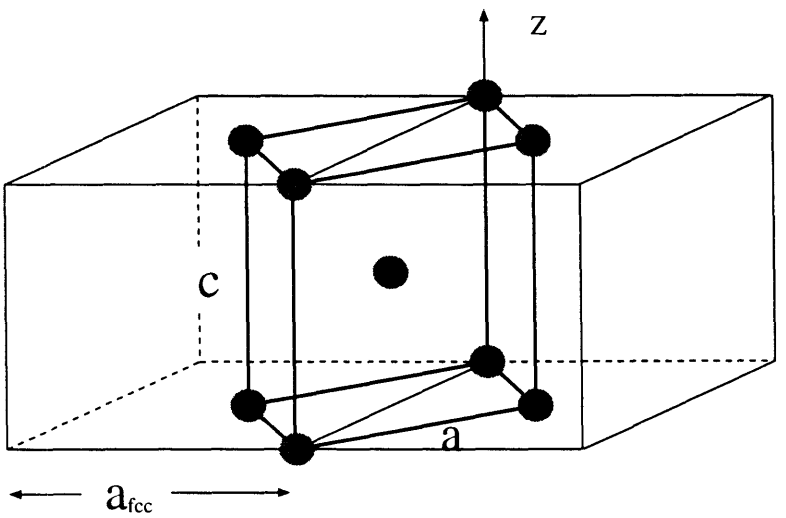

Figure 3-3: Structural representation of the fcc-bct transformation.

going to use the latter in the form

$$\beta(r) = \beta_o(\frac{r}{r_o})^5, \tag{3.30}$$

where β_o is the hopping integral between nearest neighbors in a reference lattice and r=$|\mathbf{R}_{i,j}|$. It has been shown [20] that the hopping integrals satisfy the following relationships: $|dd\sigma| > |dd\pi| >> |dd\delta|$ and $1.7 < |dd\sigma|/dd\pi < 2.5$, while $dd\sigma/dd\delta > 10$. We have used the following values of the parameters: $dd\pi/dd\sigma = -0.5$ and $dd\delta = 0$ for the hopping integrals between first-nearest neighbors in the fcc lattice taken as the reference lattice.

The following section applies the moment analysis model described above to the study of the relative stability of the phases related to the Bain transformation.

3.3.2 Application to the Bain transformation

We applied the TB moment analysis to study the tetragonal or Bain transformation that takes an fcc into a bcc structure, commonly found in relation to martensitic transformations. Figure 3-3 shows the geometric relations for this transforma-

tion. The cell outlined in the figure is a body-centered tetragonal cell (bct). The bct cell dimensions are described by two lattice constants, $a(=b)$ and c. Taking the fcc lattice as the reference lattice, it can be shown that $c = (1-v)a_{fcc}$ and $a = b = (1+u)\,(\sqrt{2}/2)\,a_{fcc}$ where a_{fcc} is the lattice constant of the fcc lattice and u and v represent the expansion normal and parallel to the $\hat{z}$ axis, respectively. If we assume that the transformation occurs at constant atomic volume then $\mathrm{Vol_{fcc}}/4 = \mathrm{Vol_{bct}}/2$ because there are four atoms per unit cell in the fcc lattice but only two in the bct lattice. Then, replacing the values of a and c in the latter expression we obtain $(1-v)(1+u)^3 = 1$. This shows that u and v are not independent and we can then characterize the tetragonal distortion of the lattice with a single parameter, for instance:

$$\frac{c}{a} = (1-v)^{3/2}\sqrt{2} \tag{3.31}$$

or alternatively,

$$\alpha = 1 - \frac{c/a - 1}{\sqrt{2}-1}, \tag{3.32}$$

where c/a takes values 1 ($\sqrt{2}$) for an ideal bcc (fcc) lattice while α varies from 0 (fcc) to 1 (bcc). Figure 3-4 shows the nearest-neighbor vectors in the bct lattice and the distribution of neighbors with distance as a function of α.

It has been shown that the second-moment approximation to the cohesive energy cannot discriminate between energies of different structures along the Bain transformation (at least in the first nearest-neighbor approximation) [18]. We must then study higher-order moments to explain the relative stability between the different structures. Using Eq. 3.28, we have computed the first five moments of the DOS versus the tetragonality parameter α.

As expected, we find that the second moment remains nearly constant along the transformation (from $\mu_2 = 14.475$ in the fcc lattice to $\mu_2 = 15.01$ in the bcc one). Figure 3-5 shows the third, fourth and fifth moments. All moments are normalized with respect to $\mu_2^{n/2}$ where n is the order of the moment. Notice that μ_3 and μ_4 remain practically constant, and only the fifth moment, μ_5, shows a significant variation, with α. This important result tells us that any model set up to study structural energy

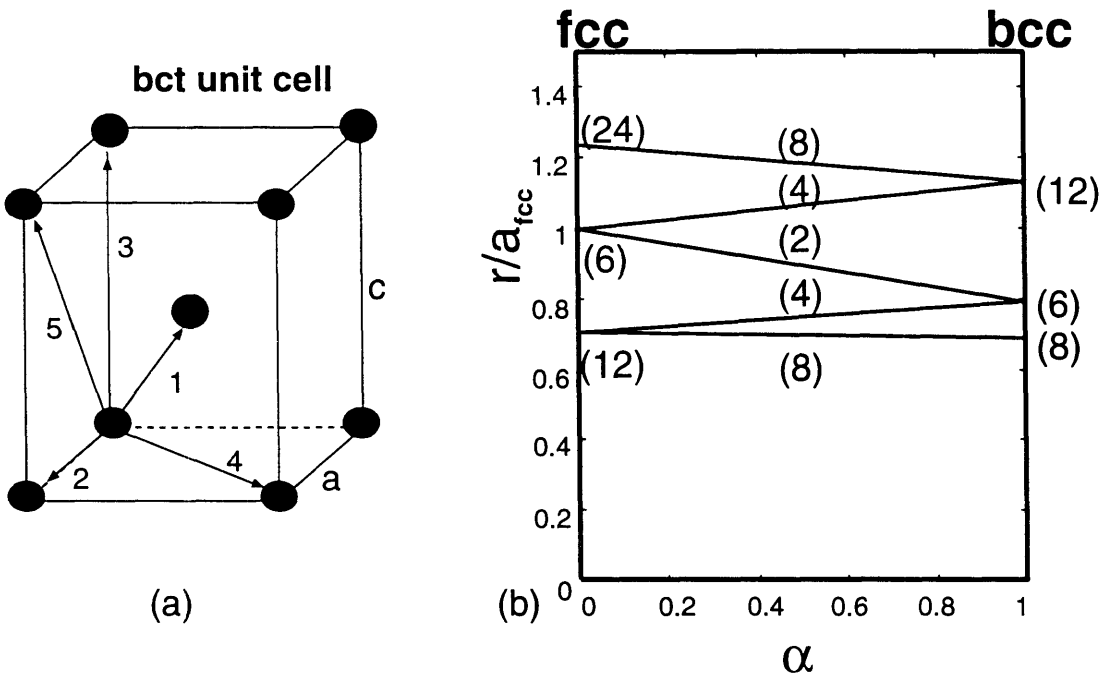

Figure 3-4: (a) Unit cell of the bct cell displaying the first five nearest-neighbor vectors. (b) Distribution with distance (in units of the first nearest-neighbor distance in the fcc lattice) of neighbors as a function of the tetragonality parameter α (the number of bonds at a given distance is indicated in parentheses). Adapted from [21].

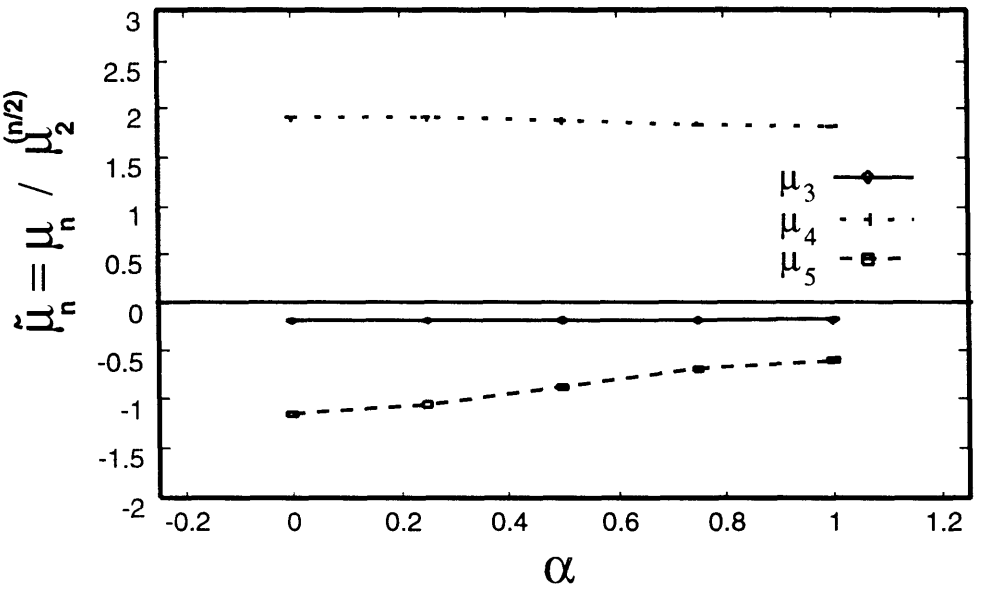

Figure 3-5: First moments of the density of states as a function of the tetragonality parameter α. All moments are normalized with respect to $\mu_2^{n/2}$, where n is the order of the moment.

differences between these phases must include at minimum the first five moments in the description of the DOS.

The DOS for three values of α are shown if Fig. 3-6. As expected from the values of the second moment, all the DOS display nearly the same width. Notice also in the same figure the bimodal behavior as predicted by the parameter s defined in Eq. 3.20, which is less than 1 in all cases ($s = 0.8718$ for $\alpha = 0.0$, $s = 0.8479$ for $\alpha = 0.5$, and $s = 0.7989$ for $\alpha = 1.0$).

Figure 3-7 shows the energy difference between the fcc and bcc structures versus the filling of the band, N, calculated within the TB model. Notice that the curve crosses the horizontal axis three times. This agrees with the prediction by a theorem of Ducastelle and Cyrot-Lackmann [20]: if the first n+1 moments of the DOS of two structures are the same, i.e. $\delta\mu_0 = 0, \cdots, \delta\mu_n = 0$, then the function δE_b(N), the difference of band energies vs. number of electrons, has at least n extremes, and therefore at least (n-1) zeros, beyond those corresponding to an empty or a filled band. This result confirms the need to study the fifth moment to establish the

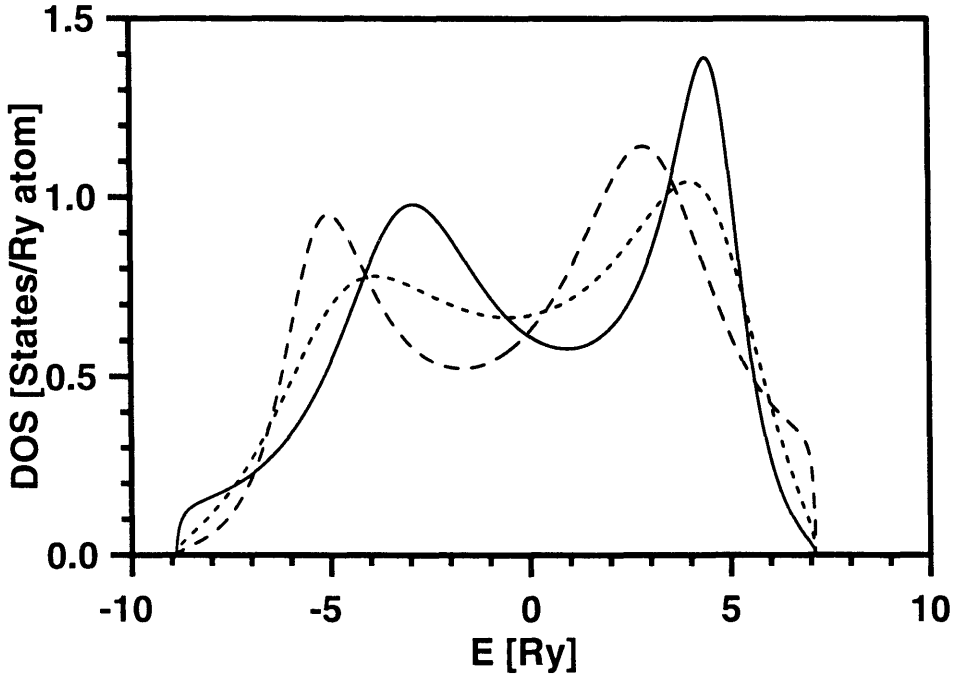

Figure 3-6: Density of states for three values of α: solid line, $\alpha = 0.0$ (fcc); short-dash line, $\alpha = 0.5$ (bct); dashed line, $\alpha = 1.0$ (bcc).

possible relationship between the local environment and the relative stability of the structures.

We should notice that the DOS's (and thus energies) for the different structures were computed with the recursion method (see the Appendix for a brief description of this technique). The coefficients a_i and b_i of the continued fraction (Eq. A.2) are intimately related to the moments of the density of states μ_p. This relation can be put in analytical form [19]. For the first moments we have

$$\begin{aligned} \mu_0 &= 1 \\ \mu_1 &= a_1 \\ \mu_2 &= a_1^2 + b_1^2 \\ \mu_3 &= a_1^3 + 2a_1 b_1^2 + a_2 b_1^2 \\ &\vdots \end{aligned} \tag{3.33}$$

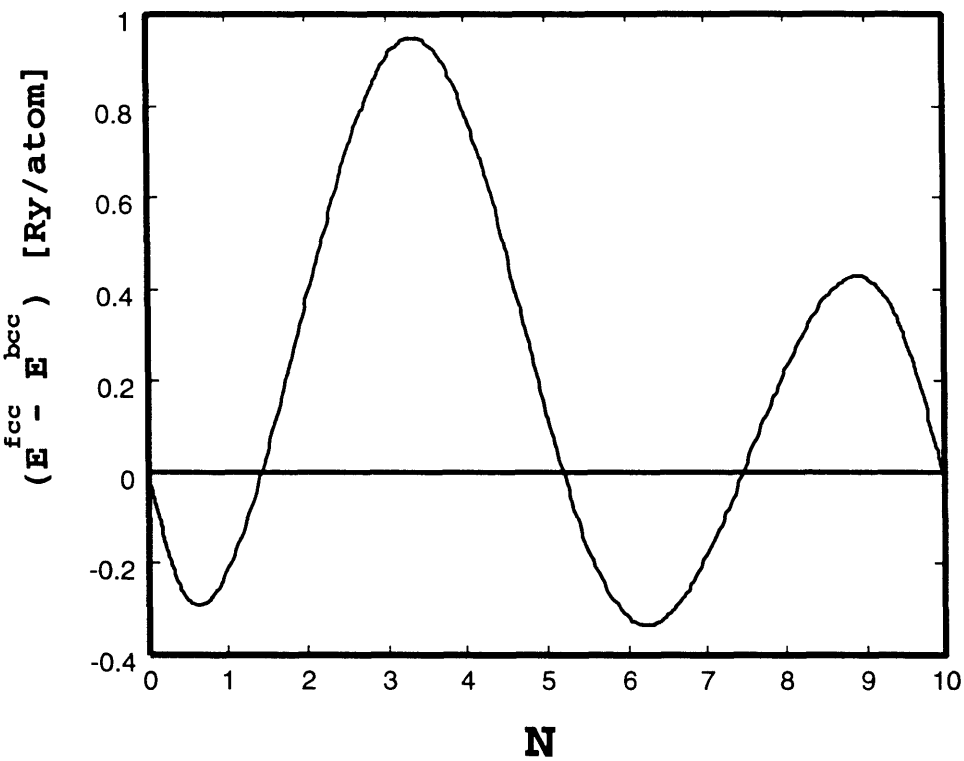

Figure 3-7: Variation of the band energy difference between the fcc and bcc phases as a function of the average band filling N ($0 < \mathrm{N} < q = 10$).

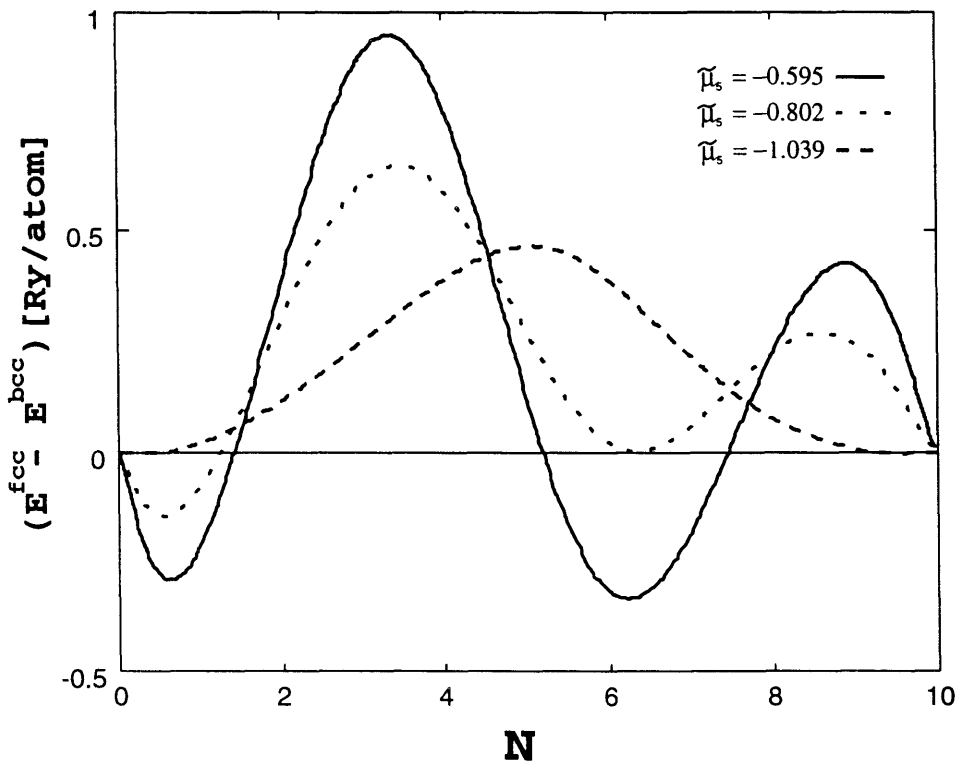

Figure 3-8: Difference of band energies between the fcc and bct structures with different values of $\tilde{\mu}_5$.

In general, the knowledge of n levels of the continued fraction implies we can obtain $2n + 1$ exact moments of the DOS (and vice versa).

Going back to Fig. 3-5, we can see that $|\mu_5|$ decreases along the transformation path from the fcc to the bcc lattice. This leads to the relative stability of the fcc and bcc (bct) phases as shown in Fig. 3-7. The effect of the fifth moment on this stability curve is shown in Fig. 3-8, where $\delta E_{fcc-bcc} = E^{fcc} - E^{bcc}$ is plotted for different values of $\tilde{\mu}_5$ (at constant normalized values for $\tilde{\mu}_3$ and $\tilde{\mu}_4$). When $\tilde{\mu}_5$ approaches the value of $\tilde{\mu}_5^{bcc} (\approx -1.039)$, it reduces to the second-moment approximation and the bcc structure is more stable for all values of band filling (if $\delta E_{X-Y} < 0$ then X is more stable than Y).

Including first and second nearest neighbor jumps, one can identify 14 different circuits that contribute to μ_5 in the bcc lattice. As the lattice distorts into a bct lattice, these paths split to a total of 34 non-equivalent circuits. At the other end,

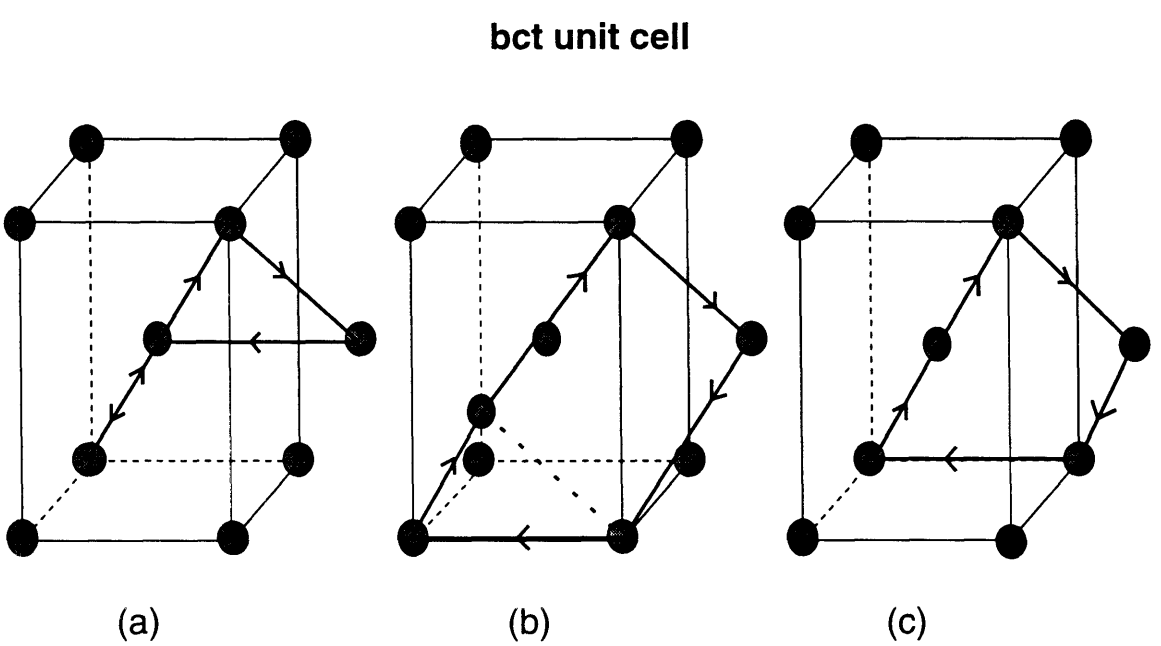

Figure 3-9: Geometric description of the most important five-jump circuits that contribute to the fifth moment. (a) and (c) are planar circuits, (b) has an out-of-plane component.

there are 24 different paths in the fcc lattice. It is possible to follow the transformation of each path as a function of the distortion of the lattice and compute the individual contributions to the fifth moment, including not only the contribution of a single circuit but the degeneracy of the circuit (i.e., the number of equivalent paths per unit cell), as well. The contribution of each path can be factorized into a radial term and an angular term, $\mu_5 = (1/5)\,\mu_5^{rad}\mu_5^{ang}$. The angular term turns out to be the most important factor. (Not all the paths follow this trend.) We have identified three particular self-avoiding paths that make up the largest contribution to the relative change in the fifth moment from the fcc to the bcc structures. These paths are shown in Fig. 3-9. Figure 3-10 shows the total contribution of these three circuits (including their degeneracy) compared to the total μ_5 (with $\tilde{\mu}_5(\alpha = 0)$ as the bottom value, i.e., $\tilde{\mu}_5^{new} = \tilde{\mu}_5(\alpha = 0) + \Delta\tilde{\mu}_5(\text{contrib. of paths in Fig 3-9}))$.

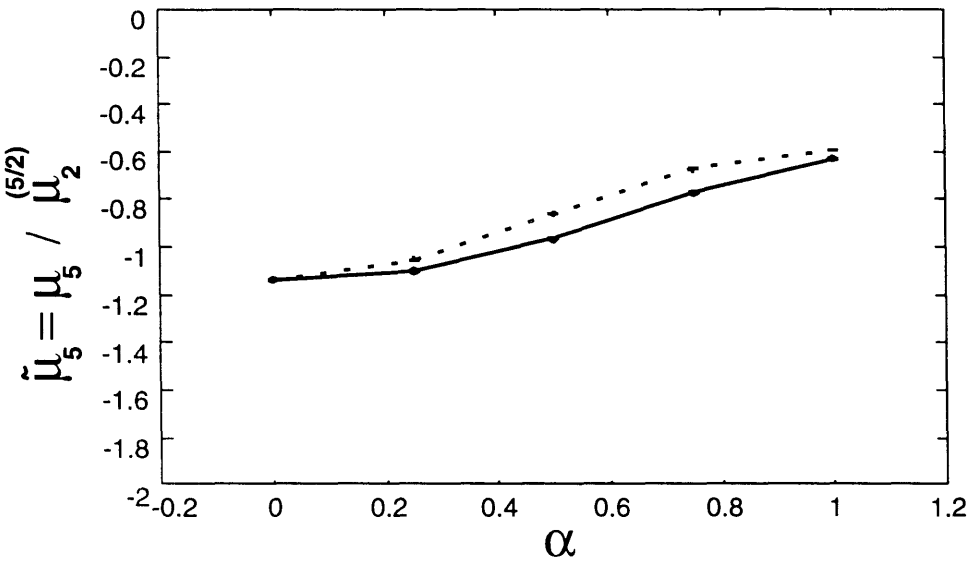

Figure 3-10: Normalized fifth moment of the density of states as a function of the tetragonality parameter α. The solid line represents the total moment. The dashed line is the contribution from the paths shown in Fig. 3-9. See text.

3.3.3 Conclusions

The relative structural stability for the Bain transformation has been interpreted in terms of the topology of the local atomic environment through the behavior of the first few moments of the electronic density of states. The moment analysis was based in a simple "canonical" TB model of *d*-bonded systems. The normalized fifth moment was found to be the important requirement to explain the structural energy difference. The main contributing paths to the fifth moment have been described. The identification of similar paths in more complex structures might help to determine and understand the relative stability of those structures in relation to the simpler phases.

3.4 Total-Energy Model

3.4.1 Introduction

One potential application of the tight-binding model is in realistic simulations such as molecular dynamics (MD) and Monte Carlo, methods that have rapidly developed in the past few years. The application of these methods is limited by our knowledge of the interaction potentials or forces among the atoms. To be useful, the working models should be computationally efficient in order to allow treating a large number of atoms while providing a reliable representation of the structural and energetic properties of the systems under study. Methods such as the Car-Parrinello [5] scheme can treat the interatomic interactions accurately in the framework of *ab initio* density-functional theory within the local-density approximation. However, to perform realistic simulations involving a large number of atoms this scheme has been rather limited by the large computational effort which is required. More recently, MD simulations based on TB [6] and the embedded atom method (EAM) [22] approaches have been emerging as powerful methods for studying various structural, dynamic, and electronic properties in systems with localized electrons like transition metals and their alloys, or in covalent systems (such as Si or C).

Most of the current TB and EAM MD models express the band energy using a second-moment approximation. This approximation gives a poor description of the DOS. As we have shown in the previous section, a good description of the DOS for transition metals and alloys is important in determining the relative energies of the crystal structures. Even the inclusion of fourth-moment terms does not substantially improve the description of properties of the bulk bcc TM [23], and we have to go beyond this approximation. Another drawback of the current TB and EAM methods is that, although they use a small basis set for the electronic calculation, solving the electronic structure at every MD step is still computational demanding if the number of atoms, N, in the simulation is large. If one uses a matrix diagonalization procedure, the cpu time scales as N^3 [6]. The model we propose here is based in the recursion technique, briefly mentioned in the previous section (see also the Appendix).

This method does not require the diagonalization of the Hamiltonian, and it allows us to make successive approximations, beyond the second (and fourth) moment, as required by the level of accuracy sought in the simulation. The advantage of this approach is that quantities such as inter-atomic forces between two atoms will be mostly determined by the disposition of the atoms in the neighborhood of where the force is acting.

3.4.2 Model

Up to this point, we have only discussed the band energy of the system. This is basically an attractive (negative) contribution to the total energy. Obviously, some other forces stabilize the system, preventing the atoms from collapsing into each other. In TB models, this balancing energy is usually represented by a sum of short-range repulsive pair potentials. Thus, the cohesive energy of the system per atom is given as the sum of two contributions,

$$E_{coh} = E_{Band} + E_{Rep}, \tag{3.34}$$

where E_{Band} is the one-electron band energy calculated for a parametrized tight-binding (TB) Hamiltonian, and E_{Rep} is a short-range repulsive energy that ensures crystal stability. The TB Hamiltonian takes the usual form given by Eq. 3.11. The validity of mapping the total energy obtained in the self-consistent DFT onto the non-self-consistent TB energy expression, Eq. 3.34, has been proved by Foulkes and Haydock [24] using a variational principle.

The TB parameters are required to be both transferable and suitable to use in extensive Monte Carlo or molecular-dynamics simulations. They are typically extracted from (or fitted to) *ab initio* band structure calculations.

The repulsive term is usually expressed as a sum of two-center potentials,

$$E_{Rep} = \sum_{i<j} \Phi(r_{ij}), \tag{3.35}$$

Table 3.1: TB Parameters used in the present calculation.

$dd\sigma$ (Ry)	$dd\pi$ (Ry)	$dd\delta$ (Ry)	Q
-0.08594	0.06444	-0.02402	3.57

where r_{ij} is the distance between atoms i and j, with $r_{ij} < r_c$ and where r_c is a cut-off radius.

In this thesis, the repulsive term is modeled via a Born-Mayer (BM) type potential,

$$\Phi(r_{ij}) = Ae^{-p\, r_{ij}/r_o}, \tag{3.36}$$

where A and p are obtained by fitting the bulk modulus and the equilibrium lattice constant, and r_o is a reference distance.

3.4.3 Computation and Results

We illustrate our techniques with molybdenum using the TB parameters suggested in the work of Masuda *et al.* [25] which were extracted from d-band self-consistent LMTO calculations. The variation of the hopping integrals with distance is given by the following power-law equation

$$\beta(r) = \beta(r_o)\, (\frac{r_o}{r})^Q, \tag{3.37}$$

where r_o is the first nearest-neighbor distance in the bcc Mo lattice. The calculation is restricted to d-orbitals, and the hopping integrals extend up to the second nearest-neighbor shell. The parameters are given in Table 3.1.

A recursion calculation was performed to compute eleven levels (i.e., 22 exact moments of the density of states) for the continued fraction expansion of the Green's function which describes the electronic properties of the bcc, fcc, and $A15$ crystalline structures. For this maximum number of levels of continued fraction, the band energies converge within 0.1 mRy; these will be taken as reference energies to which the results of further approximations will be compared.

The recursion method is a relatively fast technique but still not computational

Table 3.2: Computed energies as defined in Eq. 3.34 for the three different structures, and repulsive potential parameters.

		Approximation	
Struc.	(Energy in Ry)	up to μ_6	up to μ_{22}
bcc	E_{band}	-0.8256	-0.8300
	E_{rep}	0.2938	0.2962
	E_{coh}	-0.5318	-0.5338
fcc	E_{band}	-0.7866	-0.7916
	E_{rep}	0.2877	0.2901
	E_{coh}	-0.4985	-0.5015
A15	E_{band}	-0.8252	-0.8363
	E_{rep}	0.3129	0.3153
	E_{coh}	-0.5123	-0.5210
E_{rep}	A (Ry/at.)	0.03155	0.03178
param.	p	9.8159	9.7886

convenient to use in MD simulations. Keeping in mind that we want a reliable but computationally tractable method for obtaining the energetics of the system, we need to resort to some simplifications. The first step was to determine the minimum number of levels of continued fraction necessary to obtain reliable results. We found that three levels, or which is equivalent, a sixth-moment approximation, were necessary for a reasonable description of the energetics of the system.

The results for the three structures are shown in Table 3.2. The two parameters of the repulsive term were obtained by fitting the calculated equilibrium lattice parameter and bulk modulus (of the bcc structure) to the experimental values given for Mo ($B = 1.80$ Ry atom^{-1}). We can see that the error in the approximation is about 10 mRy or less which is within the accuracy usually attributed to the experimental determination of the elastic constants. The two parameters used in this repulsive contribution are shown in the last row of Table 3.2.

Although coefficients for a three-level continued fraction can be obtained in fractions of a second in CPU time, the bottle-neck in the computation of the total energy is the actual energy integral for the band energy (i.e., Eq. 2.20). Trying to overcome this obstacle, we study the suitability of the linearized Green's function method (LGM). In the LGM (see [19, 26] for extensive studies of the method) the band en-

ergy differences are expanded as a sum of "universal" functions which are defined for a convenient reference medium, multiplied by fluctuations of continued fraction coefficients (which in turn are related to the difference between the moments of the density of states),

$$\Delta E_{X-Y}^{(p,q)} = \sum_{n=1}^{p} \phi_n \, \delta a_n + 2 \sum_{m=1}^{q} \psi_m \, \delta b_m, \tag{3.38}$$

where ϕ_n and ψ_n refer to "universal" functions, and a_i and b_i are the coefficients of the continued fraction. The quantities ϕ_n and ψ_n are calculated from the Green's function elements G_{1n} which characterize the reference medium. The actual expressions for these integrated quantities are

$$\phi_n(E) = -\frac{\mathrm{Im}}{\pi} \lim_{\eta \to 0} \int_{-\infty}^{E} dt \, (t - E) \, G_{1n}^2(t + i\,\eta) \tag{3.39}$$

and

$$\psi_n(E) = -\frac{\mathrm{Im}}{\pi} \lim_{\eta \to 0} \int_{-\infty}^{E} dt \, (t - E) \, G_{1n}(t + i\,\eta) \, G_{1n+1}(t + i\,\eta). \tag{3.40}$$

Ideally, the reference medium would be a topologically disordered medium (an amorphous state). In the present case, since ϕ_n and ψ_n are not so sensitive to the details of the average medium DOS, we define its coefficients (a_n, b_n) as those of the bcc structure (another possibility is to define a reference medium through coefficients computed as average of the coefficients for the three structures fcc, bcc and $A15$). To be consistent with the previous approximation we consider $E_{X-Y}^{(3,3)}$ (see Eq. 3.38). Figure 3-11 shows the "exact" and the LGM approximation for the band energy differences between the A15 and bcc structures as a function of the d-band filling. The LGM curve follows the "exact" curve qualitatively with differences of the same magnitude as in Table 3.2.

Figures 3-12 (a) and (b) compare the energy differences between the three structures obtained with the LGM. Notice that, only after including the repulsive contribution does the bcc structure become more stable at the band filling value which corresponds to Mo (i.e., 4.4).

Finally, we present in Table 3.3 the values of the calculated and experimental

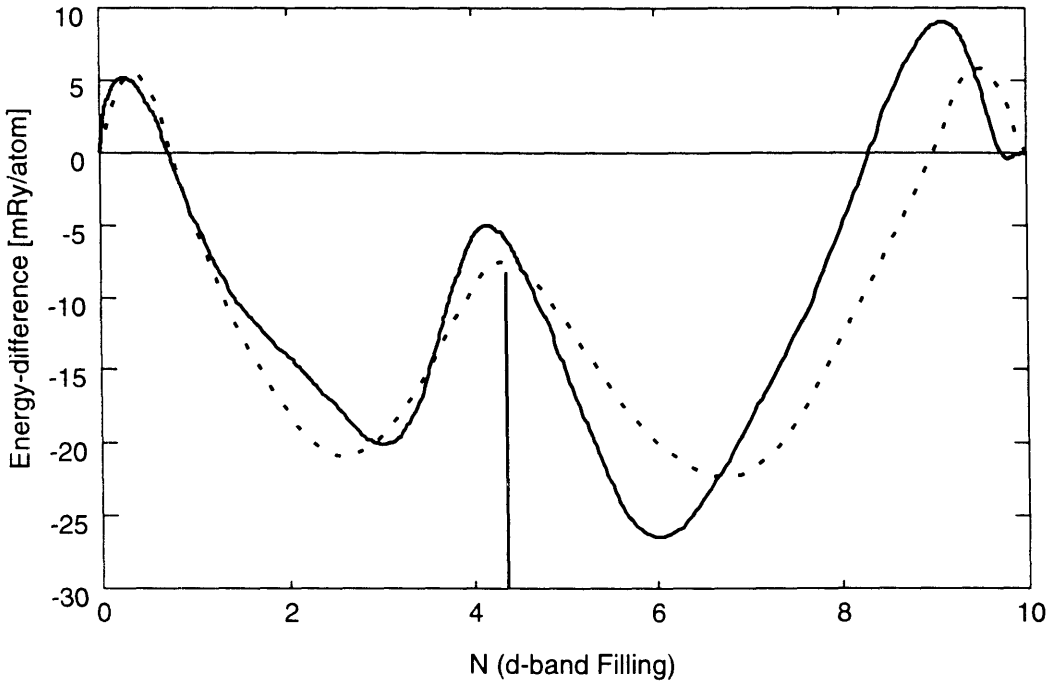

Figure 3-11: Band energy difference between A15 and bcc phases (Mo): full line, "exact"; dotted line, LGM. The vertical line shows the actual d-band filling for Mo (N = 4.4).

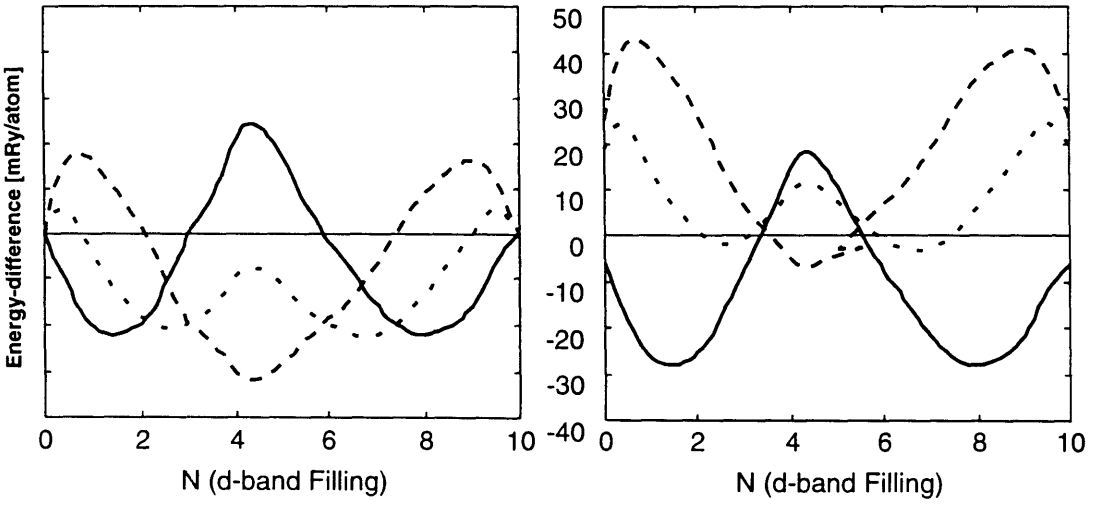

Figure 3-12: Band energy differences: full line, fcc-bcc; dotted line, A15-bcc; dashed line, A15-fcc: (a) band energy only, (b) total energy (band energy plus repulsive contribution). The sign convention is such that $\Delta E^{X-Y} < 0$ implies that X is more stable than Y.

Table 3.3: Shear Elastic Constant C_{44} for bcc-based Mo in Ry atom^{-1} calculated with different approximations. The experimental value is taken from Ref. [27]

	C_{44}			
Approximation	Band contrib.	Rep. contrib.	Total	Exper.
μ_6	-1.5035	1.9948	0.49129	0.782
μ_{22}	-1.4592	1.9958	0.53664	0.782

elastic constant C_{44} for bcc-based Mo. This allows us to check the consistency of the BM potential parameters. In order to compute this quantity we need to express the total energy as a function of the lattice strain. This strain can be chosen so that the energy is an even function of the strain, and at the same time, in the case of cubic phases, so as to preserve the volume of the unit cell [28]. The following (monoclinic) strain tensor was used in the calculation of C_{44},

$$\epsilon = \begin{pmatrix} 0 & \frac{\eta}{2} & 0 \\ \frac{\eta}{2} & 0 & 0 \\ 0 & 0 & \frac{\eta^2}{4-\eta^2} \end{pmatrix}. \tag{3.41}$$

With this strain tensor the energy can be written as

$$E(\eta) = E(-\eta) = E(0) + \frac{1}{2} C_{44}\, V\, \eta^2, \tag{3.42}$$

where η represents the strain and V the volume of the unit cell.

We notice that the model underestimates the value of this elastic constant. As shown the Table 3.3, the actual value of C_{44} is obtained as the sum of two large numbers with opposite signs: the band contribution which is negative, and the repulsive contribution which is positive. Both contributions are very sensitive to the approximations and parameters involved in the model. On one hand, the choice of number of d-electrons is somehow arbitrary and a small change of N_d can have a big effect on the the values of the repulsive parameters A and p; on the other hand, we have ignored hybridization which can also be important [25].

In order for this TB-LGM model to be useful in MD simulations, we must be

able to write the formulae for the forces. The "fluctuations" of the continued fraction coefficients in Eq. 3.38, around a convenient initial set, can be written in terms of the variation of the hopping integrals [30], yielding analytical formulae for the forces which would not have to be updated at each simulation step [29]. Since the method does not require the diagonalization of the Hamiltonian, we might expect the scaling of cpu time to be less that N^3, with respect to the number of atoms N. The applicability of the model to MD simulations is being investigated [31].

3.4.4 Conclusion

An application of the Linear Green's Function Method coupled with a Born-Mayer potential was presented to describe relative stability in transition metal systems. The need for a repulsive contribution was demonstrated in order to stabilize the correct bcc ground state crystalline structure of Mo. A sixth-moment approximation of the density of states seems to be sufficient to reproduce the energetics of the "exact" recursion method. This simple approach, that goes beyond the fourth-moment approximation, may be particularly suited for describing the evolution of realistic systems during a molecular dynamics simulation.

3.5 Summary

We have presented in this chapter two applications of the TB method: a study of relative phase stability through the computation of moments of DOS, and a total-energy calculation using the linearized Green's Function method, both showing the versatility and power of the simple TB method. The following chapter describes a TB-based scheme to study the electronic structure of multicomponent alloys.

Chapter 4

Energetics of Alloys

4.1 Introduction

Any theoretical study of ordering and phase stability in substitutional alloys, and ultimately of their phase diagrams, must begin with reliable and accurate expressions for the energy and entropy as a function of alloy composition and temperature. Over the last few years it has been possible to combine "first-principles" electronic structure calculations for alloy energetics with statistical mechanics methods for the entropy. These statistical mechanics methods are based on the so called generalized Ising model within various approximations. They range from the simpler Bragg-Williams (BW) approximation [32] to the more sophisticated cluster-variation method (CVM) (see Chapter 5) and Monte Carlo simulations [10]. In these models it is assumed that the internal energy can be written as a rapidly convergent sum of pair and multisite interactions. Several approaches have been developed to provide the link between the electronic structure calculations and the statistical models, among them the embedded-cluster method (ECM) [33], the generalized perturbation method (GPM) [34], the Connolly-Williams method (CW) [35], and the direct configurational averaging method (DCA) [36].

To date, applications of these electronic structure and statistical mechanics methods have been mostly confined to binary alloys. Ternary and higher-order alloys, by contrast, remain relatively unexplored. The BW method has been used to study or-

dering in bcc ternary alloys [37, 38, 39, 40, 41] with special emphasis on the Heusler structures [42, 43, 44, 45, 46], and in fcc lattices [47]. In these examples, "canonical" EPI's were used to study general trends, or were inferred experimentally for more quantitative studies. Kikuchi *et al.* [48] studied the fcc Cu-Ag-Au phase diagram using the CVM method in the tetrahedron approximation. Colinet *et al.* [49] reported a similar study on phase equilibrium in bcc Fe-Co-Al alloys using the irregular tetrahedron. Examples of Monte Carlo simulations can be found in a review by Inden and Pisch [50], and Traiber [51], who studied phase equilibria in the bcc Ni-Al-Ti alloys. In all cases, concentration-independent interactions estimated from experimental results were used. More recently, the DCA method has been used to compute interactions to study site substitutions in fcc Ni-Al-X alloys [52], and effective interactions and formation energies for fcc-based Rh-V-Ti, Pd-Rh-V and Ag-Pd-Rh alloys [53].

This chapter is focused in one particular alloy theory to study multi-component alloys, the GPM implemented within the TB approximation. In the GPM, a perturbation treatment is derived by choosing a reference medium which is close to any particular configuration of the alloy. Hence, intuitively, the appropriate reference medium to use is the completely disordered state, as the one described by the coherent-potential approximation (CPA, see section 4.3.1) [19, 34]. This TB-CPA-GPM scheme combined with the CVM has been successfully applied to binary alloys. For instance, Sluiter *et al.* used this approach to study phase equilibria in Ti-Rh and Ti-Ir alloys [54] with only *d*-orbitals. Sluiter and Turchi [55] carried out an investigation of phase equilibria in Ti-V and Ti-Cr alloys. Their study accurately reproduces the energetics properties of Ti-V alloys and provides insight into the possible metastables phases in the Ti-Cr system. Colinet and Pasturel [56] presented a phase diagram for Ni-Ti in good agreement with the experimental one (they used the Cluster Bethe Lattice Method for the liquid phases). Rubin and Finel [57] reported phase diagram calculations for three ternary systems (Ti-Al-Mo, Ti-Al-Nb and Ti-Al-W) using the CPA-GPM-CVM approach to write the free energy, but all the parameters (disordered energies and effective interactions) were obtained fitting to binary phase diagrams, and making the assumption that the ternary parameters do not change significantly

with the ternary addition. This rough approximation led to a poor agreement of the ternary phase diagram with the experimental evidence. To our knowledge, no study of ternary systems have been carried out using the method to the full extent that is now possible.

Before outlining the rest of this chapter, we must comment on a broader issue regarding the computation of the energetics of a given alloy. In this thesis, we are *only* considering substitutional rearrangements of atoms residing on ideal lattice sites of a fixed lattice. Of course, relaxation, vibrational, and even electronic excitation contributions to the alloy energetics can be crucial towards obtaining the small energy differences between structures that is necessary for an accurate phase diagram determination. The relaxation or elastic contribution is probably the most important effect to take into account, particularly when the size-mismatch between alloy constituents is substantial. Usually, one distinguishes between a *global* volume relaxation, when molar volumes are not ideal, and *local* volume relaxations, when atoms do not reside on ideal lattice sites [58, 59]. Some of the global relaxation effects are included in our CPA-GPM approach because Hamiltonian matrix elements and effective interactions are, in fact, parametrized with respect to the alloy volume through their dependency on the concentration of the alloy, although alloy volumes will be given by the (ideal) Zen's law as described in 4.2.2. Recent studies that incorporate lattice vibration effects into theoretical phase diagram computations have shown that the inclusion of these effects can have a significant impact on the predicted phase diagrams [58, 60]. These studies use some simple models like the Debye-Grüneisen approximation. A formalism to include the vibration effects directly into the first-principle models (through "vibrational effective cluster interactions") is currently being developed [61].

The rest of this chapter is divided into three sections; the first section, 4.2, describes in detail the scaling of the tight-binding parameters obtained from the *ab initio* calculations. To asses the reliability of these parameters we compare the density of states and band structures which are obtained with them, to the density of states and band structures given by the first-principles computations; the second section, 4.3, is concerned with the formalism of the electronic structure methods, CPA and

GPM, including their extension to study partially ordered alloys; and lastly, section 4.4 presents and discusses results for the binary Zr-Ru, Ru-Pd, and Zr-Pd alloys, and for ternary Zr-Ru-Pd alloys.

4.2 The TB Parameters

4.2.1 Background

Until the seminal paper by Slater and Koster [16], transfer integrals were computed analytically involving cumbersome integrals that included the atomic orbitals and potentials [62, 63]. Slater and Koster derived a method where the TB parameters were to be regarded as adjustable parameters determined by fitting to calculated energy eigenvalues at various points in the Brillouin zone. These energy values are now computed with more accurate density-functional methods like the augmented plane-wave method or APW (see for example [13]).

More empirical approaches, mostly used in conjunction with realistic computer simulations, have developed alternative semi-empirical models for the TB integrals. These models include a number of parameters which are obtained by fitting to some experimental values such as cohesive energies, lattice constants and independent elastic constants. These models range from the simple second-moment approximation to more sophisticated multiparameter exponentials and polynomial functions [64, 65, 66, 67].

The approach we are going to follow for obtaining the TB parameters uses the TB formulation of the linear muffin-tin orbital (LMTO) Hamiltonian, in the atomic sphere approximation (ASA), developed by Anderson *et al.* [14]. The *ab initio* nature of the TB-LMTO approach makes empirical fitting unnecessary for obtaining the Slater-Koster (SK) or fundamental transfer integrals. Also, unlike the fitted SK parameters, the TB-LMTO SK parameters are defined with reference to the Coulomb potential so that no arbitrary rigid shift of the on-site energies is needed when alloys are considered.

4.2.2 Parameters for metals and alloys

We have mentioned that the hopping integrals can be written in terms of Slater-Koster parameters which depend on the occupation of sites n and m and the distance joining the two sites. This relation can be written as [16]

$$\beta^{\lambda\mu}_{i(n)j(m)} = \sum_h c^h_{nm} w^h_{ij}(\mathbf{R}_{n,m}), \tag{4.1}$$

where $w^h_{ij}(r_{n,m})$ are the SK parameters, the coefficients c^h_{nm} depend on the direction cosines of vectors $\mathbf{R}_{n,m}$ and $i(n)$ and $j(m)$ show the explicit dependence on the species at sites n and m (i, $j = A$, B or C in a ternary alloy). The superscript h runs over the ten possible fundamental SK parameters, $h = dd\sigma, dd\pi, \ldots$, etc.

It is well known that the SK parameters depend on interatomic distance. Our approach is to fit exponential curves to SK parameters obtained with the LMTO-ASA calculations of the pure elements at different volumes and lattice structures (bcc and fcc). It has been shown that atomic environment has little influence on the potential parameters [68]. Figure 4-1 shows the fitting in the case of Zr. The fitting curves are of the form

$$w^h_i = \mathcal{A}^h_i \, e^{-\mathcal{P}^h_i d}, \tag{4.2}$$

where d is the interatomic distance in a.u., $\mathcal{A}^h_i$ and $\mathcal{P}^h_i$ are the fitting parameters, and i is the element type (Zr in this case). Similar results were obtained for Ru and Pd. (In Fig. 4-1, the interatomic distance was normalized to a reference distance, d_o, in this case, the nearest-neighbor distance for the $B2$ RuZr structure computed with the LMTO method: $d_o = (\sqrt{3}/2)\, a^{\mathrm{RuZr}}_{B2} = 5.3503$ a.u.) Table 4.1 shows the parameters computed for the three elements.

Slater-Koster parameters for a particular alloy were approximated according to

$$\beta^h_{alloy} = (\sum_i c_i \sqrt{\beta^h_{ii}})^2, \tag{4.3}$$

where c_i is the concentration of species i present in the alloy. (We have changed the notation of SK parameters to β as it is customary.) This equation is arrived at when

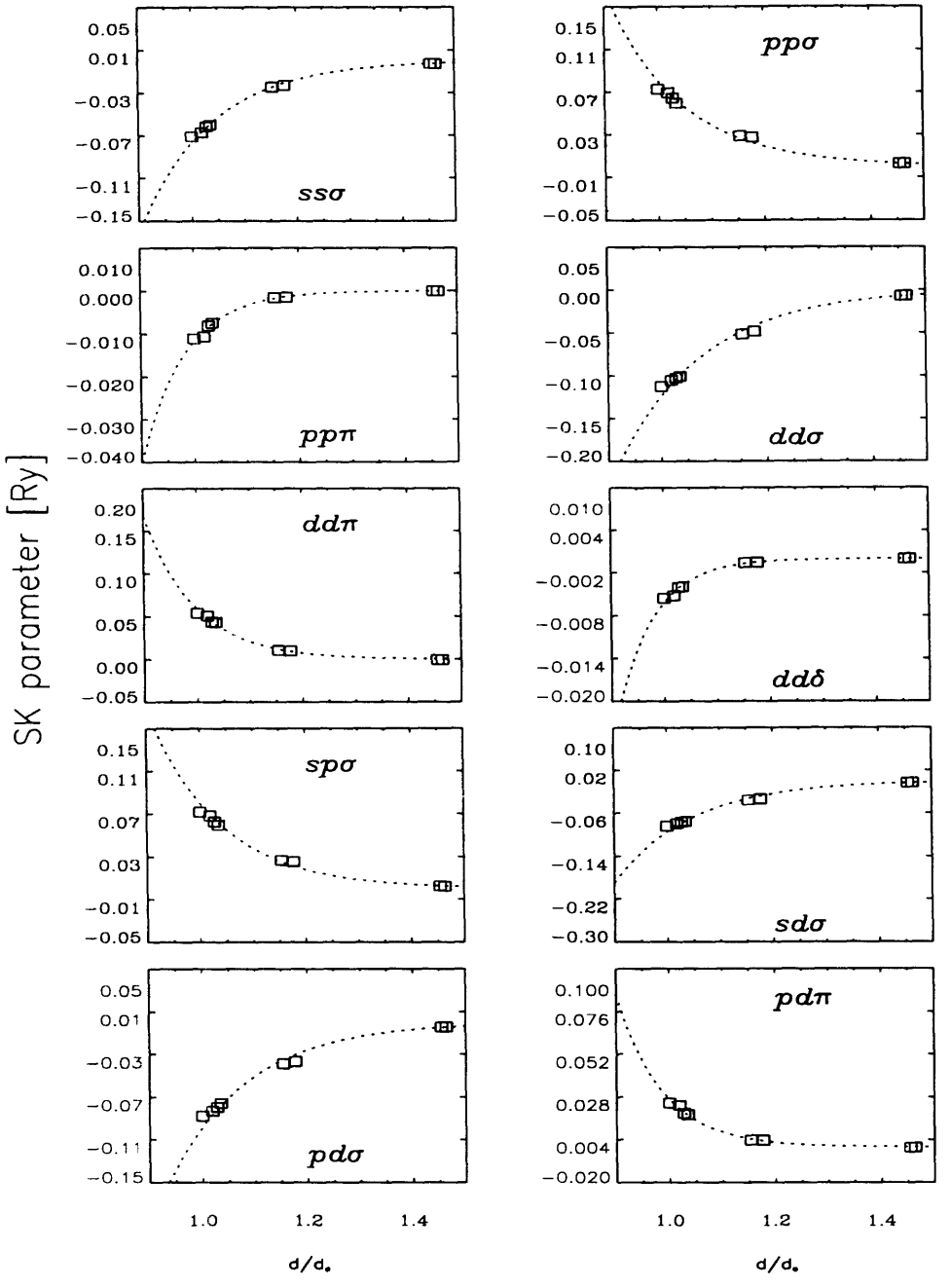

Figure 4-1: Transfer parameters for Zr as a function of the interatomic distance as computed with the exponential fitting (dashed line) of the LMTO-ASA results (square dots).

Table 4.1: Tight-bindig fitting parameters $\mathcal{A}_i^h$ and $\mathcal{P}_i^h$ for Zr, Ru and Pd. See Eq. 4.2. ($\mathcal{A}^h$ in [Ry], $\mathcal{P}^h$ in [(a.u.)$^{-1}$].)

	Zr		Ru		Pd	
SK Parameter (h)	$\mathcal{A}^h$	$\mathcal{P}^h$	$\mathcal{A}^h$	$\mathcal{P}^h$	$\mathcal{A}^h$	$\mathcal{P}^h$
$ss\sigma$	-74.8759	1.2668	-113.1613	1.3912	-112.0270	1.3823
$pp\sigma$	57.7912	1.1981	137.4739	1.3378	137.7712	1.3240
$pp\pi$	-54.1653	1.5654	-289.4552	1.8810	-188.6586	1.7817
$dd\sigma$	-40.4902	1.0714	-39.9683	1.1774	-28.3505	1.1708
$dd\pi$	208.5139	1.5235	293.2882	1.7263	204.3557	1.7090
$dd\delta$	-373.1065	2.0514	-619.6101	2.3208	-421.0329	2.2903
$sp\sigma$	74.5814	1.2541	142.0822	1.3885	141.3045	1.3765
$sd\sigma$	-62.4407	1.1972	-76.4761	1.3148	-64.1410	1.3068
$pd\sigma$	-47.8802	1.1358	-73.5461	1.2592	-61.8225	1.2484
$pd\pi$	129.0867	1.5787	358.0203	1.8423	241.0660	1.7833

averaging the hopping integrals for all ij bonds in random alloys, assuming that the hopping between unlike atoms is given by the geometric mean of the appropriate pure element integrals, $\beta_{ij}^h = \sqrt{\beta_{ii}^h \beta_{jj}^h}$ [Shiba approximation [69]]. The interatomic distance of the alloy is obtained from the concentration average of atomic volumes for the pure species (also known as Zen's law):

$$\bar{\Omega} = \sum_i c_i \, \Omega_i. \tag{4.4}$$

This is not a bad approximation for the present case. For example, the equilibrium atomic volume for the (ordered) ZrRu alloy computed with the LMTO-ASA method is about 2% lower than the ideal value given by Eq. 4.4.

4.2.3 On-site energies

Usually the variation of on-site energies with atomic volume is ignored in electronic structure calculations. Our LMTO calculations clearly showed a significant variation that should be taken into account. In this work, on-site energies were extracted from a polynomial fit of first-principles data at different atomic volumes. A common energy shift to all orbitals for each particular site was added to obtain local neutrality for the bcc-based ZrPd and ZrRu disordered alloys using the CPA approximation (described

Table 4.2: Polynomial coefficients for the on-site energies. See Eq. 4.6.

Zr			
λ	A [Ry]	B [Ry (a.u.)$^{-1}$]	C [Ry (a.u.)$^{-2}$]
s	12.264350	-3.184679	0.206417
p	1.413209	0.073624	-0.033483
t_{2g}	7.620164	-1.913354	0.119266
e_g	7.078303	-1.781268	0.110827
Ru			
λ	A [Ry]	B [Ry (a.u.)$^{-1}$]	C [Ry (a.u.)$^{-2}$]
s	9.750855	-2.737415	0.188767
p	9.586590	-2.544969	0.169262
t_{2g}	6.973325	-2.030726	0.141034
e_g	6.492289	-1.904228	0.132484
Pd			
λ	A [Ry]	B [Ry (a.u.)$^{-1}$]	C [Ry (a.u.)$^{-2}$]
s	7.608464	-2.156563	0.148761
p	8.526845	-2.294863	0.153963
t_{2g}	5.163944	-1.578082	0.111592
e_g	4.789320	-1.478577	0.104818

in the next section). This shift can be expressed as

$$\epsilon_i^\lambda = \epsilon_{i(0)}^\lambda + \delta_i, \tag{4.5}$$

where the index 0 denotes the on-site energy of the particular element and δ_i are the shifts. In our particular case, the shifts used were $\delta_{\mathrm{Zr}} = 0.0$ Ry, $\delta_{\mathrm{Ru}} = 0.313$ Ry and $\delta_{\mathrm{Pd}} = 0.3673$ Ry. When using these values in the computation of the RuPd random alloy, the resulted charge transfer is about 0.1 electron/atom. Figure 4-2 shows the fitting for the on-site energies corresponding to Zr. Similar results were obtained for Ru and Pd. We used a second-order polynomial of the form

$$\epsilon_{i(0)}^\lambda = A_i^\lambda + B_i^\lambda\, r + C_i^\lambda\, r^2, \tag{4.6}$$

with r in atomic units. Table 4.2 shows the polynomial coefficients for the three elements.

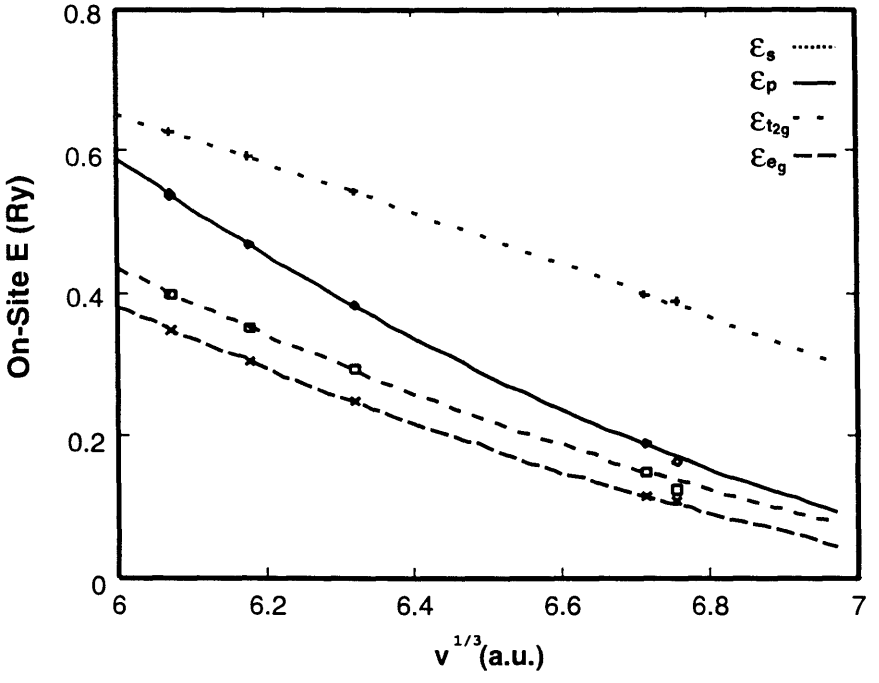

Figure 4-2: On-site energies in Ry for Zr as a function of $v^{1/3}$ (where v is the atomic volume) in a.u. Symbols represent the LMTO results, broken lines are the polynomial fit.

4.2.4 Discussion of the TB approximation

Before embarking on the study of the chemically disordered alloys it is important to analyze the approximations we have introduced and how the results would differ from the more accurate first-principles calculations. To illustrate this point we will compare the band structures (BS) and DOS for an ordered $B2$ ZrRu alloy. Our most "exact" results correspond to the LMTO calculation of the $B2$-type structure. We will call it case (a). A first level of approximation is the TB-LMTO result (that is a TB Hamiltonian with potential parameters obtained from the LMTO calculation of the $B2$ alloy), first taking into account off-diagonal disorder (see next section for a definition), case (b), and second, in a further approximation, defining an "average" SK parameter using Eq. 4.3, case (c). The final approximation, case (d), uses the tight-binding parameters for the pure elements using the TB-LMTO scheme. Again, using these results, we define an average alloy with the SK parameters given by Eq. 4.3 with no off-diagonal disorder.

Figures 4-3 shows the band structure for the different approximations. The overall agreement between the band structures, especially below the Fermi energy, where we are most concerned, is very good. Figure 4-4 compares the total DOS corresponding to cases (c) and (d) in Fig. 4-3. The DOS in these cases were computed using the recursion method. Again, we obtained a good agreement. This shows that an accurate description of the electronic structure (in terms of band structure and DOS) can be achieved within the TB framework. Based on these results we will use this simpler approximation in the rest of this work.

We have described the tight-binding approximation placing special emphasis on the TB parameters. The parameters are extracted form LMTO-ASA calculations and scaled with a novel scheme. We found a good agreement between the TB and the *ab initio* calculations of band structures and density of sates. The following sections deal with the energetics of binary and ternary alloys within this TB framework.

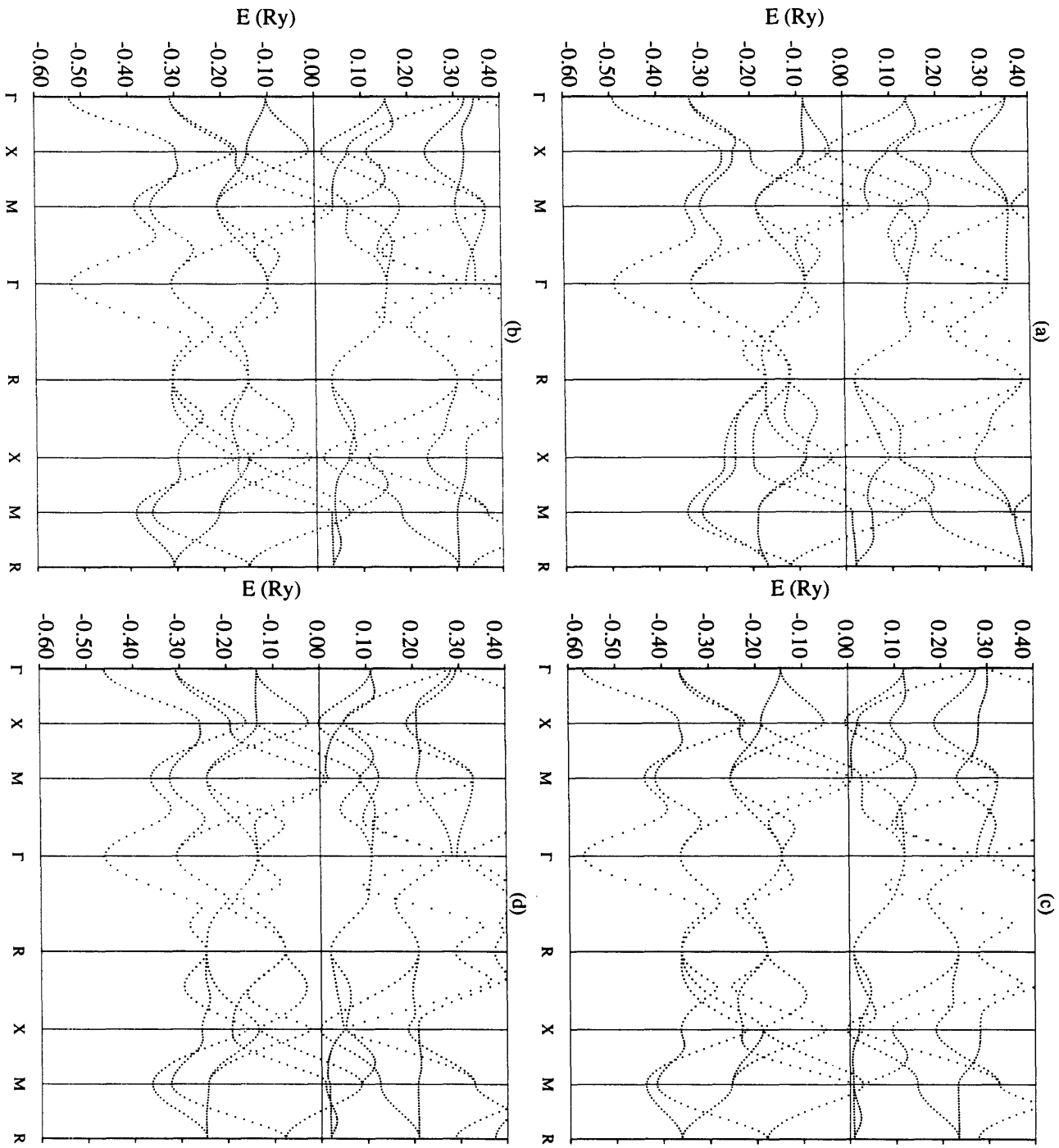

Figure 4-3: Band structure for the $B2$ RuZr compound along special directions of the irreducible wedge of the primitive cubic Brillouin zone. (a) from LMTO calculation; (b) from TB-LMTO calculation; (c) from TB-LMTO using an "average" SK parameter (see text); (d) using SK parameters extrac ted from TB-LMTO calculations performed for the pure elements, and with the definition of "average" SK parameters for the alloy case.

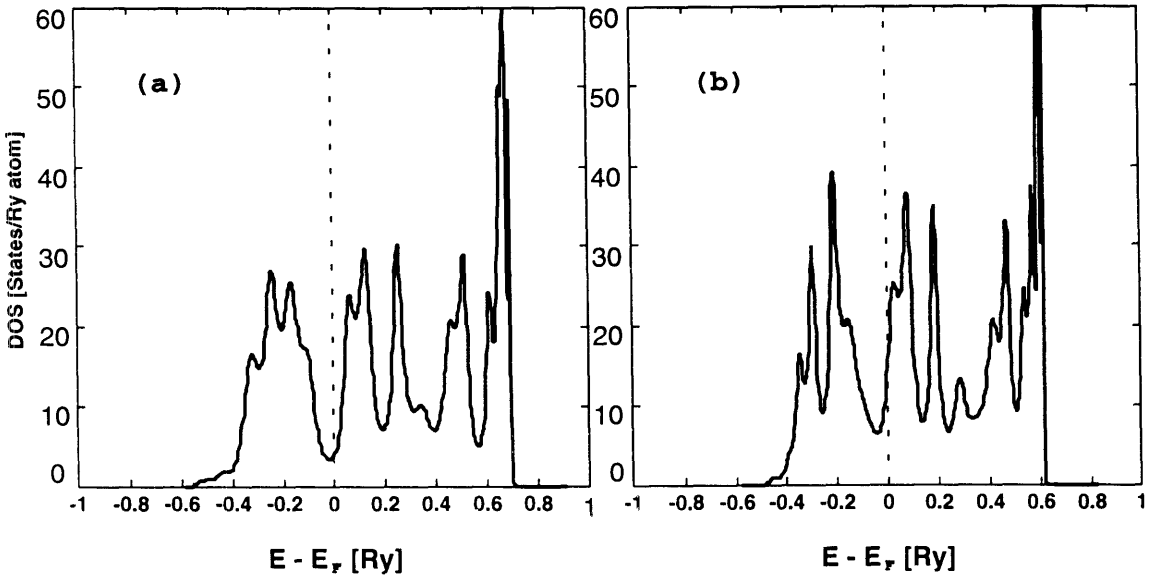

Figure 4-4: Total density of states (in Ry/atom) of the $B2$ RuZr compound as a function of energy (the Fermi energy is taken as zero of energy) computed with the recursion method, (a) same approximation as Fig. 4-3 (c), and (b) same approximation as Fig. 4-3 (d).

4.3 Electronic Structure Methods

The total energy of an alloy characterized by some ordered structure can be decomposed as follows:

$$E = \sum c_i \, E_i(N_e^i) + \Delta E_{dis}(\bar{N}_e) + \Delta E_{ord}(\bar{N}_e) \tag{4.7}$$

where E_i and N_e^i are the energy and the number of valence electrons per atom of the pure element i, respectively. $\Delta E_{dis}(\bar{N}_e)$ is the energy of the totally disordered state,

$$\Delta E_{dis}(\bar{N}_e) = E_{dis}(\bar{N}_e) - \sum c_i \, E^i(N_e^i) \tag{4.8}$$

also known as the *energy of mixing*, and $\Delta E_{ord}(\bar{N}_e)$ is the ordering energy

$$\Delta E_{ord}(\bar{N}_e) = E_{ord}(\bar{N}_e) - E_{dis}(\bar{N}_e). \tag{4.9}$$

Notice that $\bar{N}_e$ is the average number of electrons, $\bar{N}_e = \sum c_i \, N_e^i$ and that the energy of each element is computed with its own Fermi energy $E_F^i(N_e^i)$. Alternatively, we could define a segregation energy ΔE_{seg} given by

$$\Delta E_{seg} = E_{seg} - E_{dis}, \tag{4.10}$$

where E_{seg} is computed using an average DOS,

$$E_{seg} = \int_{-\infty}^{E_F(\bar{N}_e)} \bar{n}(E) \, E \, \mathrm{d}E, \tag{4.11}$$

where $\bar{n}(E) = \sum_i c_i \, n_i(E)$. If interface energies are neglected, the total energies corresponding to both situations (using E_{seg} or $\sum c_i \, E^i$) should be identical. Finally the *formation energy* is defined as:

$$\Delta E_{form} = \Delta E_{dis} + \Delta E_{ord}. \tag{4.12}$$

The following sub-sections deal with the computation of the disordered and ordering energies introduced in Eq. 4.7.

4.3.1 Disordered Alloys and the Coherent-Potential Approximation

The coherent-potential approximation (CPA) [70] is a mean-field theory that describes the average electronic structure of the completely disordered state of an alloy. It is considered the best single-site model for treating random alloys. In the absence of short-range order, the constituents of the alloy are placed randomly on the periodic underlying lattice, thus Bloch's theorem does not apply. The CPA restores the translational invariance by defining an average medium, represented by an on-site energy (or coherent potential) σ. This potential is located at all sites except the central one, which is occupied by a particular atom i. Thus, this fixed atom is assumed to be embedded in the uniform medium of the disordered state, and as such the CPA is a

single-site approximation. This central atom causes scattering of electrons by the potential difference $\Delta\epsilon^{\lambda}_{\mathrm{i(O)}} = \epsilon^{\lambda}_{\mathrm{i(O)}} - \sigma^{\lambda}(z)$ between the potential at site O occupied with atom i and that of the uniform medium. Here, z is the energy plus an infinitesimal imaginary part. We also assume that the alloy is homogeneous, i.e., that all the sites are equivalent and σ does not depend on the site n, but we allow for multiple orbitals λ. The scattering can be described by the t-matrix element

$$t^{\lambda}_{\mathrm{i}} = \frac{\Delta\epsilon^{\lambda}_{\mathrm{i(O)}}(z)}{1 - \Delta\epsilon^{\lambda}_{\mathrm{i(O)}}(z) G^{\lambda\lambda}_{00}(z)} \tag{4.13}$$

where $G^{\lambda\lambda}_{00}$ is the diagonal matrix element of the Green's function for the random medium, $\bar{G}$. The coherent potential σ^{λ} can be obtained self-consistently if we require that the scattering 'on average' vanishes. For a ternary alloy we have:

$$\langle t^{\lambda} \rangle = c_A t^{\lambda}_A + c_B t^{\lambda}_B + c_C t^{\lambda}_C = 0. \tag{4.14}$$

The notation $\langle \cdots \rangle$ is taken to be the so-called configurational average which is the average over all possible atomic configurations on the lattice sites at the average concentration of the alloy. As t^{λ}_{i} is a function of z, ϵ^{λ} and $\bar{G}$, σ^{λ} must be found iteratively. The first guess for the coherent potential is given by the Virtual Crystal Approximation (or VCA) value, $\sigma^{\lambda}_0 = \sum c_i \, \epsilon^{\lambda}_i$. To formally describe the coherent potential and $\bar{G}(z)$, we start with the Hamiltonian of the alloy written as follows,

$$H = W + V \tag{4.15}$$

$$W = \sum_{mn,\mu\lambda} |n,\lambda\rangle \, \beta^{\lambda\mu}_{nm} \, \langle m,\mu| \tag{4.16}$$

$$V = \sum_{n,\lambda} |n,\lambda\rangle \, \epsilon^{\lambda}_n \, \langle n,\lambda|. \tag{4.17}$$

The hopping integrals $\beta^{\lambda\mu}_{nm}$ are assumed to be independent of the nature of the atoms located at sites n and m, and W is then the translationally invariant part of the alloy

Hamiltonian. ϵ_n^λ's are distributed randomly in the alloy and are defined as

$$\epsilon_n^\lambda = \sum_i p_n^i \, \epsilon_i^\lambda, \tag{4.18}$$

where the *occupation number* $p_n^i = 1$ if atom of type i occupies site n, otherwise $p_n^i = 0$.

As it was defined in the previous chapter, the Green's function for a particular configuration is given by $G(z) = (z - H)^{-1}$. The self-energy $\Sigma(z)$ is then defined for the average Green's function $\bar{G}$:

$$\bar{G}(z) = \langle G(z) \rangle = (z - V - \Sigma(z))^{-1}. \tag{4.19}$$

Within the CPA, the resulting self-energy is site-diagonal;

$$\Sigma(z) = \sum_{n,\lambda} |n, \lambda\rangle \, \sigma^\lambda \, \langle n, \lambda|. \tag{4.20}$$

Equation (4.14) actually represents nine equations that must be solved simultaneously. The average Green's function is given by an integration in reciprocal space over the first Brillioun zone (BZ) performed with a technique of special k-points [71],

$$\bar{G}(z) = \frac{1}{\Omega_{\mathrm{BZ}}} \int_{\mathrm{BZ}} (z - \sigma - W(\mathbf{k}))^{-1} \, \mathrm{d}^3\mathbf{k}, \tag{4.21}$$

where $W(k)$ is the Fourier transform of W and Ω_{BZ} is the volume of the first BZ. Partial densities of states can be obtained from the Green's function according to

$$n_{\mathrm{i}}^\lambda(E) = -\frac{2}{\pi} \lim_{\eta \to 0^+} \mathrm{Im} \langle 0\lambda | \bar{G}(E + i\eta) | 0\lambda \rangle, \tag{4.22}$$

whereas band energies can be obtained as

$$E_b^{CPA} = \int_{-\infty}^{E_F} E \, n(E) \, \mathrm{d}E. \tag{4.23}$$

Here $n(E)$ is the total density of states, $n(E) = \sum_{i,\lambda} (c_i/q) \, n_i^\lambda(E)$ and E_F the Fermi

energy. The factor 2 in Eq. 4.22 accounts for the spin degeneracy.

4.3.2 Ordered Alloys

Ordering processes in alloys are normally described by the use of an Ising model. This model was first introduced to study magnetic systems in which each atom of the lattice is supposed to have a magnetic moment (Ising spin) σ_n which can take on one of two possible values. Then the Hamiltonian of the system takes the form:

$$H = -\sum_{nm} J_{nm}\sigma_n\sigma_m, \tag{4.24}$$

where J_{nm} is an exchange integral between spins on sites n and m and the spin variable σ_n is 1 (-1) if the spin at site n points 'upwards' ('downwards'). The summation is over interacting neighbor pairs. We can use the same concept to approximate random or partially ordered multicomponent substitutional alloys, writing the configurational energy (with only pair interactions) as

$$E = \frac{N}{2}\sum_{i,j=1}^{M}\sum_{n,m=1}^{N} V_{nm}^{i,j}\, p_n^i\, p_m^j, \tag{4.25}$$

where $V_{n,m}^{i,j}$ is the effective real-space pair potential between species i and j at sites n and m, respectively. There are N sites and M chemical species. The factor $1/2$ is required to avoid double counting. One important difference between the alloy system and the Ising model is that the magnetic interactions J_{nm} in the Ising model are postulated to be independent of both temperature and concentration (of spins in either direction). On physical grounds, there is no compelling reason to assume that interatomic interactions in alloys possess these properties [72], although the temperature dependence of the interactions seems to be most important for magnetic systems [50]. An exhaustive analysis of the approximations involved in the use of this "generalized" Ising model when mapping the real free energy of an alloy is discussed in Ref. [73]. We will return to the Ising model in the next chapter when we discuss phase stability.

The generalized perturbation method (GPM) [34] attempts a direct determination of concentration-dependent multi-site interactions in real-space. The method is a perturbation treatment of a reference medium which is close to any particular configuration of the alloy, such as the complete disordered state described by the CPA. Any chemical configuration is completely specified by the set of occupation numbers $\{p_n^i\}$. For a particular configuration $\{p_n^i\}$ the GPM allows the band energy $E(\{p_n^i\})$ to be expressed (see [74] for a derivation of the equations) as:

$$E(\{p_n^i\}) = E_{dis}(c) + \Delta E_{ord}(\{p_n^i\}), \tag{4.26}$$

where the energy of the disordered state E_{dis} is concentration-dependent but independent of the $\{p_n^i\}$ (thus. configuration-independent) as calculated with the CPA method, and ΔE_{ord} is the ordering energy which can be expanded as follows:

$$\Delta E_{ord} = \frac{1}{2N} \sum_{\substack{ij \\ n,m,n\neq m}} V_{nm}^{ij,(2)} \delta c_n^i \delta c_m^j + \frac{1}{3N} \sum_{\substack{ijk \\ n,l,m, \\ n\neq m,m\neq l,n\neq l}} V_{nml}^{ijk,(3)} \delta c_n^i \delta c_m^j \delta c_l^k + \cdots, \tag{4.27}$$

where δc_n^i is the concentration deviation from the average composition at site n, $\delta c_n^i = p_n^i - c^i$ and $V_{nm\cdots}^{ij\cdots(l)}$ are the concentration-dependent l-site effective cluster interactions between atoms $i, j, \ldots$ at sites $n, m, \ldots$. Usually, higher-order terms (greater than two) in expression (4.27) are negligible. In the following we will only consider the second-order terms which comprise the effective pair interactions (EPI's), and redefine the EPI's by the quantities V_s^{ij}. In terms of Green's function matrix elements, these interactions are written as:

$$V_s^{ij} = -\frac{1}{\pi} \mathrm{Im} \int^{E_F} \mathrm{d}E \sum_{\lambda\mu} G_{(s)}^{\lambda\mu} G_{(s)}^{\mu\lambda} \Delta t_{ij}^{\lambda} \Delta t_{ij}^{\mu}, \tag{4.28}$$

where E_F is the Fermi energy of the CPA medium, $G_{(s)}^{\lambda\mu}$ is the off-diagonal matrix element of the CPA Green's function between s'th-neighbors and $\Delta t_{ij}^{\lambda} = t_i^{\lambda} - t_j^{\lambda}$. Notice that if $V_s^{ij} > 0$ then clustering of unlike sth-neighbors is favored. Finally, the

ordering energy for the ternary system can be expressed as

$$\Delta E_{ord} = \frac{1}{2} \sum_{i \neq j,s} (c_i \, c_j \, z_s - \delta q_s^{ij}) \, V_s^{ij} = \sum_{i \neq j,s} q_s^{ij} \, V_s^{ij} \,, \tag{4.29}$$

where z_s is the coordination number, δq_s^{ij} is the number of ij pairs, per atom, associated with the s-th shell, and q_s^{ij} are the GPM expansion coefficients.

The EPI's for a given lattice depend on:

(i) The composition (via the concentration-dependent self-energy of the CPA medium).

(ii) The interatomic distance.

(iii) The diagonal disorder defined by $\delta_\lambda^{AB} = (\epsilon_i^\lambda - \epsilon_j^\lambda)/\bar{W}$, where $\bar{W}$ is the averaged half bandwidth of the DOS for elements i and j. (Notice in Eq. 4.28 that the total EPI can be decomposed into orbital-dependent contributions, $V_s^{ij} = \sum_{\lambda\mu} V_s^{ij,\lambda\mu}$.)

(iv) The off-diagonal disorder characterized by the ratio $(W^i - W^j)/\bar{W}$. It is generally smaller than the diagonal disorder parameter for TM alloys and may be neglected [15]. The off-diagonal effect can be taken into account by allowing the hopping integrals to be site-occupation dependent [69] and by using a CPA adapted to that effect [75].

(v) The filling of the band,

$$N_e(E_F) = \int_{-\infty}^{E_f} \mathrm{d}E \; n_{\mathrm{CPA}}(E).$$

As an example of the GPM expansion, consider the $L2_1$ (Heusler) ordered structure of a C_2AB ternary alloy, as illustrated in Fig. 4-5. Here, atoms C fully occupy one of the two interpenetrating primitive cubic sublattices that form the bcc structure and atoms A and B the second sublattice in a NaCl-type of ordering. Then, within the GPM framework, the ordering energy associated with this particular alloy

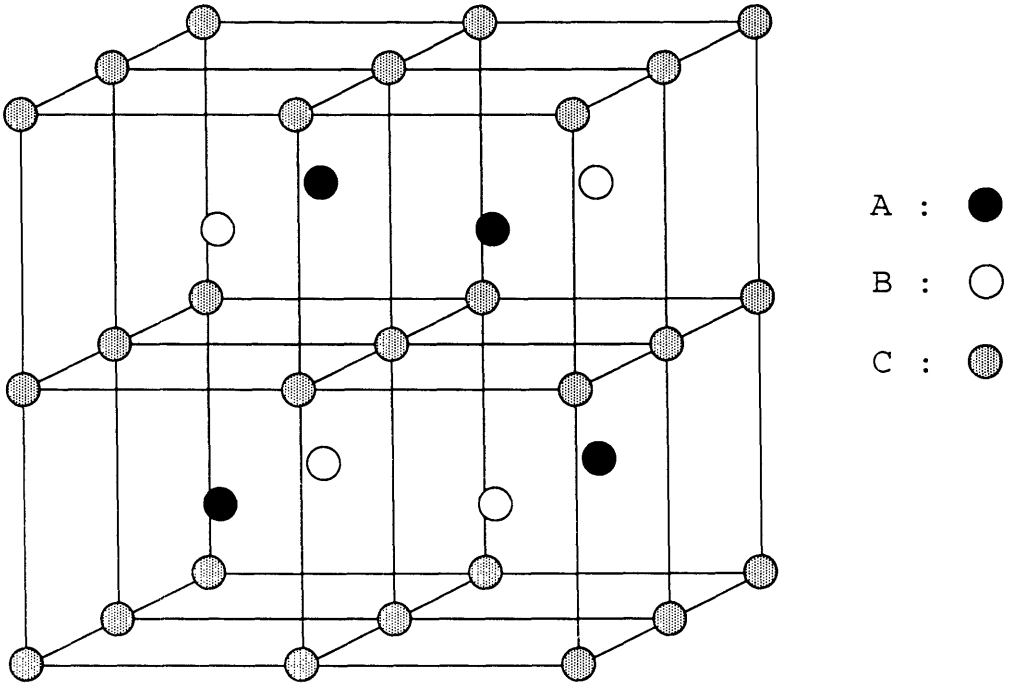

Figure 4-5: Heusler structure ($L2_1$) of a C_2AB alloy.

configuration will be expressed as

$$\begin{aligned}\Delta E_{ord}^{(L2_1)} &= -\frac{1}{2}(V_1^{AC}+V_1^{BC})+\frac{1}{4}V_1^{AB}+\frac{3}{8}(V_2^{AC}+V_2^{BC}) \\ &\quad -\frac{9}{16}V_2^{AB}+\frac{3}{4}(V_3^{AC}+V_3^{BC})+\frac{3}{8}V_3^{AB}+\cdots . \end{aligned} \tag{4.30}$$

In order to test the validity of the GPM expansion we compare in Fig. 4-6 the ordering energy of a hypothetical Zr_2RuPd Heusler structure as given by Eq. 4.30, with that computed using the recursion technique with 15 levels of the continued fraction. Here, $\Delta E_{\rm ord}^{\rm rec} = E^{\rm rec} - E^{\rm CPA}$, where E^{rec} is the band energy associated with the DOS obtained with the recursion method. In reference to Eq. 4.30, we have Zr $\equiv C$, Ru $\equiv A$, and Pd $\equiv B$. First and second EPI's were computed according to Eq. 4.28. We can see that the agreement between the "exact" method and the GPM is very satisfactory except at low levels of band-filling. We are confident then that the GPM , with an expansion in pair potentials including first and second nearest-neighbors, can be used to reproduce the ordering energy.

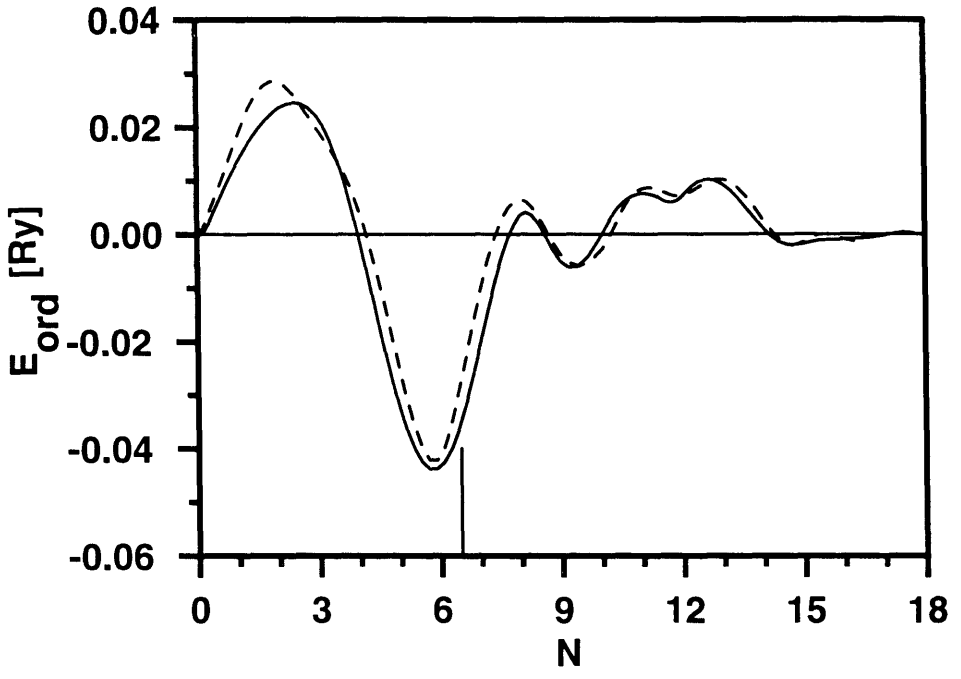

Figure 4-6: Ordering energy in Ry/atom vs. band-filling for the $L2_1$ Zr_2RuPd alloy computed with the recursion method (dotted line) and the GPM expansion (solid line). The vertical line shows the band filling for the composition of this particular compound.

4.3.3 Partially Random Alloys

As we mentioned in Chapter 2, the stable phase along the $Zr_{0.5}(Ru,Pd)_{0.5}$ pseudobinary system has a $B2$ structure beyond the martensitic region. We have studied the characteristics of partially random alloys where, for example, Zr occupies one of the two primitive cubic sublattices which constitute the bcc lattice, and Pd and Ru randomly occupy the other sublattice. Although the present theory is applicable to more complicated compounds, we restrict the following arguments to those particular bcc-based intermetallic compounds, represented by $(A_{1-x}B_x)_{0.5}C_{0.5}$. They consist of two sublattices, α where A and B atoms are distributed randomly, and β which is occupied by only C atoms. This corresponds to having A and B randomly occupying the primitive cubic sublattice in Fig. 4-5. The values of the on-site energies are given by (we drop the orbital superscript for simplicity),

$$\epsilon_n = \begin{cases} \epsilon_A \text{ or } \epsilon_B & \text{if } n \in \alpha \\ \epsilon_C & \text{if } n \in \beta \end{cases} \tag{4.31}$$

A rigorous treatment of this system would require, for example, the use of the two-site cluster CPA (CCPA) (see, for instance, Ref. [76]) where the disordered material is considered to be a collection of clusters chosen so that the entire lattice can be generated by the translation of the points in a cluster through a set of translation vectors. Each cluster or cell contains several atoms (two in our case), and we apply the CPA equation to the cell rather than to a single site. The cluster Green's function now becomes a matrix and the scalar CPA self-consistent condition given by Eq. 4.14, is generalized to a matrix self-consistent condition. The CPA self-energy σ is replaced by a (18 x 18) cluster diagonal matrix, $\mathbf{\Sigma}$.

We can rewrite the Hamiltonian matrix of the disordered material in terms of cluster quantities. Let $\underline{\epsilon}_C$ denote the cluster-diagonal part of H, where $C = \alpha$ or β,

and $\underline{\mathrm{W}}_{CC'}$ the cluster off-diagonal part. We have then (dropping orbital superscripts)

$$(\underline{\epsilon}_C)_{ij} = \begin{cases} \epsilon_i\,\delta_{ij} & \\ \beta_{ij}\,(1-\delta_{ij}) & i,j \in C, \end{cases} \tag{4.32}$$

and

$$(\underline{\mathrm{W}}_{CC'})_{ij} = \beta_{ij} \qquad i \in C, j \in C', C \neq C'. \tag{4.33}$$

To avoid the tedious calculations involved in the CCPA computations we applied the following approximation. The self-energy of the effective medium is required to be not only cluster-diagonal but also site-diagonal, that is $(\mathbf{\Sigma})_{ij} = \sigma\delta_{ij}$. Furthermore, the coherent potential σ is placed only on the random sublattice. This approach is similar to the self-consistent boundary-site approximation of the cluster CPA [77]. We impose the additional restriction of fixing the on-site energies in the fully ordered sublattice, and apply the CPA condition on the random sublattice, restoring the scalar nature of the single-site CPA.

If we consider the full $s-p-d$ bands, the Σ-matrix takes the form

$$\Sigma = \left(\begin{array}{cccc|cccc} \epsilon_n^{\lambda_1} & & & & \beta_{nm}^{\lambda_1\lambda_2} & \beta_{nm}^{\lambda_1\lambda_2} & \cdots & \beta_{nm}^{\lambda_1\lambda_9} \\ & \epsilon_n^{\lambda_2} & & & \beta_{nm}^{\lambda_2\lambda_1} & \beta_{nm}^{\lambda_2\lambda_2} & \cdots & \beta_{nm}^{\lambda_2\lambda_9} \\ & & \ddots & & \vdots & \vdots & \ddots & \vdots \\ & & & \epsilon_n^{\lambda_9} & \beta_{nm}^{\lambda_9\lambda_1} & \beta_{nm}^{\lambda_9\lambda_1} & \cdots & \beta_{nm}^{\lambda_9\lambda_9} \\ \hline \beta_{mn}^{\lambda_1\lambda_1} & \beta_{mn}^{\lambda_1\lambda 2} & \cdots & \beta_{mn}^{\lambda_1\lambda_9} & \sigma^{\lambda_1} & & & \\ \beta_{mn}^{\lambda_2\lambda_1} & \beta_{mn}^{\lambda_2\lambda_2} & \cdots & \beta_{mn}^{\lambda_2\lambda_9} & & \sigma^{\lambda_2} & & \\ \vdots & \vdots & \ddots & \vdots & & & \ddots & \\ \beta_{mn}^{\lambda_9\lambda_1} & \beta_{mn}^{\lambda_9\lambda_2} & \cdots & \beta_{mn}^{\lambda_9\lambda_9} & & & & \sigma^{\lambda_9} \end{array}\right). \tag{4.34}$$

To test this approximation, which we call "partial CPA" (PCPA), we have compared results with the rigorous two-site cluster CPA treatment of the alloy. In Fig. 4-7, we can see the good agreement between the total DOS for the $Zr_{0.5}(Ru_{0.5}Pd_{0.5})_{0.5}$ alloy computed with both methods. We plot in Fig.4-8 the values of the coherent potential $\sigma^{t_{2g}}$ and on-site energy $\epsilon_{\mathrm{Zr}}^{t_{2g}}$ as a function of energy, as computed with the CCPA.

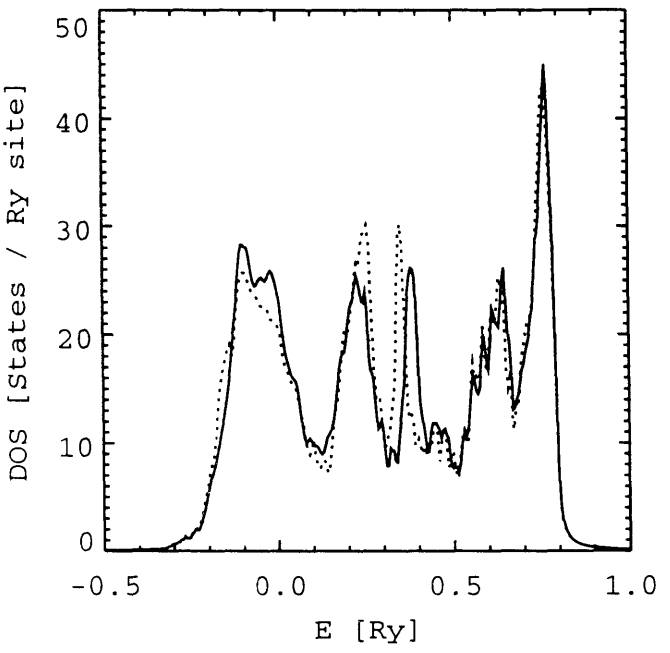

Figure 4-7: DOS (in Ry/atom) for a bcc $Zr_{0.5}(RuPd)_{0.5}$ pseudo-binary alloy vs. energy (in Ry) as computed with the cluster CPA (solid line) and the partial CPA (dashed line).

Notice the different scaling in the ordinate axis. We obtained similar behavior for the other on-site orbitals. This figure shows that the fluctuation of the on-site energy for the ordered sublattice is vanishing compared with respect to the atomic (Zr) on-site energy value. We can then consider a fixed on-site energy on this ordered sublattice, and apply the partial CPA to the fully random sublattice only.

The GPM, discussed in the previous section, can be also applied to partially random alloys. When this is done, the computed interactions are associated with the primitive cubic random sublattice. The energy for a particular ternary configuration may be then obtained with two different expansions (see Eq. 4.29):

$$E_{ord} = E_{CPA} + \sum_{i \neq j, s} q_s^{ij} V_s^{ij} = \tilde{E}_{CPA} + \sum_{i,j \in \alpha, s} \tilde{q}_s \tilde{V_s^{ij}} \,, \tag{4.35}$$

where $\tilde{q}_i$ and $\tilde{V}_i$ are respectively the expansion coefficients and EPI's associated with the specific sublattice (α) where ordering takes place (here the primitive cubic sublattice), and $\tilde{E}_{CPA}$ is the energy of the partially random alloy. We have then two

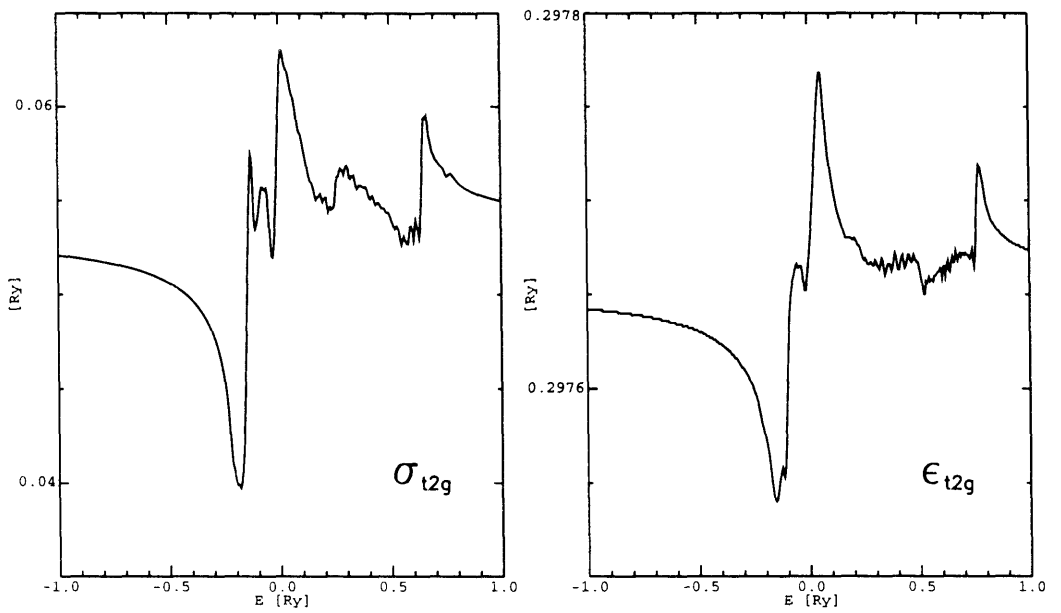

Figure 4-8: On the left: real part of the self energy $\sigma^{t_{2g}}$ corresponding to the random sublattice for the $Zr_{0.5}(RuPd)_{0.5}$ pseudo-binary alloy computed with the CCPA. On the right: on-site energy $\epsilon^{t_{2g}}$ of the fully ordered sublattice for the same alloy. Notice the different scaling on the ordinate axis.

different approaches to study stability and ordering energies in multicomponent alloys. The first one has the fully random alloy as the starting point, while the second one starts by considering a partially ordered system.

4.4 Results

4.4.1 Binary Alloys

We studied the electronic structure of bcc-based Ru-Zr, Pd-Zr and Ru-Pd alloys at different compositions using the TB-CPA-GPM formalism. For example, Fig. 4-9 shows the CPA-DOS for the three alloys at equiconcentration. They all exhibit a pseudo-gap around the half-filled band with two peaks of strong *d*-character. This is typical for DOS of bcc metals and alloys where the lower half region is related to *bonding* states and the upper half region, to *antibonding* states [3]. According to Friedel's theory of the cohesive energy for TM , the essential contribution to the

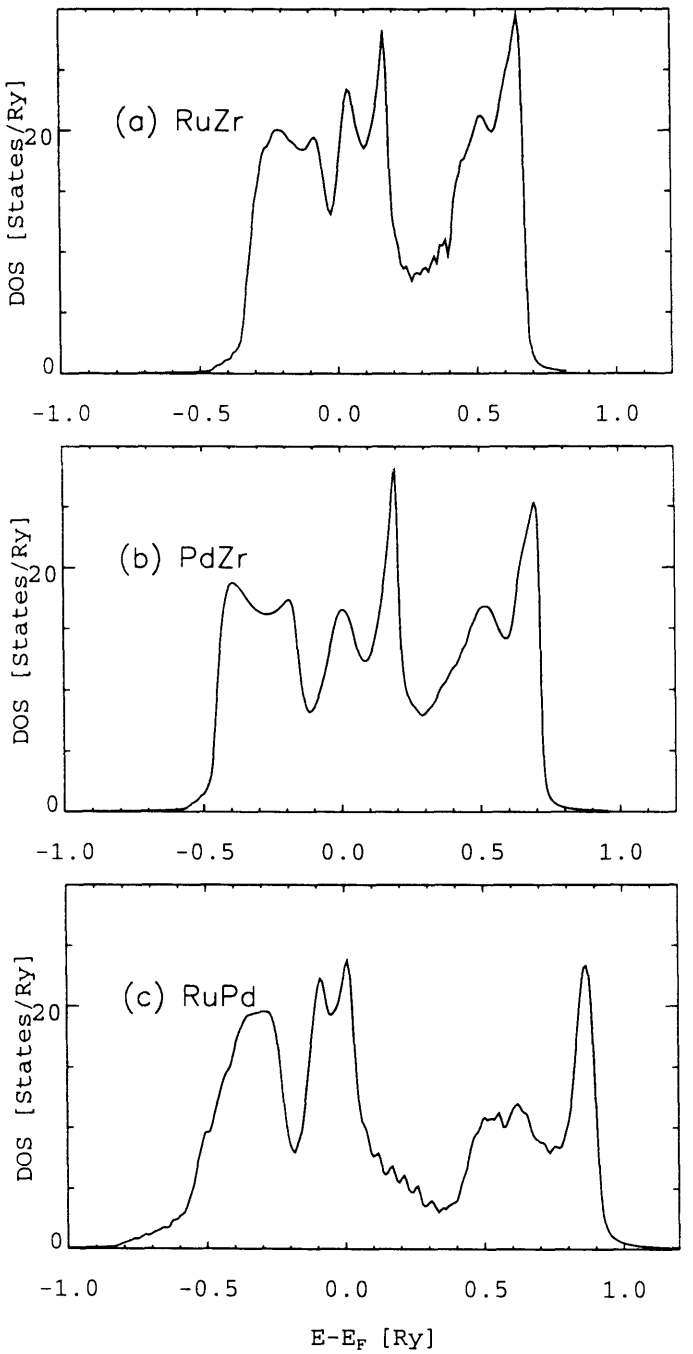

Figure 4-9: Total DOS (in Ry/atom)vs. energy (in Ry) for the binary alloys (a) RuZr, (b) PdZr, and (c) RuPd, as computed with the CPA. The Fermi energy is taken as zero of energy.

shell	1	2	3	4	5
V^{RuZr}	31.18	1.75	0.80	0.81	-2.37
V^{PdZr}	20.28	1.13	1.20	1.59	-2.13
V^{RuPd}	-1.57	-2.51	-0.14	-0.28	0.57

Table 4.3: Effective pair interactions (in mRy/atom) for the binary alloys at 50% composition computed within the CPA-GPM formalism. All interactions in mRy.

cohesion of TM compounds is the broadening of the TM d band; filling bonding or antibonding states will increase or reduce the cohesion (or stability). In the case of Ru-Pd the Fermi energy falls far from the pseudo-gap, lying on a peak of the antibonding states. This may be associated to the instability of the bcc Ru-Pd solution (e.g., see [78] for similar analysis of TM DOS). Furthermore Table 4.3 shows that the first four EPI's between Ru and Pd are negative and, as seen in Fig. 4-10, the mixing energy is positive suggesting a clear tendency towards phase separation. On the other hand we confirm a strong $B2$ ordering tendency in RuZr and a weaker $B2$ ordering tendency in PdZr. The $B2$ ordering is favored when $V_1 > 0$ and $V_2/V_1 < 2/3$ [79]. As expected, the mixing energies for both systems are negative as shown in Fig. 4-11.

4.4.2 Ternary Alloys

The tendency towards mixing of the ternary alloy was evaluated with ΔE_{mix}, defined as

$$\Delta E_{\mathrm{mix}}(\{c_i\}, a) = E_{\mathrm{dis}}(\{c_i\}, a) - c_{\mathrm{A}} E_{\mathrm{A}}(a_{\mathrm{A}}) - c_{\mathrm{B}} E_{\mathrm{B}}(a_{\mathrm{B}}) - c_{\mathrm{C}} E_{\mathrm{C}}(a_{\mathrm{C}}), \qquad (4.36)$$

where a and a_i represent, respectively, the lattice parameter of the random alloy and of the pure element i. This formula was used to map the energy of mixing on the Gibbs' triangle for the bcc-based Zr-Ru-Pd alloys. We found that the energy of mixing is negative except in a narrow range of concentration close to the Ru-Pd side, as expected.

We were interested in the ternary alloy $\mathrm{Zr}_{0.5}(\mathrm{Pd}_c\mathrm{Ru}_{1-c})_{0.5}$ (Fig. 4-12) for which the

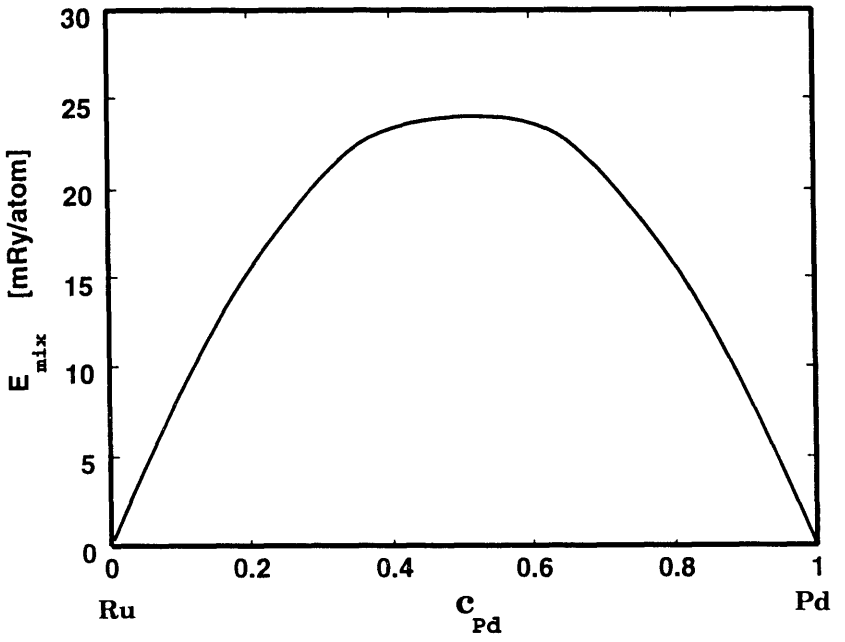

Figure 4-10: Energy of mixing for Ru-Pd alloys versus concentration computed with CPA.

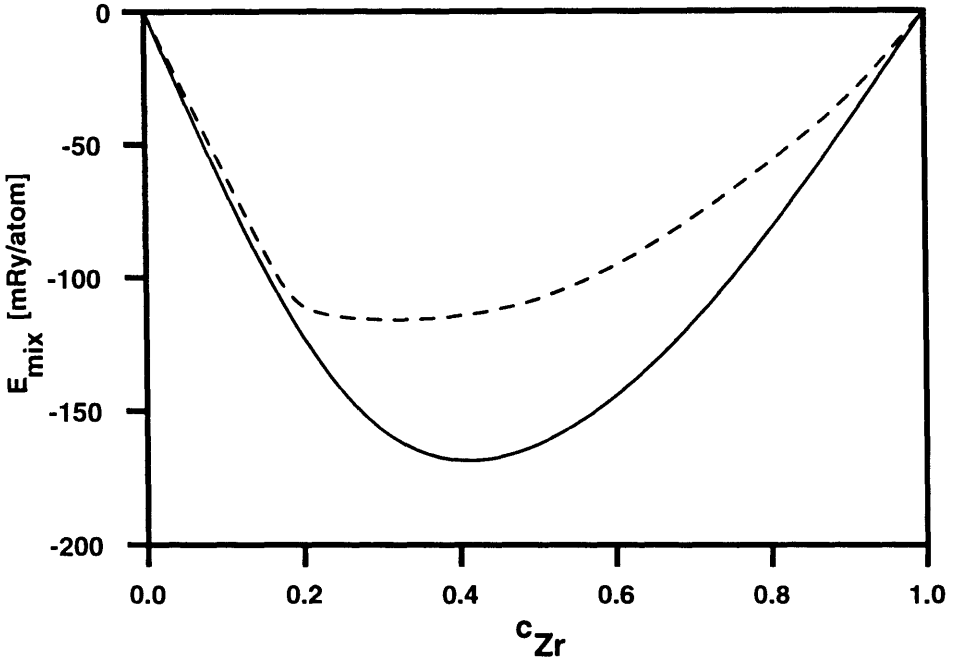

Figure 4-11: Energy of mixing for Ru-Zr (solid line) and Pd-Zr (dashed line) alloys versus concentration computed with the CPA.

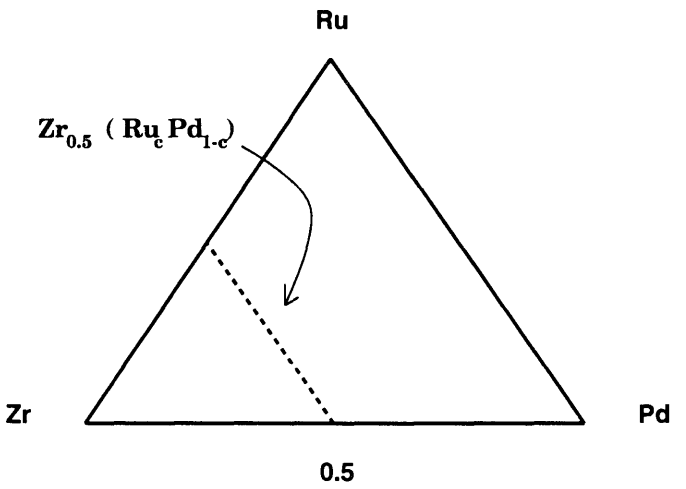

Figure 4-12: Tie line as discussed in the text in the ternary phase representation of the Zr-Ru-Pd alloy.

bulk of experimental data are available. First and second nearest-neighbor effective pair interactions were computed at different concentrations for these particular alloys. Figures 4-13 and 4-14 show the first and second nearest EPI's, V_1 and V_2, respectively, as a function of concentration c. Notice that V_1 is positive and similar in magnitude for Ru-Zr and Pd-Zr while the interaction between Pd and Ru remains negative and about one order of magnitude smaller. A ground state analysis performed with a cluster method [80] and which included nearest and next-nearest neighbor interactions predicts a tendency towards phase separation into two $B2$ phases. This is expected from the magnitude and the negative sign of the EPI's involved, particularly the next nearest-neighbor interaction, V_2^{RuPd}, between Ru and Pd.

Figure 4-15 shows the variation of this interaction with the filling of the band. This figure tell us an important result. Simple band-filling arguments show that replacing one element like Ru by a metal with lower number of valence electrons could turn this interaction positive without altering the other ones significantly. In this way we may be able to stabilize an ordered structure like the $L2_1$. That is possible because given an $A_{0.5}BC$ alloy, the ordering energy difference between a Heusler phase, $L2_1(A_2BC)$, and a mixture of two β phases, $B2(AB)/B2(AC)$, is controlled mainly by V_2^{BC}. Our own preliminary calculations agree with this analysis if Ru is replaced, for instance,

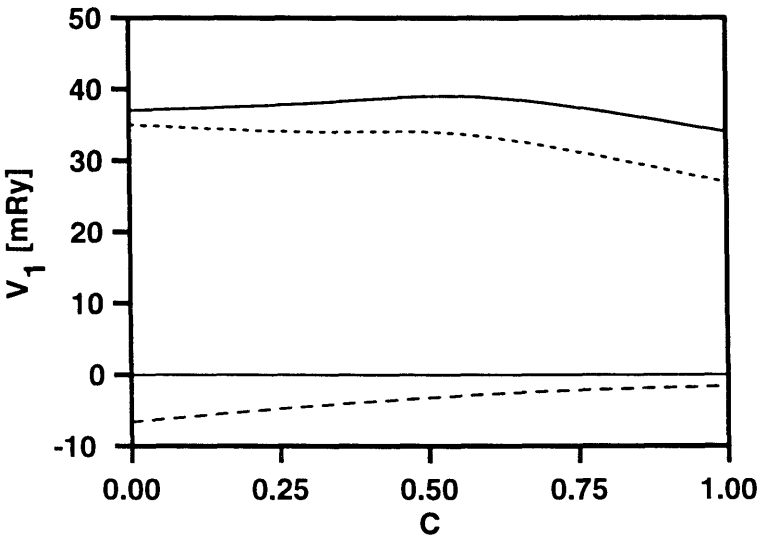

Figure 4-13: First EPI versus concentration in $Zr_{0.5}Ru_{1-c}Pd_c$. Solid line, Ru-Zr; dotted line, Pd-Zr; dashed line, Ru-Pd.

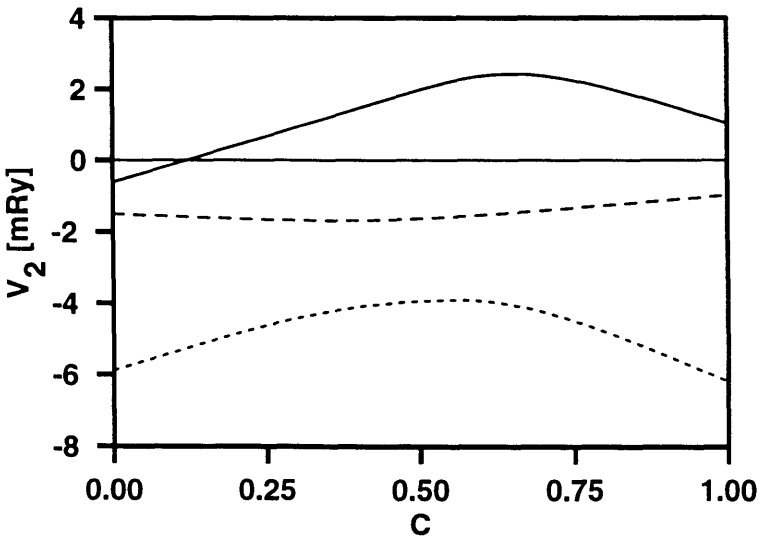

Figure 4-14: Second EPI versus concentration in $Zr_{0.5}Ru_{1-c}Pd_c$. Solid line, Ru-Zr; dotted line, Pd-Zr; dashed line, Ru-Pd.

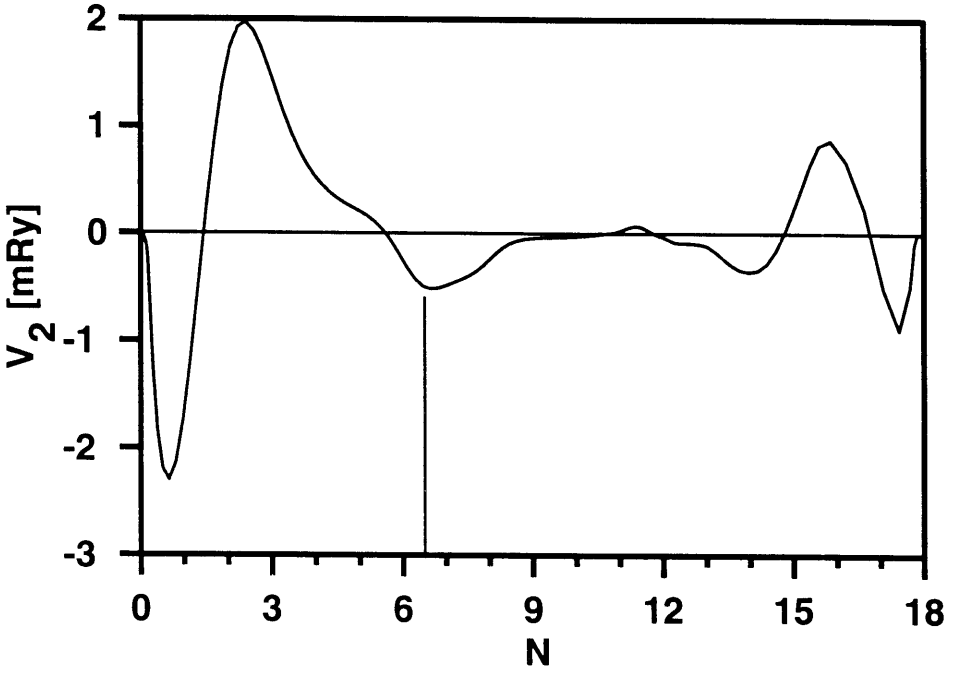

Figure 4-15: Second nearest-neighbor EPI, V_2, in mRy/atom between Ru and Pd in the $Zr_{0.5}Ru_{0.25}Pd_{0.25}$ alloy versus band-filling, as computed with the GPM applied to the fully random CPA medium. The vertical line shows the band filling that correspond to the actual alloy

by Mo.

These results motivated the study of partial order in the $Zr_{0.5}$(Ru,Pd) system as described in the previous section. We applied the partial CPA-GPM formalism to a primitive cubic sublattice occupied by Pd and Ru only. The interactions that we obtained are in agreement with those obtained using the full CPA, i.e., they are all negative so that the elements tend to segregate on this sublattice, giving rise to a phase separation into two $B2$ phases, as concluded before. Furthermore, the disordered energy of this system is more negative than the disordered energy of the fully random alloy for all concentrations, as shown in Fig. 4-16. This indicates that the former configuration should, in principle, be more stable, consistent with a preferential occupation of Zr on one sublattice, as observed in the $B2$ structures of ZrRu and ZrPd.

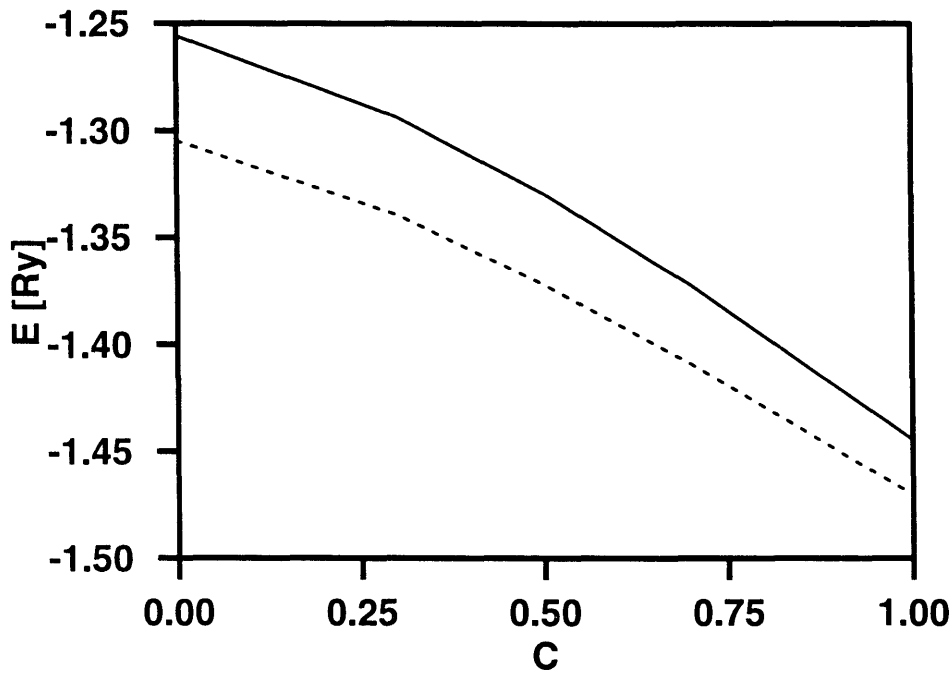

Figure 4-16: Energy of the disordered alloy $Zr_{0.5}(Pd_cRu_{1-c})$: dashed line, with partial CPA; solid line, with full CPA.

4.5 Conclusions

We have described and analyze in this chapter an electronic structure method based on the TB approximation to study the energetics of multicomponent alloys. First, a novel scaling scheme for the TB parameters was introduced. The CPA and GPM were then presented with their natural extension for treating ternary systems. The method allows the study of partially ordered systems using a reliable approximation of the cluster CPA. The results obtained with the CPA-GPM formalism compare very well with the 'exact' results obtained with the recursion method. The methodology was applied to study bcc Zr-Ru-Pd alloys. The effective interactions for the binary systems give rise to $B2$ phases at 50% concentration in agreement with experimental data (at $T = 0$). The kind of analysis given respect to the second EPI, V_2^{RuPd}, shows that the computational scheme we are using can be used to design or modify alloy composition so as to stabilize particular ordered phases. The following chapter shows how the energetic parameters obtained within the TB-CPA-GPM scheme are

used with the CVM to study phase equilibria in alloys.

Chapter 5

Phase Equilibria

5.1 Introduction

Once the energetics and ground states have been determined we can pursue the calculation of equilibrium phase diagrams. We will be concerned here with coherent phase diagrams where the underlying lattice structure is unchanged. Equilibrium is obtained by minimizing a suitable thermodynamic potential, for instance the Helmholtz free energy, $F(N_i, V, T) = U - T\,S$ can be minimized at fixed number of particles N_i; alternatively, the grand potential, $\Omega(\mu_i, V, T) = U - TS - \sum_i \mu_i N_i$ can be minimized at constant chemical potentials μ_i. Here, U is the internal energy, T the temperature, V the volume and S the entropy of the system. From statistical mechanics we have

$$F = -k_B\,T\,\ln Z, \tag{5.1}$$

with k_B the Boltzmann constant and Z the canonical partition function given by

$$Z = \sum_{all\ states\ j} e^{-\beta\,E_j}, \tag{5.2}$$

where E_j is the energy of a particular microstate of the canonical ensemble and $\beta = 1/k_B T$. Let H be the Hamiltonian of the crystal and ρ the density matrix,

$$\rho = \frac{e^{-\beta H}}{Z}, \tag{5.3}$$

so that

$$Z = \mathrm{Tr}\, e^{-\beta H} = e^{-\beta H}\, \rho^{-1}. \tag{5.4}$$

Using the property $\mathrm{Tr}\, \rho = 1$ (ρ behaves as a probability) we can rewrite the free energy as:

$$\begin{aligned} F &= -\frac{1}{\beta} \mathrm{Tr}\,(\rho)\, \ln Z \\ &= -\frac{1}{\beta} \mathrm{Tr}\,(\rho \ln Z) \\ &= -\frac{1}{\beta} \mathrm{Tr}\,(\rho \ln(e^{-\beta H} \rho^{-1})) \\ &= -\frac{1}{\beta} \mathrm{Tr}\,(\rho(-\beta H - \ln \rho)) \qquad (5.5) \\ F &= \mathrm{Tr}\,(\rho H) + k_b T\, \mathrm{Tr}\,(\rho \ln \rho). \qquad (5.6) \end{aligned}$$

It can be shown that if F is considered as functional of ρ, i.e. $\hat{F}(\rho)$, then the free energy can be found as the minimum of this functional:

$$\hat{F}(\rho) \geq F, \tag{5.7}$$

where the equality holds when ρ takes its real value at equilibrium. The task is then to construct the free energy function and find its minimum.

There are a number of models for the configurational free energy, for example the generalized Bragg-Williams (BW) model based on single-site averaging or point-clusters, Taylor and Fourier expansions of the free energy, and Landau-Lifshitz theories. More sophisticated approaches include Monte Carlo (MC) simulations and the cluster-variation method (CVM). In general the BW methods are not quantitatively reliable and can yield incorrect phase diagrams which overestimate transition tem-

peratures as much as 50%; in certain circumstances, the BW model is known to give incorrect order of the order-disorder transition [82]. As a rule, the lowest approximation gives the highest critical temperatures for the same set of energy interactions [81]. On the other hand, CVM calculations can have an accuracy within 3% of that for MC, the latter considered the most reliable [82].

5.2 The Cluster-Variation Method

5.2.1 General Description

Let us consider Eq. 5.2. Following the spirit of the Ising model, each microstate corresponds to a particular configuration of the system, compatible with the thermodynamic constraints of the ensemble. Having a lattice with N sites, we define the spin-like variable (or site operator) σ_n, which takes integral values depending on the type of atom located at site n. For example, in binary systems $\sigma_n = 1$ or -1 , while in ternary systems, $\sigma_n = 1$, 0, or -1. Any configuration of the system can be completely specified by the N-dimensional vector: $\boldsymbol{\sigma} = (\sigma_1, \sigma_2, \ldots, \sigma_N)$. Then, the partition function is written as:

$$Z = \sum_{\{\boldsymbol{\sigma}\}} e^{-\beta F_{\boldsymbol{\sigma}}}, \tag{5.8}$$

where $F_{\boldsymbol{\sigma}}$ is the 'nonequilibrium' free energy of the particular configuration $\boldsymbol{\sigma}$. Notice that this energy should account for all the possible 'excitations' compatible with the configuration, such as atomic displacements, vibrational contributions, etc. In what follows, we will assume that these contributions are configuration-independent and can be factored out from the partition function because they will not contribute to the free energy of mixing.

It is clear that the number of different configurations $\{\boldsymbol{\sigma}\}$ is too large to be workable. Thus, we introduce the concept of clusters on the Ising lattice. A cluster α is the set of r points in the lattice. The smallest cluster is a point, the next one a pair, then a triplet, and so on. The largest cluster corresponds to the lattice itself, denoted

by α_N. A configuration on a cluster of r sites is given by $\boldsymbol{\sigma}_r = (\sigma_1, \sigma_2, \ldots, \sigma_r)$. We define a cluster spin or cluster function for every cluster α of $r_\alpha = |\alpha|$ sites as $\sigma_\alpha = \prod_{i\in\alpha}^{r_\alpha} \sigma_i$. We also introduce the correlation function ξ_α defined as the thermodynamic average (or ensemble average) of the cluster function (in the canonical ensemble, the thermodynamic average of a quantity Q is given by $\langle Q \rangle = \mathrm{Tr}\,(\rho Q)$, where Tr is the trace of the operator):

$$\xi_\alpha = \langle \sigma_\alpha \rangle = \underset{\{\boldsymbol{\sigma}\}}{\mathrm{Tr}}\ \rho(\{\boldsymbol{\sigma}\})\sigma_\alpha, \tag{5.9}$$

where now we have made explicit that ρ is a function of the particular lattice configuration (microstate) $\boldsymbol{\sigma}$. Likewise, the density matrix can be expanded in terms of correlation functions [83]:

$$\rho(\{\boldsymbol{\sigma}\}) = \frac{1}{2^N} \sum_\alpha \xi_\alpha \sigma_\alpha. \tag{5.10}$$

The idea of the CVM is to develop an approximate expression for the configurational entropy, $S = -k_B \mathrm{Tr} \rho \ln \rho$, taking into account only the correlations up to a maximal cluster size. These maximal clusters are considered uncorrelated independent species. The derivation of the CVM can be found in several publications (see for instance [15] or [84]). We present here the final equation for the entropy:

$$S = -k_b \sum_{\alpha\subseteq\alpha_M} a_\alpha \underset{\alpha}{\mathrm{Tr}}\ \rho_\alpha \ln \rho_\alpha, \tag{5.11}$$

where the summation is performed over clusters smaller or equal to a maximal cluster α_M. a_α are the so-called Kikuchi-Barker coefficients which only depend on the geometry of the lattice, and ρ_α are the (finite) cluster probabilities. The former are determined using

$$\sum_{\beta\subseteq\alpha_M} a_\beta = 1, \tag{5.12}$$

which is valid for each subcluster of the maximum cluster and the sum extends over all subclusters β of the maximum clusters that contain α. The cluster probabilities ρ_α in Eq. 5.11 are defined as:

$$\rho_\alpha = \underset{\beta\subset\alpha_N/\alpha}{\mathrm{Tr}}\ \rho(\{\boldsymbol{\sigma}\}). \tag{5.13}$$

In the previous equation, the sum is over all the configurations of the sites within α_N but outside α, i.e. within the set α_N/α. Replacing $\rho(\{\boldsymbol{\sigma}\})$, by Eq. 5.10 above, we obtain:

$$\rho_\alpha = \underset{\alpha_N/\alpha}{\mathrm{Tr}} \frac{1}{2^N} \sum_\beta \xi_\beta \sigma_\beta = \sum_\beta \xi_\beta \frac{1}{2^N} \underset{\alpha_N/\alpha}{\mathrm{Tr}} \sigma_\beta = \frac{1}{2^{|\alpha|}} \sum_{\beta \subset \alpha} \xi_\beta \sigma_\beta, \tag{5.14}$$

where $|\alpha|$ is the number of sites in cluster α.

In practice, the CVM is implemented for particular ordered phases of the parent lattice one at a time (for instance the $B2$ phase in the bcc lattice). This reduces the infinite number of cluster probabilities ρ_α to a finite number. The cluster probabilities are then written in terms of correlation functions ξ_α according to Eq. 5.14, and the free energy is minimized with respect to these new variables.

5.2.2 Implementation of the CVM on Binary Systems

Having just presented the CVM expression for the configurational entropy, Eq. 5.11, we should now consider the internal energy, U. This quantity will be approximated by the energy of the ground-state, i.e. we neglect its temperature dependence. Within the CPA-GPM formalism this energy is given by:

$$U = \Delta E_{dis}^{\mathrm{CPA}} + \Delta E_{ord}^{\mathrm{GPM}} \tag{5.15}$$

In terms of pair-correlation functions, the ordering energy for binary alloys can be rewritten as:

$$\Delta E_{ord}(\{\xi_s\}) = \frac{1}{2} \sum_s z_s V_s(c) (\xi_s - \xi_s^R) \tag{5.16}$$

where z_s is the coordination number in the s'th shell, V_s the effective pair interaction and ξ_s^R the pair-correlation function for the random state, $\xi_s^R = (2c-1)^2$. We can now write the final form of the CVM free energy functional, for a particular structure:

$$F(\{\xi_\alpha\}, c, T) = \Delta E_{dis}(c) + \Delta E_{ord}(\{\xi_s\}, c) + k_b T \sum_{\alpha \subseteq \alpha_M} \mu_\alpha a_\alpha \mathrm{Tr}_\alpha \rho_\alpha \ln \rho_\alpha, \tag{5.17}$$

where μ_α is the multiplicity of the cluster type α in an unit cell. The cluster probability can be written as:

$$\rho_\alpha = \frac{1}{2^{|\alpha|}} [1 + \sum_{\beta \in \alpha, \beta \neq \emptyset} v(\beta, \alpha)\, \xi_\alpha \ ], \tag{5.18}$$

where $|\alpha|$ is the number of lattice points in the cluster α, $\emptyset$ is the empty cluster, and the matrix $v(\beta, \alpha)$ is known as the 'V-matrix'. This matrix is unique to the particular crystal structure and needs to be computed only once for a given CVM approximation (maximal cluster).

Minimization of the free energy, Eq. 5.17, with respect to the correlation functions was performed with the Newton-Raphson method. Because the disordered energy and EPI's are concentration-dependent, we have fitted calculated values to spline functions of the concentration and used their derivatives in the minimization.

The CVM was applied to Ru-Zr and Pd-Zr bcc-binary alloys. We used the tetrahedron approximation in the bcc lattice, i.e., the maximal cluster is a tetrahedron which includes first- and second-nearest neighbors. The experimental phase diagram for Ru-Zr is well characterized [85]. It shows the presence of only two compounds: a very stable $B2$ intermetallic compound near 50% Zr, and a Laves phase $C14$ with a Ru_2Zr structure at high temperature. The phase diagram we have obtained for the bcc-based lattice, Fig. 5-1(a), reproduces the $B2$ structure. The fact that the $B2$ intermetallic remains stable far above the melting point (2130°C) precludes a direct comparison of the calculated transition temperatures with the experiment.

The experimental Zr-Pd phase diagram [85] depicts a series of intermetallic compounds, Pd_3Zr ($D0_{24}$), Pd_2Zr ($C11_b$), and $PdZr_2$ ($C11_b$), none of them based in the bcc structure. It also shows a ZrPd phase with the structure $A1$ (fcc) as strictly stoichiometric and melting congruently at 1600°C. There is now wide evidence [12] that a $B2$-type structure is stable at temperatures above about 670°C. Our phase diagram Fig. 5-1(b) reproduces the $B2$ structure and we have also found a $D0_3$ structure below about 1800°C in Pd-rich alloys.

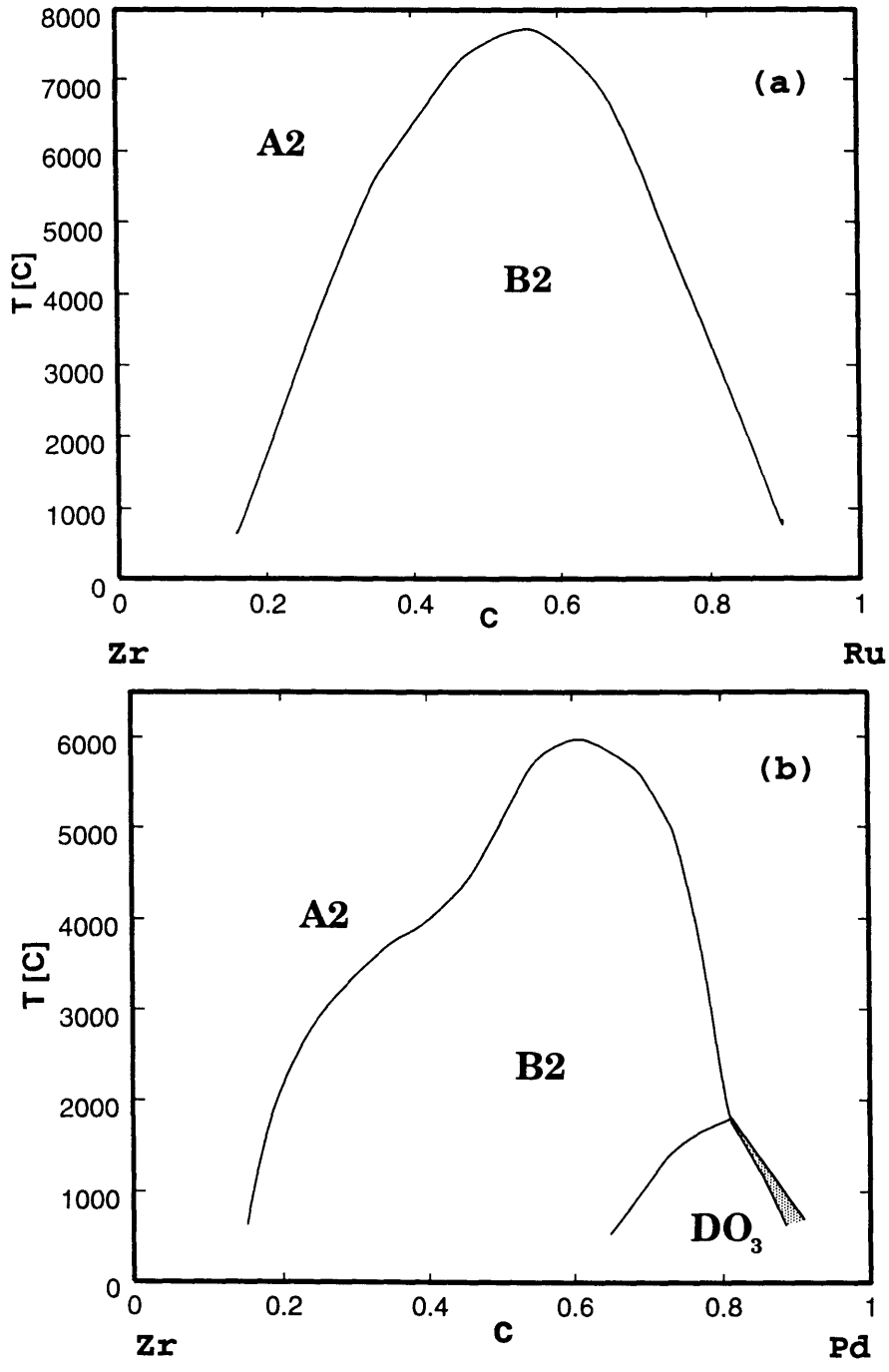

Figure 5-1: Phase diagrams computed with the CVM in the tetrahedron approximation: (a) Ru-Zr alloy, (b) Pd-Zr alloy.

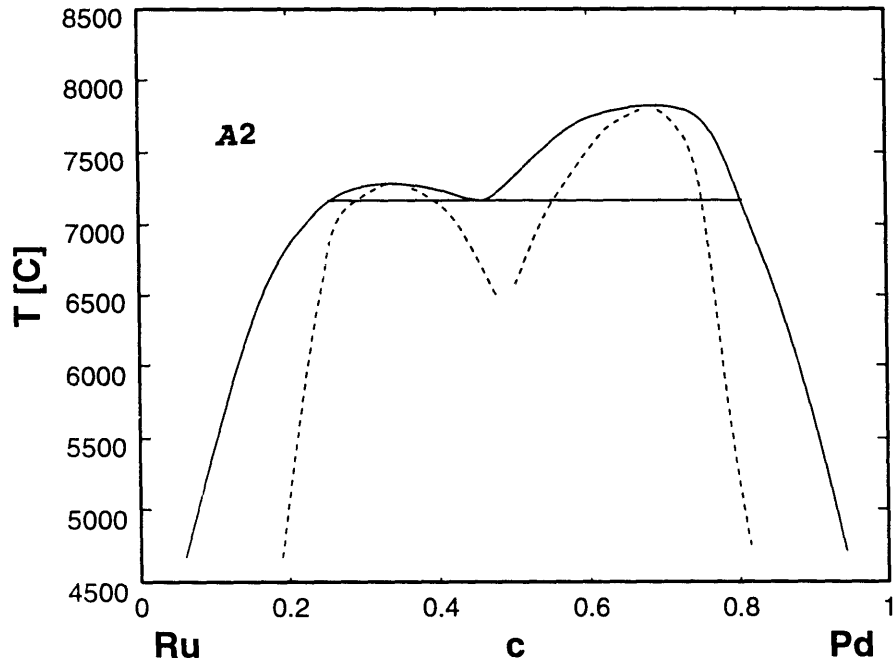

Figure 5-2: Phase diagram of the bcc-based Ru-Pd alloy computed with the CVM in the tetrahedron approximation.

The calculated bcc-based phase diagram for Ru-Pd, shown if Fig. 5-2, presents a miscibility gap at low temperature. This is expected from the positive energy of mixing (and negative pair interactions) between Ru and Pd as computed in the previous chapter. Qualitatively, this result agrees with the observed phase diagram, although the phases involved in the real system are hcp (Ru) and fcc (Pd).

5.2.3 Application to Pseudo-binary Alloys

The case of the ternary Zr-Ru-Pd alloy was limited to the study of the equilibrium properties of the $Zr_{0.5}(Ru,Pd)_{0.5}$ system. From the ground-state analysis we would expect this ternary system to phase separate in two $B2$ phases. Thus, we populated one sublattice fully with Zr and studied the stability of Ru-Pd in the second sublattice. We then applied the CVM to this sublattice taking the simple-cube as the maximal cluster. Twenty-one correlation functions are necessary to describe the equilibrium configuration for the phase separating system in this approximation. Figure 5-3 shows

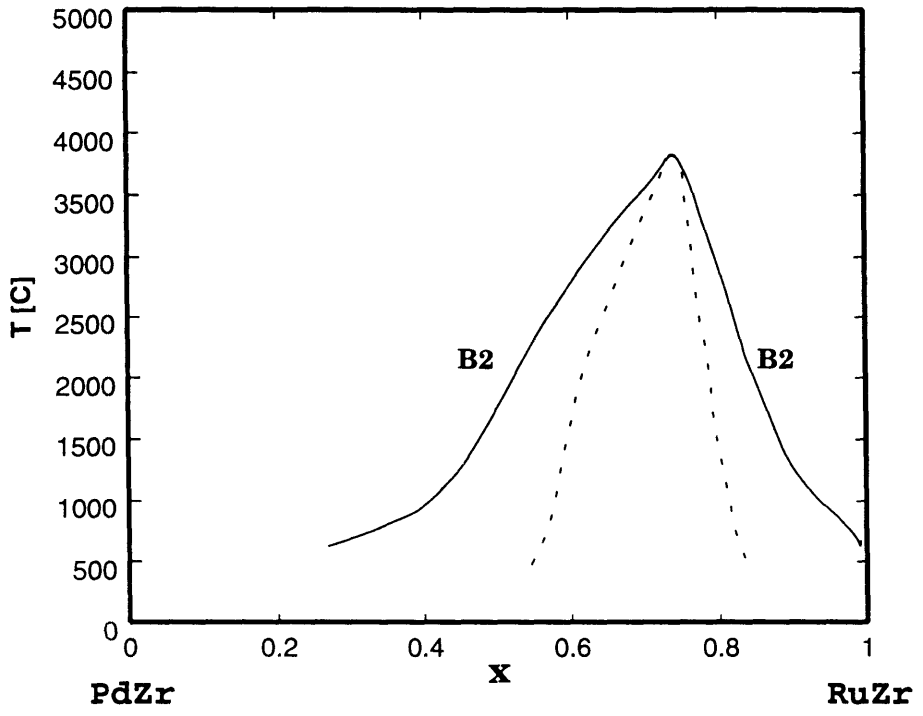

Figure 5-3: Phase diagram for the pseudo-binary system $Zr_{0.5}(Ru_xPd_{(1-x)})$ computed with the CVM in the simple cube approximation. The dashed line correspond to the spinodal line

the results we obtained for this pseudo-binary system using effective pair interactions $\tilde{V}_j^{\mathrm{RuPd}}$ calculated with the GPM applied to the partial CPA medium, as described in the previous chapter. The interactions are all negative, which is consistent with the phase diagram having a miscibility gap at low temperatures, that is a $B2/B2$ phase separation. Experimentally, the system has been only characterized by a $B2$ solid solution on the Ru-rich side at low temperature [11, 12]. In the following section we will see how the two-phase field could explain the observed behavior of the electronic specific heat in these alloys.

5.3 Calculation of the Electronic Specific Heat

If there is one theme we want to emphasize in this thesis, it is the close relationship between electronic structure and ordering phenomena in alloys. One goal is to predict the occurrence and type of ordering from the knowledge of the electronic structure.

At the same time, we want to study how ordering can influence certain electronic properties. One possible macroscopic observable to consider is the linear coefficient of the low-temperature specific heat, γ, which is related to the properties of the electrons at the Fermi energy. Usually the specific heat of a metal or an alloy obeys the law:

$$C(T) = \gamma T + \beta T^3 + \cdots, \tag{5.19}$$

where the first term is the electronic contribution, and the second term is the lattice (phonon) contribution. The coefficient γ turns out to be proportional to the density of states at the Fermi energy [88], $n(E_F)$:

$$\gamma = \frac{\pi^2}{3} k_b^2 \, n(E_F), \tag{5.20}$$

where k_b is the Boltzmann constant. Actually, the electron-phonon coupling (λ_{e-p}) and the spin fluctuations (λ_{sf}) can increase the bare DOS and γ is given by [86]

$$\gamma = \frac{\pi^2}{3} k_b^2 \, (1 + \lambda_{e-p} + \lambda_{sf} + \cdots) \, n(E_F). \tag{5.21}$$

Figure 5-4 shows the variation of the electronic specific heat coefficient γ with composition for the pseudo-binary $Zr_{0.5}(Ru_{1-x}Pd_x)_{0.5}$ as obtained from low-temperature calorimetry [87]. It shows a fairly linear increase of γ with composition until it drops around x=0.68 where a martensitic transformation takes place. This behavior has been observed in similar $B2$-type pseudo-binaries. For instance, γ for $Ti_{0.5}(Ni,Fe)_{0.5}$ presents a rounded peak around the concentration where the martensitic transformation takes place, whereas in $Ti_{0.5}(Ni,Os)_{0.5}$ and $Ti_{0.5}(Ni,Ru)_{0.5}$ the rounded peak is larger and can be thought of as forming a "plateau" like in the $Zr_{0.5}(Ru,Pd)_{0.5}$ case [86].

Assuming that the electron-phonon coupling and spin fluctuations are constant upon alloying, we could explain the linear behavior if we think of the alloy as being phase separated into two $B2$ phases, PdZr and RuZr, i.e. the coefficient γ for the alloy would be simply given by the concentration-weighted average of γ(RuZr) and γ(PdZr).

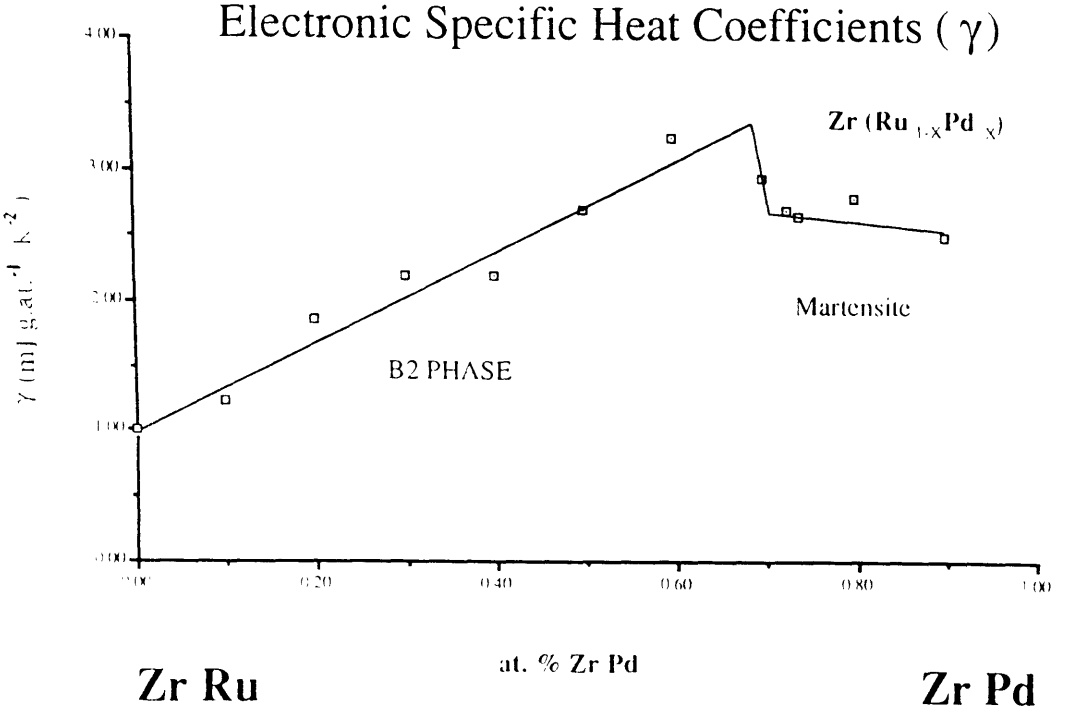

Figure 5-4: Electronic specific heat coefficient in mJ(g at)$^{-1}$ K^{-2}

Curve (b) in Fig. 5-5 shows the $n(E_F)$ that corresponds to a phase separating system for which the total DOS was computed as the concentration-weighted average of the DOS's of the two $B2$-type binary alloys RuZr and PdZr. We confirmed a fairly linear increase of $n(E_F)$ with composition. Furthermore, after converting the appropriate units, the rate of increase (taking only the end points) agrees to within 15% of the measured one.

Using the partial CPA we also calculated the DOS for the partially ordered alloy and plotted $n(E_F)$ versus composition (see Fig. 5-5, curve (a)). The calculated $n(E_F)$ flattens out towards the Pd-rich size. We can explain this behavior by examining the variation of the Fermi surface between RuZr and PdZr $B2$-type alloys. Figures 5-6 and 5-7 show the band structure and Fermi surface cuts for the two compounds. The band structure of RuZr displays a virtual gap at the Fermi level in the M-Γ-R-X plane, while the sixth band barely touches the Fermi level at the X point. As the concentration of Pd increases the Fermi level will "move" upwards, cutting through higher energy bands and increasing the number of valence electrons. At a certain

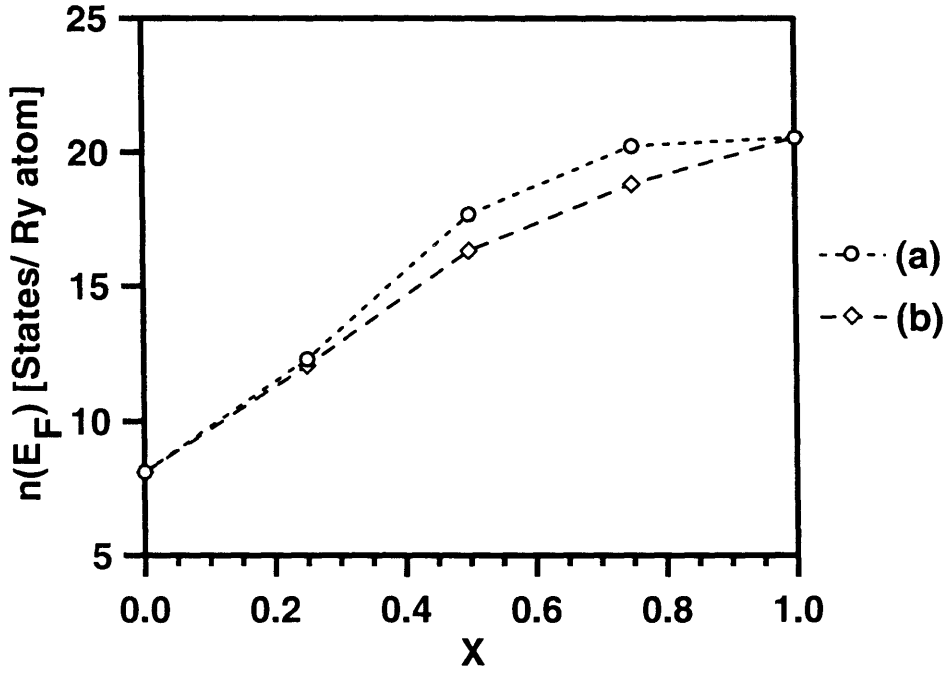

Figure 5-5: DOS (in States/ Ry atom) at the Fermi energy for (a): $Zr_{0.5}(Pd_xRu_{1-x})_{0.5}$ from a partial CPA computation, and (b): $(PdZr)_x^{B2}(RuZr)_{1-x}^{B2}$. See text.

composition the number of states at the Fermi energy levels off until the composition reaches the PdZr alloy.

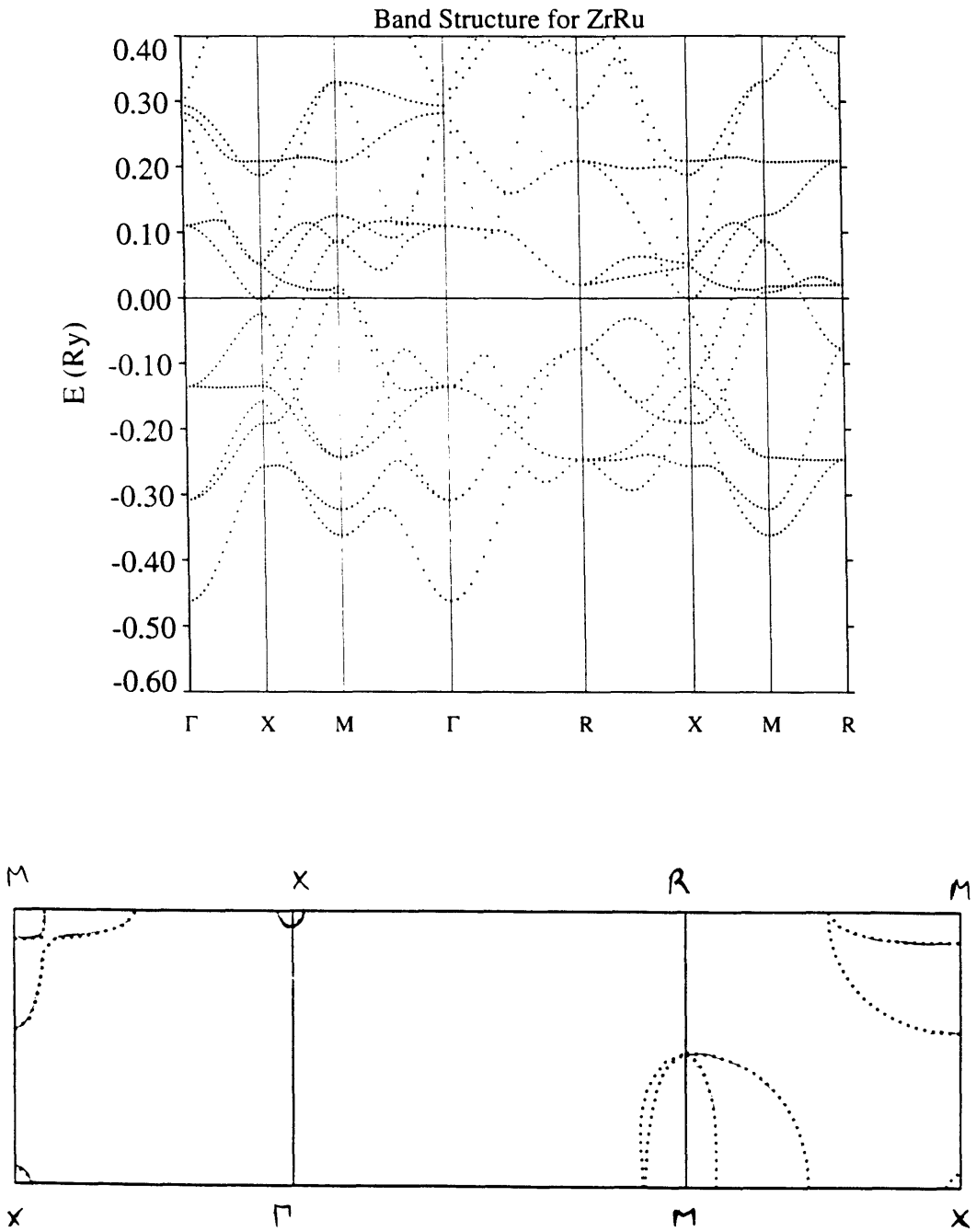

Figure 5-6: Band structure along special directions of the sc Brillouin Zone and Fermi surface cuts for the *B*2-phase of RuZr.

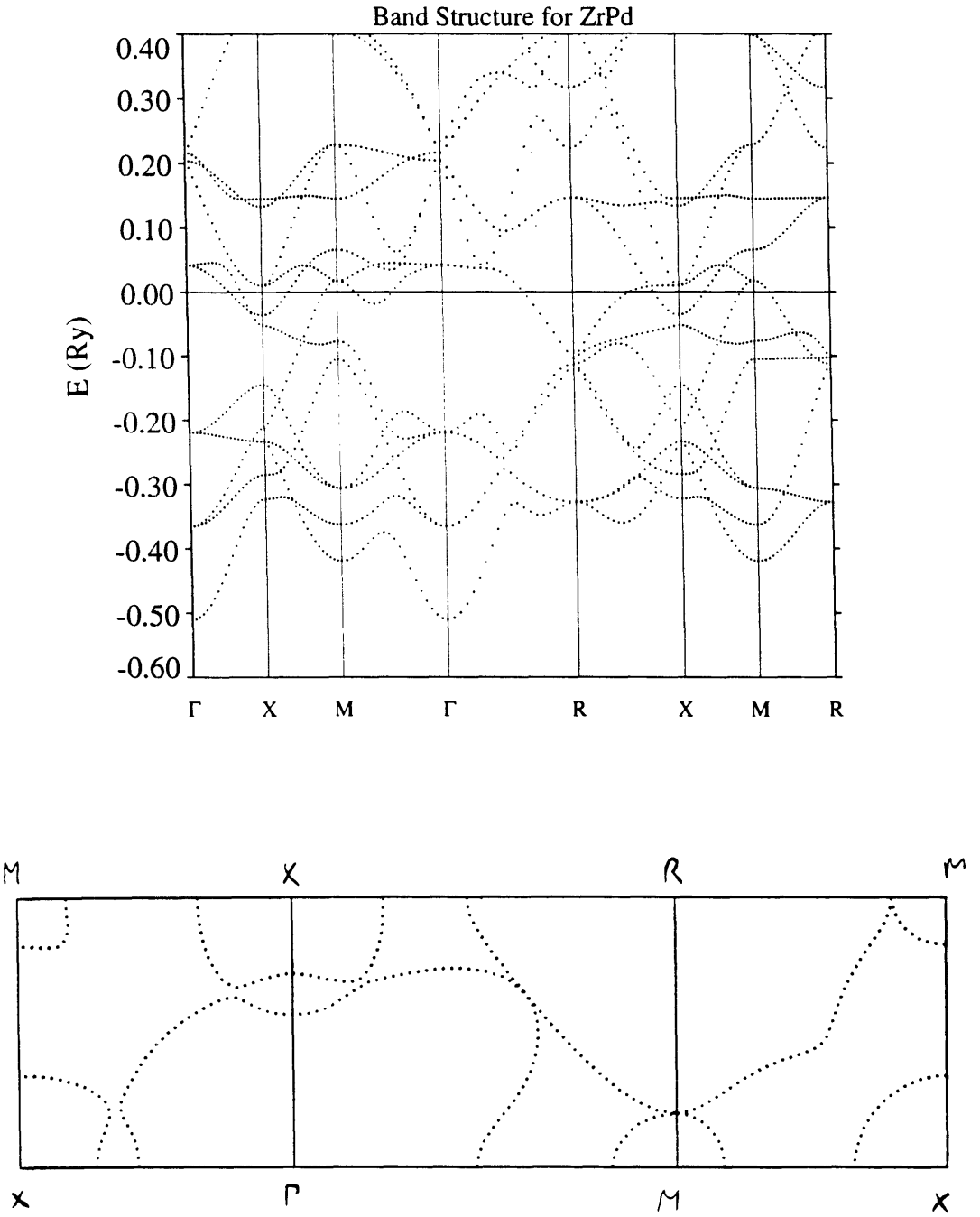

Figure 5-7: Band structure along special directions of the sc Brillouin Zone and Fermi surface cuts for the $B2$-phase of PdZr.

5.4 Conclusions

Using energetic parameters obtained with the TB-CPA-GPM model, we have applied the cluster-variation method to compute bcc-based phase diagrams of binary Ru-Zr, Pd-Zr, and Ru-Pd alloys, and pseudo-binary $Zr_{0.5}$(Ru,Pd) alloys. Qualitatively, the equilibrium phases that were obtained for the binary systems agree with the experimental phase diagrams. Based on the ($B2$)+$B2$) two-phase field predicted for the ternary alloy, we proposed an explanation for the observed variation of the electronic specific heat coefficient, γ, with composition in $Zr_{0.5}$(Ru,Pd) alloys.

Chapter 6

Summary and Conclusions

The study of alloy phase equilibria from 'first-principles' requires two distinctive components: the computation of the electronic structure of the system leading to band energies and interaction parameters, and the determination of ground states and phase diagrams by solving the Ising model using some appropriate method. The emphasis of this thesis has been mainly on the first point. The formalism we have presented was based on the tight-binding approximation. We have shown how this simple approximation can provide a qualitative solution to the problem of determining the stable structure for metals through the study of the first few moments of the electronic density of states. In addition, this formalism provided the basis for an efficient total-energy model using the linearized Green's function method based on the recursion technique.

Even though the implementation of fully self-consistent calculations has improved considerably in recent times, the use of a reliable and computational efficient TB approximation is still very much sought for the study of complex structures and large-scale simulations. To obtain reliable quantitative results we have described a new scaling of the TB parameters based on LMTO-ASA calculations, and we have demonstrated good agreement of the band structure and DOS with the *ab initio* results. We applied the CPA-GPM formalism within this TB frame to study binary and ternary alloys and presented a novel approximation to the cluster CPA coupled with the GPM to study partially ordered alloys. The TB-CPA-GPM approach has

proven to give an efficient description of the electronic structure of alloys and we have shown that it can be used to design or modify alloys to achieve desired properties.

Finally, we have used the energetic parameters from the TB-CPA-GPM combined with the CVM to compute phase diagrams of binary and pseudo-binary systems. The predicted bcc ordered phases and phase separation tendencies for the binary systems agree quantitatively with the experimental results. We have also shown how, in the case of the particular alloy, $Zr_{0.5}$(Ru,Pd), the results can explain the behavior of the specific heat coefficient γ or what is similar, of $n(E_F)$.

The following diagram illustrates how the alloy methods we touch upon in this work connect with each other. It can also serve as a flow-chart for performing phase equilibria computations:

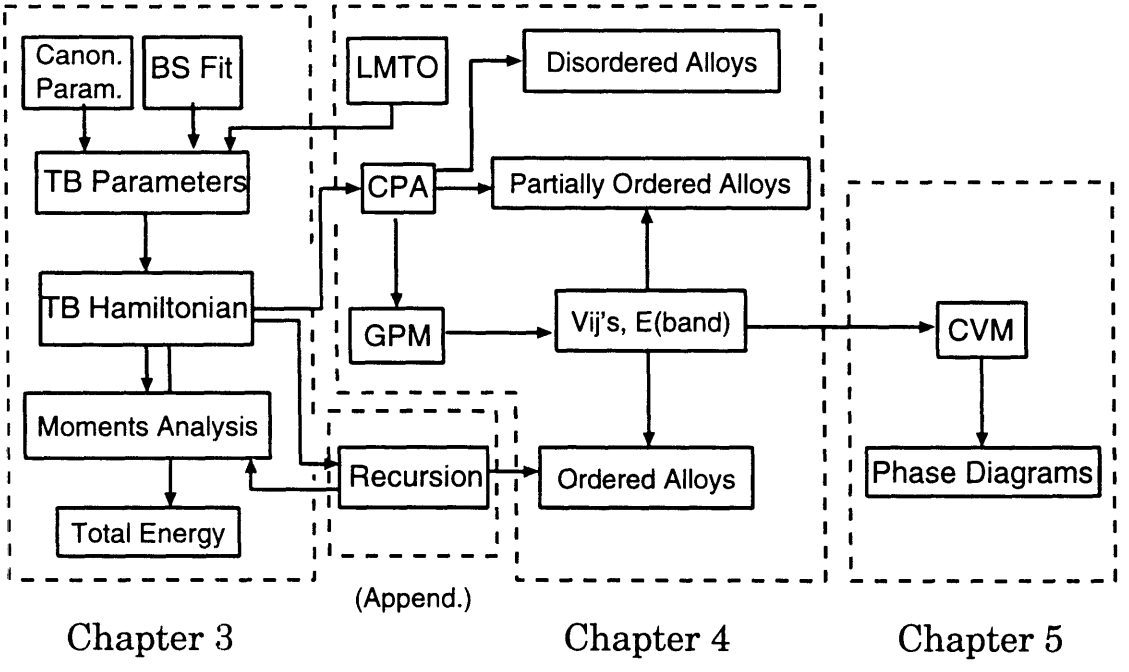

In conclusion, the main points we have laid out in this dissertation are:

- An analysis of the moments of the DOS computed with the recursion method using a canonical TB model along the Bain transformation. We have shown the relevance of the fifth moment to determining the relative stability of the metal phases.

- A model for total-energy calculation using the linearized Green's function method to compute the band contribution and a Born-Mayer type potential for the repulsive contribution. A sixth-moment approximation of the density of states seems to be sufficient to reproduce the energetics of the "exact" recursion method. This model can have important applications in molecular dynamics simulations that look for reliable, yet tractable models to describe the energetics of sizable systems.

- The study of the electronic structure of a ternary system within the CPA-GPM framework, based on a TB approximation, including the description of a new scaling of the TB parameters obtained from LMTO calculations. The DOS and band structures are in good agreement with the *ab initio* results. The TB-CPA-GPM scheme proved to be a consistent and reliable way to treat the alloy problem, and it has the capability of assisting in the design of materials with specific electronic properties. The study also included a novel formalism to study partially ordered alloys, based in a simplification of the cluster CPA.

- An application of the interaction parameters and energies obtained with the TB-CPA-GPM approach to the study the phase diagram of Zr-Ru-Pd alloys using the CVM. The results are consistent with the bcc-based phases found experimentally for the binary constituents. The two-phase field found for the ternary $Zr_{0.5}$(Ru,Pd) alloys can explain the observed behavior of the linear coefficient of the electronic specific heat in these alloys.

Chapter 7

Suggestions for Future Research

• Recent studies have tried to explain the occurrence of martensite phase transformations of some transition-metal alloys by studying special features of the band structure of the β-phase showing up in the Fermi surface, leading to a softening of particular branches of the phonon spectra (for instance, calculations have been performed on NiTi [89, 90], Ni_xAl_{1-x} [91], and PdTi [90]). It has been shown that for a phonon $\mathbf{q_1}$ going soft, the dynamical matrix of phonons $\xi(\mathbf{q})$ must have a maximum at $\mathbf{q} = \mathbf{q_1}$. For that purpose, there must be nesting regions in the Fermi surface which are connected by $\mathbf{q_1}$ and produce a maximum in the generalized susceptibility of non-interacting electrons $\chi_o(\mathbf{q})$. A second condition for a maximum of $\xi(\mathbf{q})$ is a saddle point of the Fermi surface in the direction of the vector $\mathbf{q_1}$ connecting the nesting hole and the electron Fermi surface regions. In most of these cases, these phonon anomalies and nesting features depend on the concentration, temperature and applied stress, and occur at those phonon wave vectors related to the transformation displacements. Although *ab initio* methods can easily evaluate the electronic structure of ordered compounds, the consideration of concentration changes or disorder requires further approximations. We believe that the TB-CPA approach outlined in this thesis, including the treatment of partially ordered alloys, can be successfully applied to study the electronic origin of the martensite transformation in $Zr_{0.5}(Ru_xPd_{1-x})$ alloys and similar systems.

- Obtaining phase diagrams from first-principles calculations is a long standing dream and continuing objective for material scientists. Most of the work of the past decades has been confined to binary systems. The CVM formalism using the GPM interactions can be extended to the full ternary alloys. As we mentioned in the introduction of Chapter 3, there are several works in the literature which have applied an extension of the CVM to study a small collection of ternary systems, using a limited number of phases. Additional work must be done to handle the concentration-dependent interactions that would require, for instance, a good interpolation scheme on the Gibbs triangle. The main problem, though, remains in designing a reliable scheme to compute the equilibrium phases, i.e., while *binary* phase diagram computations have to deal with common-tangent constructions on free energy *curves*, common tangential *planes* on free energy *surfaces* are needed for *ternary* phase diagrams. The implementation of Monte Carlo simulations on ternary systems may be also worth exploring.

Appendix A

The Recursion Method

We have seen that the local density of states can be obtained as a diagonal element of the Green's function. One technique to compute these elements is the recursion method [92]. The basic idea of the method is to tridiagonalize the Hamiltonian matrix by replacing the atomic-orbital basis by a new basis $\{|u_1\rangle, |u_2\rangle, \cdots\}$ such that

$$H = \begin{pmatrix} a_1 & b_1 & 0 & 0 & \cdots \\ b_1 & a_2 & b_2 & 0 & \cdots \\ 0 & b_2 & a_3 & b_3 & \cdots \\ 0 & 0 & b_3 & a_4 & \cdots \\ \vdots & \vdots & \vdots & \vdots & \ddots \end{pmatrix}. \tag{A.1}$$

The basis is chosen to be orthonormal. It can be shown that the diagonal element $\langle u_1|G|u_1\rangle$ can be expressed in terms of a continued fraction

$$\langle u_1|G(z)|u_1\rangle = G_{11}(z) = \cfrac{1}{z - a_1 - \cfrac{b_1^2}{z - a_2 - \cfrac{b_2^2}{z - \cdots}}}. \tag{A.2}$$

The recursion method directly computes the coefficients a_i and b_i. Using the new orbital basis it is not difficult to prove the following recursive equation

$$H|u_n\rangle = a_n|u_n\rangle + b_{n-1}|u_{n-1}\rangle + b_n|u_{n+1}\rangle \tag{A.3}$$

with $b_0|u_0\rangle = 0$. We also have

$$a_n = \langle u_n|H|u_n\rangle, \tag{A.4}$$

and

$$b_{n-1} = \langle u_{n-1}|H|u_n\rangle = \langle u_n|H|u_{n-1}\rangle. \tag{A.5}$$

Defining the vectors $|\tilde{u}_n\rangle = b_{n-1}|u_n\rangle$ and replacing in Eq. A.3, we obtain

$$|\tilde{u}_{n+1}\rangle = (H - a_n)|u_n\rangle - b_{n-1}|u_{n-1}\rangle. \tag{A.6}$$

We notice that

$$b_n = \langle \tilde{u}_{n+1}|\tilde{u}_{n+1}\rangle^{1/2}, \tag{A.7}$$

so that

$$|u_{n+1}\rangle = \frac{|\tilde{u}_{n+1}\rangle}{\langle \tilde{u}_{n+1}|\tilde{u}_{n+1}\rangle^{1/2}}. \tag{A.8}$$

Applying recursively Eqs. A.4, A.6, A.8 and A.7, we can obtain $a_n, |\tilde{u}_n\rangle, |u_{n+1}\rangle$ and b_n. To start the recursion we have to select the first eigenvector $|u_1\rangle$. We usually choose it as the orbital from which we want to compute the density of states, that is, $|u_1\rangle = |n, \lambda\rangle$. The recursion method has proven to be very efficient and numerically stable. It is obvious that the continuous fraction must be truncated after a finite number of steps (usually 10 to 30). The analytical continuation of the continuous fraction has been extensively studied and a number of techniques are reported in the literature [93]. Off-diagonal elements of the Green's function can also be obtained with this method: from the identity

$$(\langle u_n| + \langle u_m|)G(|u_n\rangle + |u_m\rangle) = \langle u_n|G|u_n\rangle + \langle u_m|G|u_m\rangle + 2\langle u_n|G|u_m\rangle, \tag{A.9}$$

we can obtain $\langle u_n|G|u_m\rangle$. In this case it is necessary to run the recursion method three times, once for each $|u_n\rangle$, $|u_m\rangle$, and $(|u_n\rangle + |u_m\rangle)$.

Physically, the Hamiltonian in Eq. A.3 connects the state $|u_1\rangle = |n, \lambda\rangle$ at a central site (whose local DOS we want to obtain) to the nearby atoms limited by the range

of the Hamiltonian (i.e., transfer integrals), producing an orbital $|u_2\rangle$ that extends over these neighboring sites. As the recursion progresses, the subsequent states, $|u_3\rangle$, $|u_4\rangle$,... , $|u_k\rangle$,... extend further and further from the central site while their contribution to the DOS decreases as k increases.

A clear advantage of the recursion method is that it does not require a periodic lattice, making it suitable to study non-periodic systems such as amorphous materials and surfaces. It also provides an analytical form for describing the Green's function which is convenient to calculate derived quantities such as integrated DOS and band energies.

Bibliography

[1] W. Kohm and L. J. Sham, 1965, Phys. Rev. **140**, p. 1133.

[2] P. Hohenberg and W. Kohn, 1964, Phys. Rev. **136**, p. 864.

[3] J. Friedel, 1969, Physics of Metals I: Electrons, ed. J. M. Ziman, (Cambridge University Press, Cambridge) p. 340.

[4] D. G. Pettifor, 1987, in Solid State Physics V. 40, eds. H. Ehrenreich, F. Seitz and D. Turnball, (Academic Press, New York), p. 43.

[5] R. Car and M. Parrinello, 1985, Phys. Rev. B **55**, p. 2471.

[6] C. Z. Wang, K. M. Ho C. T. Chan, 1994, Comput. Matter. Sci. **2**, p. 93, and refs. therein.

[7] Ahmet Isik, 1994, Ph.D. Thesis, MIT, unpublished.

[8] R. Kikuchi, 1950, Phys. Rev. **79**, p. 718.

[9] R. Kikuchi, 1951, Phys. Rev. **81**, p. 988.

[10] K. Binder, 1986, in Monte Carlo Methods in Statistical Mechanics, Topics in Current Physics Vol. 7, ed. K. Binder, (Springer, Berlin), p. 1.

[11] R. M. Waterstrat, 1993, Platinum Metals Rev. **37**, p. 194.

[12] R. M. Waterstrat, L. A. Bendersky, and R. Kuentzler, 1992, Mat. Res. Soc. Symp. Proc. **246**, p. 115.

[13] D. A. Papaconstantopoulos, 1986, Handbook of the Band Structure of Elemental Solids, (Plenum. New York).

[14] O. K. Andersen, O. Jepsen, and D. Glotzel, 1985, in Highlights of Condensed Matter Theory, eds. F. Bassani, F. Fermi and M. P. Tosi, (North-Holland, Amsterdam), p. 59.

[15] F. Ducastelle, 1991, Order and Phase Stability in Alloys, eds. F. R. de Boer and D. G. Pettifor, Cohesion and Structure Series V3, (North-Holland, Amsterdam).

[16] J. C. Slater and G. F. Koster, 1954, Phys. Rev. **94**, p. 1498.

[17] F. Cyrot-Lackmann, 1968, J. Phys. Chem. Solids **29**, p. 1235.

[18] Adrian P. Sutton, 1993, Electronic Structure of Materials, (Oxford Science Publications, Oxford).

[19] P. Turchi, 1984, Thèse de Doctorat d'Etat, Université Paris VI, unpublished.

[20] F. Ducastelle and F. Cyrot-Lackmann, 1971, J. Phys. Chem. Solids **32**, p. 285.

[21] P. E. A. Turchi, 1990, Materials Science and Eng. **A127**, p. 145.

[22] M. S. Daw and M. I. Baskes, 1984, Phys. Rev. B **29**, p. 6443.

[23] S. M. Foules, 1993, Phys. Rev. B **48**, p. 4287.

[24] W.Matthew C. Foulkes and Roger Haydock, 1989, Phys. Rev. B **39**, p. 12520.

[25] K. Masuda, N. Hamada and K Terakura, 1984, J. Phys. F: Met Phys. **14**, p. 47.

[26] P. Turchi and F. Ducastelle, 1984, Continued Fractions and Perturbation Theory: Applications to Tight Binding Systems, Paper presented at the Conference "The Recursion Method and its Applications" (London).

[27] J. P. Hirth and L. Lothe, 1965, Theory of Dislocations, (McGraw-Hill, New York).

[28] Michael J. Mehl, 1993, Phys. Rev. B **47**, p. 2493.

[29] F. Ducastelle, 1991, in Computer Simulation in Materials Science, eds. M. Meyer and V. Pontikis, (Kluwer, Dordrecht), p. 233.,

[30] D. G. Pettifor, 1989, Phys. Rev. Lett. **63**, p. 2480.

[31] P. E. A. Turchi, private communication.

[32] W. L .Bragg and E. J. Williams, 1934, Proc. Roy. Soc. A **145**, p. 699; 1935, A **151**, p. 540; 1935, A **152**, p. 231.

[33] A. Gonis, X.-G. Zhang, A. J. Freeman, P. Turchi, G. M. Stocks, and D. M. Nicholson, 1987, Phys. Rev. B **36**, p. 4630, and refs. therein.

[34] F. Ducastelle and F. Gautier, 1976, J. of Phys. F: Mat. Phys. **6**, p. 2036.

[35] J. W. D. Connolly and A. R. Williams, 1983, Phys. Rev. B **27**, p. 5169.

[36] H. Dreyssé, A. Berera, L. T. Wille, and D. de Fontaine, 1989, Phys. Rev. B **39**, p. 2442.

[37] J. L. Meijering, 1950, Philips Res. Rep. **5**, p. 333.

[38] J. L. Meijering, 1951, Philips Res. Rep. **6**, p. 183.

[39] T. Nishizawa, S. M. Hao, M. Hasebe, and K. Ishida, 1983, Acta Metall. **31**, p. 1403.

[40] Masuhiro Fukaya, Toru Miyazaki, Pi Zhi Zhao, and Takao Kozakai, 1990, J. Mater. Sci. **25**, p. 522.

[41] Masuhiro Fukaya, Toru Miyazaki, and Takao Kozakai, 1991, J. Mater. Sci. **26**, p. 5420.

[42] K. F. Wojciechowski, 1958, Acta Metall. **6**, p. 396.

[43] K. F. Wojciechowski, 1959, Acta Metall. **6**, p. 376.

[44] M. Schoijet and L. Muldawer, 1970, Bull. Am. Phys. Soc. **15**, p. 360.

[45] S. Hosoya, 1954, J. Phys. Soc. Japan **4**, p. 489.

[46] S. Matsuda, 1953, J. Phys. Soc. Japan **8**, p. 20.

[47] D. C. Chrzan and L. M. Falicov, 1988, Phys. Rev. B **37**, p. 3894.

[48] R. Kikuchi, J. M. Sanchez, D. de Fontaine and H. Yamauchi, 1990, Acta Metall. **28**, p. 651.

[49] C. Colinet, G. Inden and R. Kikuchi, 1993, Acta Metall. Mater. **45**, p. 1109.

[50] G. Inden and W. Pitsh, 1991, in Phase Transformations in Materials, Vol. 5, ed. P. Haasen, (Verlag Chemie, Weinheim).

[51] A. J. S. Traiber, 1991, Master of Science in Materials Science Thesis, MIT, unpublished.

[52] C. Wolverton and D. de Fontaine, 1994, Phys. Rev. B **49**, p. 12351.

[53] C. Wolverton and D. de Fontaine, 1994, Phys. Rev. B **49**, p. 8627.

[54] M. Sluiter, P. Turchi, Fu Zezhong, and D. de Fontaine, 1988, Phys. Rev. Lett. **60**, p. 716.

[55] M. Sluiter and P. E. A. Turchi, 1991, Phys. Rev. B **43**, p. 12251.

[56] C. Colinet and A. Pasturel, 1993, Physica B **192**, p. 238.

[57] G. Rubin and A. Finel, 1993, J. Phys.: Condens. Matter. **5**, p. 9105.

[58] J. M. Sanchez, J. P. Stark, and V. L. Moruzzi, 1991, Phys. Rev. B **44**, p. 5411.

[59] Z. W. Lu, S.-H. Wei, A. Zunger, S. Frota-Pessoa, and L. G. Ferreira, 1991, Phys. Rev. B **44**, p. 512.

[60] C. Colinet, J. Eymery, A. Pasturel, A. T. Paxton , and M. van Schilfgaarde, 1994, J. Phys.: Condens. Matter **6**, p. L47.

[61] G. D. Garbulsky and G. Ceder, 1994, Phys. Rev. B **49**, p. 6327.

[62] H. Jone and N.F. Mott, 1937, Proc. Roy. Soc. A **162**, p. 49.

[63] G. C. Fletcher, 1952, Proc. Phys. Soc. (London) A **65**, p. 192.

[64] V. Rosato, M. Guillope, and B. Legrand, 1989, Phil. Mag. A **59**, p. 321.

[65] Fabrizio Cleri and Vittorio Rosato, 1993, Phys. Rev. B **48**, p. 22.

[66] L. Goodwin, A. J. Skinner, and P. G. Pettifor, 1989, Europhys. Lett. **9**, p. 701.

[67] James L. Mercer. Jr. and M. Y. Chou, 1993, Phys. Rev. B **47**, p. 9366.

[68] Marcel H. F. Sluiter and Prabhakar P. Singh, 1994, Phys. Rev. B **49**, p. 10918.

[69] Hiroyuki Shiba, 1971, Prog. Theor. Phys. **46**, p. 77.

[70] Paul Soven, 1967, Phys. Rev. **156**, p. 809 ; B. Velicky, S. Kirkpatrick, and H. Ehrenreich, 1968, Phys. Rev. **175**, p. 747.

[71] D. J. Chadi and M. L. Cohen, 1973, Phys Rev. B **8**, p. 5747.

[72] A. Gonis, P. E. A. Turchi, X. G. Zhang, G. M. Stocks, D. M. Nickolson, W. H. Butler, 1989, in Atomistic Simulation of Materials, eds. V. Vitek and D. J. Srolovitz, (Plenum, New York), p. 15.

[73] G. Ceder, 1993, Comput. Mater. Sci. **1**, p. 144.

[74] F. Ducastelle, 1989, in Alloy Phase Stability, eds. G.M. Stocks and A. Gonis, (Kluwer, Boston), p. 293.

[75] A. Bieber and F. Gautier, 1981, Physica **107A**, p. 71.

[76] A. Gonis, 1992, Green's Functions for Ordered and Disordered Systems, chap. 9, (North-Holland, Amsterdam).

[77] William H. Butler, 1973, Phys. Rev. B **8**, p. 4499.

[78] Jian-hua Xu and A. J. Freeman, Phys. Rev. B **40**, p. 11927.

[79] S. M. Allen and J. W. Cahn, 1972, Acta Metall. **20**, p. 423.

[80] Ariel J. S. Traiber and Samuel M. Allen, 1992, Acta Metall. Mater. **40**, p. 1403.

[81] D. de Fontaine, 1979, in Solid State Physics V. 34, eds. H. Ehrenreich, F. Seitz and D. Turnball, (Academic Press, New York), p. 74.

[82] B. Dünweg and K. Binder, 1987, Phys. Rev. B **36**, p. 6935.

[83] J. M . Sanchez, F. Ducastelle, and D. Gratias, 1984, Physica **128A**, p. 334.

[84] Gerbrand Ceder, 1991, Ph.D. Thesis, University of California at Berkeley.

[85] T. B. Massalski ed., 1990, Binary Alloy Phase Diagrams, (ASM Int., Metals Park, OH).

[86] R. Kuentzler and Y. Dossmann, 1991, J. de Phys. IV , vol. 1 (no. C4), p. 54.

[87] R. Kuentzler, private communication.

[88] C. Kittel, 1976, Introduction to Solid State Physic, 5th ed. (Wiley, New York), p. 85.

[89] G.-L. Zhao, T. C. Leing, B. N. Harmon, M. Keil, M. Müllner, and W. Weber, 1989, Phys. Rev. B **40**, p. 7999.

[90] G. Bihlmayer, R. Eibler, and A. Neckel, 1993, J. Phys.: Condens. Matter **5**, p. 5083.

[91] G.-L. Zhao and B. N. Harmon, 1992, Phys. Rev. B **45**, p. 2818.

[92] Roger Haydock, 1980, in Solid State Physics V. 35, eds. H. Ehrenreich, F. Seitz, D. Turnbull, (Academic Press, New York) p. 215.

[93] The Recursion Method and Its Applications, 1985, series in Solid State Sciences, eds. D. G. Pettifor and D. L. Weair, (Springer, Berlin).